

# **The Connection between Cellular Factors Essential for the Human Adenovirus Type 5 E1B-55K Protein**



## **Dissertation**

Zur Erlangung der Würde des Doktors der Naturwissenschaften  
des Fachbereichs Biologie, der Fakultät für Mathematik, Informatik und Naturwissenschaften,  
der Universität Hamburg

vorgelegt von

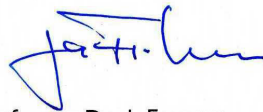
**Wilhelm Ching**

aus Hamburg

03/2012

Genehmigt vom Fachbereich Biologie  
der Fakultät für Mathematik, Informatik und Naturwissenschaften  
an der Universität Hamburg  
auf Antrag von Prof. Dr. T. DOBNER  
Weiterere Gutachterin der Dissertation:  
Priv.-Doz. Dr. N. FISCHER  
Tag der Disputation: 18. Mai 2012

Hamburg, den 03. Mai 2012



Professor Dr. J. Fromm

Vorsitzender des Promotionsausschusses  
Biologie

## **Eidesstattliche Erklärung**

Die vorliegende Arbeit wurde selbständig und ohne unzulässige Hilfe angefertigt

---

Wilhelm Ching

Promotionsgesuch eingereicht am:

Die Arbeit wurde angeleitet von:

Prof. Dr. Thomas Dobner

Prüfungsausschuss:

- Prof. Dr. Alexander Haas (Vorsitzender)
- Prof. Dr. Thomas Dobner (1. Dissertationsgutachter)
- PD. Dr. Nicole Fischer (2. Dissertationsgutachterin)
- Prof. Dr. Hans Will (1. Disputationsgutachter)
- Prof. Dr. Udo Wienand (2. Disputationsgutachter)

Teile dieser Arbeit wurden bereits veröffentlicht (beschrieben in „Part I“):

**Ching, W., Dobner, T., and Koyuncu, E.** (2012). The Human Adenovirus Type 5 E1B 55Kilodalton Protein Is Phosphorylated by Protein Kinase CK2. *J. Virol.* 86, 2400–2415.

## **Abstract**

The human adenovirus type 5 (HAdV5) early region 1B 55-kDa protein (E1B-55K) is a multifunctional phosphoprotein playing several critical roles in productive adenoviral infection and the adenoviral oncogene-mediated transformation processes, e.g., degradation of host cell proteins, viral late mRNA export and inhibition of p53-mediated transcription. Many of these functions are apparently regulated - at least partially - by phosphorylation of E1B-55K. So far, E1B-55K has been shown to interact with and manipulate several proteins of the p53 stress response pathway (e.g. p53) and DNA damage response pathway (e.g. Mre11). These functional interactions are performed mainly to avoid detrimental effects for virus growth. However, a lack of knowledge exists regarding cellular factors directly promoting adenovirus growth.

This work presents detailed analyses of two cellular proteins which are essential for adenoviral replication. Due to the nature of the investigations performed in this study and for clarity reasons, the thesis is divided into three “Parts”.

### **Part I**

In the first Part, extensive biochemical studies were performed to describe the role of the cellular protein kinase CK2 for E1B-55K. CK2 is a constitutively active serine/threonine protein kinase with more than 300 substrates and therefore intertwined in nearly every aspect of cell biology. Here, it was possible to demonstrate for the first time that specifically the  $\alpha$  subunit of CK2 binds to and efficiently phosphorylates E1B-55K. A phosphonegative-E1B-55K (E1B-P minus) virus mutant exhibited several defects: (I) the mutated E1B-55K does not bind known cellular interaction partners like p53 and Mre11 comparably to wild-type E1B-55K. (II) the stability of the mutant E1B-55K protein is cell type-dependent. (III) virus growth is severely reduced in all investigated cell types. These observations were substantiated by using different CK2 inhibitors. Concluding from the data sets, CK2 represents a very important cellular factor to promote adenoviral growth.

### **Part II**

The second Part presents data on the functional interaction of the cellular ubiquitin-specific protease 7 (Usp7) and E1B-55K.

Usp7 is an enzyme capable of cleaving ubiquitin moieties which leads to stabilization of its respective substrates like cellular p53 and Mdm2 or Herpes simplex virus type 1 ICP0. Here,

functional characterization studies were performed using a USP7 inhibitor and a Usp7 knockdown cell line. In fact, it was possible to show that E1B-55K and other adenoviral protein steady-state levels strongly depend on Usp7. Remarkably, it was possible to reduce adenoviral progeny production up to 80% by negatively affecting Usp7 in different human cell lines. In line with this observation, utilizing RNAi or the Usp7 inhibitor in focus forming assays with primary rat cells, an almost complete abolishment of E1A- and E1B-55K-induced transformation was observed. In this respect, Usp7 represents a pivotal cellular factor for both virus growth and transformation processes induced by adenoviral oncogenes.

### **Part III**

Strikingly, in Part I and Part II an essential dependence of E1B-55K from two cellular proteins is presented. Part III provides a rationale why certain similarities between Part I and Part II such as reduced E1B-55K stability and almost identically reduced virus yield are observed. In effect, CK2 phosphorylation of E1B-55K is a prerequisite for Usp7 binding which in turn stabilizes E1B-55K. As a result, a model can be generated helping to understand the intricate relationship in virus-host interaction and to develop antiviral strategies.

## Abbreviations

BSA	bovine serum albumin
C-terminus	Carboxy-terminus
CK2	casein kinase 2
dd.	double distilled
DAPI	4',6-diamidino-2-phenylindole
DBP	DNA binding protein
DMSO	Dimethyl sulfoxide
DMAT	2-dimethylamino-4,5,6,7-tetrabromo-1 <i>H</i> -benzimidazole
DMEM	Dulbecco's modified Eagle medium
dNTP	deoxyribonucleotide
dsDNA	double-stranded DNA
DTT	Dithiothreitol
EBV	Epstein-Barr virus
EDTA	Ethylenediamine-tetraacetate
FFU	fluorescence forming units
fw	forward
g	gravitational force
GAPDH	Glyceraldehyde 3-phosphate dehydrogenase
HAdV5	human adenovirus type 5
HAUSP	herpesvirus-associated ubiquitin-specific protease
HCMV	human cytomegalovirus
HSV	herpes simplex virus
h	hour or hours
h p.i.	hours post infection
ICP	Infected cell polypeptide
Ig	Immunoglobulin
kb	kilo base
kbp	kilo base pair
K/ kDa	kilo Dalton
min	minute
MLP	Major late promoter
MOI	Multiplicity of infection
nt	nucleotide
N-terminus	Amino-terminus
OD	Optical density
orf	open reading frame
PAGE	Polyacrylamide gel electrophoresis
PBS	Phosphate buffered saline
PML	promyelocytic leukaemia protein
rev	reverse
rpm	rounds per minute
RT	room temperature
s	second
SDS	Sodium dodecyl sulfate
TBB	4,5,6,7-tetrabromobenzotriazole
TBE	Tris/Borate/EDTA
TBS	Tris-buffered saline
TEMED	N, N, N', N'-Tetramethyl-ethylenediamine
Tris	Tris-(hydroxymethyl)-aminomethane
U	unit
Usp7	ubiquitin-specific protease 7
vol	volume
v/v	volume per volume
w/v	weight per volume

# Contents

1	Introduction .....	1
1.1	Adenoviruses in the context of basic and applied science.....	1
1.1.1	Adenovirus taxonomy .....	1
1.1.2	Adenovirus pathogenesis.....	2
1.1.3	Molecular structure and genome organization .....	3
1.1.4	Fundamentals of the productive infection cycle.....	5
1.1.5	Oncogenic potential of adenoviruses.....	6
1.1.6	Adenovirus-encoded oncogenes .....	7
1.1.7	Human <i>Adenovirus</i> type 5 E1B-55K.....	8
1.2	CK2 .....	10
1.2.1	CK2 regulation .....	11
1.2.2	CK2 structure and inhibition .....	12
1.2.3	CK2 in specific pathways.....	13
1.3	Usp7 .....	14
1.3.1	Structure and function of Usp7.....	16
2	Materials.....	17
2.1	Cell lines.....	17
2.1.1	Prokaryotic cell lines .....	17
2.1.2	Eukaryotic cell lines .....	17
2.2	Adenoviruses.....	18
2.3	Nucleic Acids .....	18
2.3.1	Oligonucleotides.....	18
2.3.2	Vectors.....	19
2.3.3	Recombinant plasmids.....	20
2.4	Antibodies .....	21
2.4.1	Primary Antibodies.....	21
2.4.2	Secondary Antibodies.....	21
2.4.3	Fluorophore-coupled secondary antibodies.....	22

2.5	Buffers, media and solvents .....	22
2.6	Standards and Markers .....	23
2.7	Animals .....	23
2.8	Enzymes, reagents and consumables.....	23
2.9	Commercial systems.....	24
2.10	Software and databases.....	24
3	Methods.....	25
3.1	Bacteriological techniques.....	25
3.1.1	Cultivation of bacteria .....	25
3.1.2	Transformation of <i>Escherichia coli</i> ( <i>E. coli</i> ) .....	25
3.1.3	Expression and purification of recombinant fusion proteins.....	26
3.1.4	Kinase assays.....	27
3.2	Mammalian cell lines .....	27
3.2.1	Cultivation and passaging.....	27
3.2.2	Preparation of Primary Baby Rat Kidney Cells.....	28
3.2.3	Mammalian cell counting.....	28
3.2.4	Storage of mammalian cells .....	28
3.2.5	Mammalian cell harvest .....	28
3.2.6	Transfection of mammalian cells .....	29
3.2.7	Transformation of primary BRK cells.....	30
3.2.8	Transformation of hMSCs.....	30
3.2.9	FACS-experiments .....	30
3.2.10	Experiments with Usp7 inhibitor HBX .....	31
3.2.11	MTS-based proliferation assay .....	31
3.2.12	Determination of growth behavior .....	31
3.3	Handling adenoviruses .....	31
3.3.1	Generating virus from DNA.....	31
3.3.2	Propagation and storage of high-titer virus stocks .....	32
3.3.3	Titration of adenoviruses.....	32

3.4	Handling lentiviruses.....	33
3.4.1	Titration of Lentiviral Particles .....	33
3.5	DNA techniques .....	34
3.5.1	Isolation of plasmid DNA from <i>E. coli</i> .....	34
3.5.2	Determination of DNA concentrations.....	34
3.5.3	DNA agarose gel electrophoresis .....	34
3.5.4	Isolation of DNA fragments from agarose gels.....	34
3.5.5	Polymerase chain reaction (PCR).....	35
3.5.6	Cloning of DNA fragments .....	36
3.5.7	Analysis of viral DNA synthesis .....	37
3.5.8	Pulsed-field gel electrophoresis.....	37
3.6	Protein techniques .....	38
3.6.1	Preparation of total cell lysates.....	38
3.6.2	Quantitative determination of protein concentrations .....	38
3.6.3	SDS-polyacrylamide gel electrophoresis (SDS-PAGE).....	38
3.6.4	Western blot .....	39
3.6.5	Immunoprecipitation .....	39
3.6.6	Immunofluorescence .....	40

## Part I

4	An investigation conducted to explore the role of CK2 for adenoviral infection – The connection between E1B-55K and CK2.....	42
4.1	E1B-55K is phosphorylated at highly conserved residues at the C terminus, which has similarity to the CK2 consensus phosphorylation motif .....	42
4.2	CK2 $\alpha$ interacts with E1B-55K .....	45
4.3	CK2 $\alpha$ is relocalized during adenovirus infection but in an E1B-independent manner .....	47
4.4	CK2 $\beta$ binds to E1B-55K and is relocalized during adenoviral infection in a phospho E1B-dependent manner.....	48
4.5	CK2 $\alpha$ , but not the CK2 holoenzyme, phosphorylates E1B-55K <i>in vitro</i> .....	51
4.6	The 156R splice product of E1B-55K is also targeted by CK2 $\alpha$ but not by the holoenzyme.....	52
4.7	Inhibition of CK2 during adenovirus infection abolishes E1B-55K phosphorylation and interaction with diverse cellular proteins .....	53

4.8	Alanine substitution of E1B-55K's phospho-sites results in cell type-specific profound negative effects.....	56
4.9	Inhibition of CK2 during adenovirus infection limits down regulation of Mre11 and DNA ligase IV protein levels but does not induce adenoviral genome concatemerization although virus yield is significantly reduced.....	59
5	Discussion.....	61
5.1	The CK2 E1B relationship.....	61

## Part II

6	The cellular protein Usp7 interacts with E1B-55K, promotes adenoviral replication and transformation processes.....	67
6.1	Usp7 interacts with E1B-55K.....	67
6.2	Usp7 is relocalized during adenoviral infection.....	69
6.3	Qualitative and quantitative assessment of Usp7-E1B colocalization.....	72
6.4	Usp7 is relocalized to viral replication centers during adenoviral infection.....	74
6.5	Qualitative and quantitative assessment of Usp7-DBP colocalization.....	76
6.6	Introduction into a new class of inhibitors.....	78
6.7	Analyses of the HBX effect on cell growth and viability.....	80
6.8	HBX does not affect Usp7 relocalization during adenoviral infection.....	81
6.9	Usp7 knockdown or inhibition reduces E1B-55K steady-state levels.....	84
6.10	Impact of Usp7 knockdown on adenoviral replication.....	85
6.11	Impact of Usp7 inhibition on adenoviral replication.....	87
6.12	Impact of Usp7 inhibition on adenoviral oncogene-mediated cellular transformation.....	89
7	Discussion.....	92
7.1	The Usp7-E1B relationship.....	92
7.2	Usp7 is redistributed in a complex manner during adenoviral infection.....	93
7.2.1	Usp7 knockdown or inhibition leads to similar negative effects on adenoviral replication.....	95
7.3	Usp7 in adenoviral transformation processes.....	98

## Part III

8	Connecting CK2-mediated phosphorylation of E1B-55K and Usp7 .....	100
8.1	The extent of binding deficiency toward Usp7 affects E1B-55K protein stability which is a matter of E1B-55K's phosphorylation status .....	100
8.2	Usp7 is relocalized during E1B-P minus virus ( <i>H5pm4174</i> ) infection in the same manner as during wt virus infection .....	102
8.3	TBB-mediated inhibition of CK2 results in reduced Usp7 binding of E1B-55K.....	103
8.4	Usp7 inhibition through HBX further reduces virus yield of the E1B-P minus virus.....	105
8.5	Concluding subsections – Giving an outlook of possible investigation pathways.....	106
8.5.1	The amount of PML tracks during wt and E1B-P minus virus infection differs significantly .....	106
8.5.2	Adenoviral infection induces the spatial proximity of Usp7 and PML into ring-like structures .....	109
9	Discussion.....	111
9.1	E1B-55K and the dependence upon two cellular factors .....	111
9.2	PML-NBs and phospho-E1B-55K – more complexity to the CK2-Usp7 matter .....	112
10	Thesis model .....	113
10.1	Phosphorylation of E1B-55K impacts its localization.....	113
10.2	Phosphorylation of E1B-55K – An interaction issue .....	114
10.3	Usp7 - A very special interaction partner .....	114
10.4	Possible role of CK2 $\alpha$ and Usp7 in the modulation of downstream targets.....	115
11	Conclusion and Outlook.....	119
12	References .....	121
13	List of figures .....	134
14	Acknowledgements .....	136

# 1 Introduction

## 1.1 Adenoviruses in the context of basic and applied science

Since their first discovery in the mid-20<sup>th</sup> century, scientific work with adenoviruses has borne many important and essential insights into different basic processes of DNA replication, transcription and molecular signal transduction processes in eukaryotic cells. Moreover, much knowledge about viral infection processes was and is gained from work with adenoviruses. Especially, human *Adenovirus* type 12 (HAdV12) turned out to be the first virus capable of inducing malignant tumors in rodents which was eventually the starting point of investigations into DNA tumor viruses (Trentin et al., 1962). The process of RNA splicing was first discovered by examining adenoviral gene maturation processes (Berget and Sharp, 1977; Chow et al., 1980, 2000). Nevertheless, adenoviruses are still a fertile ground for investigating a multitude of different molecular mechanisms among them tumor induction or mRNA transport.

Another important aspect of adenoviral science and application involves the use of adenoviruses as gene transfer vectors or as oncolytic viruses in the combat against cancer. H101 is one example of an oncolytic adenovirus used against head and neck cancers (Xu et al., 2005). However, approval is only given in China. Adenoviruses are also thought as being used for vaccination (Everts and Curiel, 2004; Tatsis and Ertl, 2004).

### 1.1.1 Adenovirus taxonomy

There are more than 130 adenovirus types to be found in the family of *Adenoviridae*. According to the host species tropism and other distinct attributes, adenoviruses can be classified into five genera: *Mastadenoviruses* (infecting mammals), *Aviadenoviruses* (infecting birds), *Atadenovirus* (infecting reptiles and ruminants), *Siadenoviruses* (infecting amphibians) and *Ichadenovirus* (infecting fish). Human *Adenoviruses* (HAdVs) belong to the genus of *Mastadenovirus* and are further categorized into subgroups using several characteristic hallmarks like hemagglutination properties, DNA sequence homologies and oncogenicity in immunosuppressed experimental animals. There are seven subgroups/serotypes (A-G) including 57 accepted adenovirus types (HAdV1-HAdV57) HAdV2 and HAdV5 are the most intensively studied types due to their non-oncogenic properties (for an overview: Shenk, 2001).

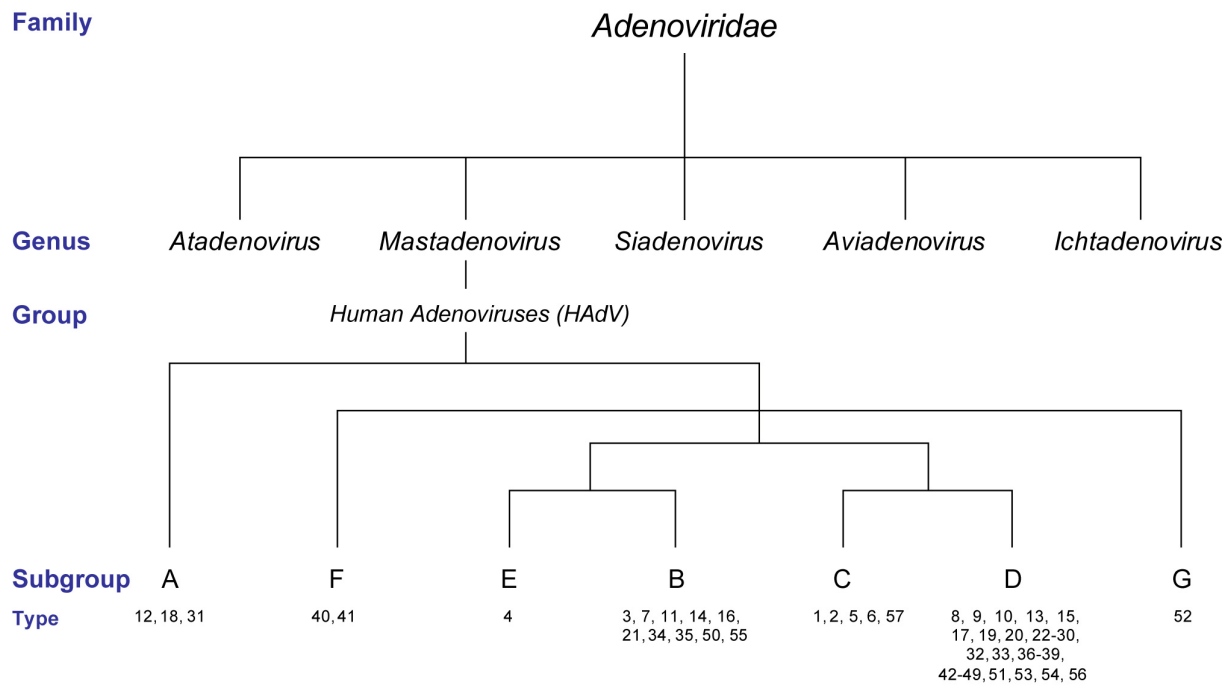


FIG 1 Simplified taxonomic illustration of the family *Adenoviridae*. The human Adenovirus taxonomic relationship is represented with 57 known adenovirus types as described in <http://www.vMRI.hu/~harrach/AdVtaxlong.htm>.

### 1.1.2 Adenovirus pathogenesis

Adenoviruses are widespread throughout the human population and cause, in most cases, asymptomatic infections, but can also induce certain types of more severe reactions (Tab. 1). Adenovirus infections mostly target epithelial tissues of the respiratory and gastrointestinal tract, but can also target the eye. Infections usually lead to common cold-like symptoms or diarrhea. Due to their high prevalence ca. 80% of all children by the age of 5 years have encountered an adenoviral infection which is usually followed by long-term immunity. However, severe HAdV infections may occur in immunosuppressed people, for example, patients undergoing hematopoietic stem cell transplantation. In this example, HAdV-induced hemorrhagic cystitis is a recognized cause of morbidity and mortality (Benkő and Harrach, 1998; Horwitz, 2001; Davison et al., 2003).

**TAB 1 Diseases caused by adenoviruses**

<b>Subgroup/Serotype</b>	<b>Clinical Syndromes</b>
<b>A, E</b>	Acute respiratory illness, conjunctivitis, pharyngitis, pneumonia, acute/chronic appendicitis, respiratory tract infections
<b>B (3, 7, 14, 21)</b>	Fever, pharyngitis, acute respiratory illness, meningitis
<b>C (1, 2, 5, 6)</b>	Respiratory illness in children, rare in adults
<b>D (8, 19, 37)</b>	Epidemic keratoconjunctivitis
<b>E (4)</b>	Fever, pharyngitis, acute respiratory illness
<b>F, G (40, 41)</b>	Gastroenteritis

### **1.1.3 Molecular structure and genome organization**

Adenoviruses are non-enveloped and possess an ~80-110 nm protein capsid. The characteristic icosahedral capsid is composed of a multitude of different structural proteins in total 252 capsomeres. 240 hexons form the faces and 12 pentons are located at the vertices. Each penton is associated with a protruding fiber protein and together both units mediate the receptor-coordinated cell adsorption (Wickham et al., 1993, 1994; Mathias et al., 1994). The cellular receptor mediating subgroup C adenovirus entry is the same one used by Coxsackie B virus. Thus, this receptor is called Coxsackie/Adenovirus Receptor (CAR) (Bergelson et al., 1997). Minor structural components of the capsid include proteins IIIa, VI, VIII and IX (Fig. 2).

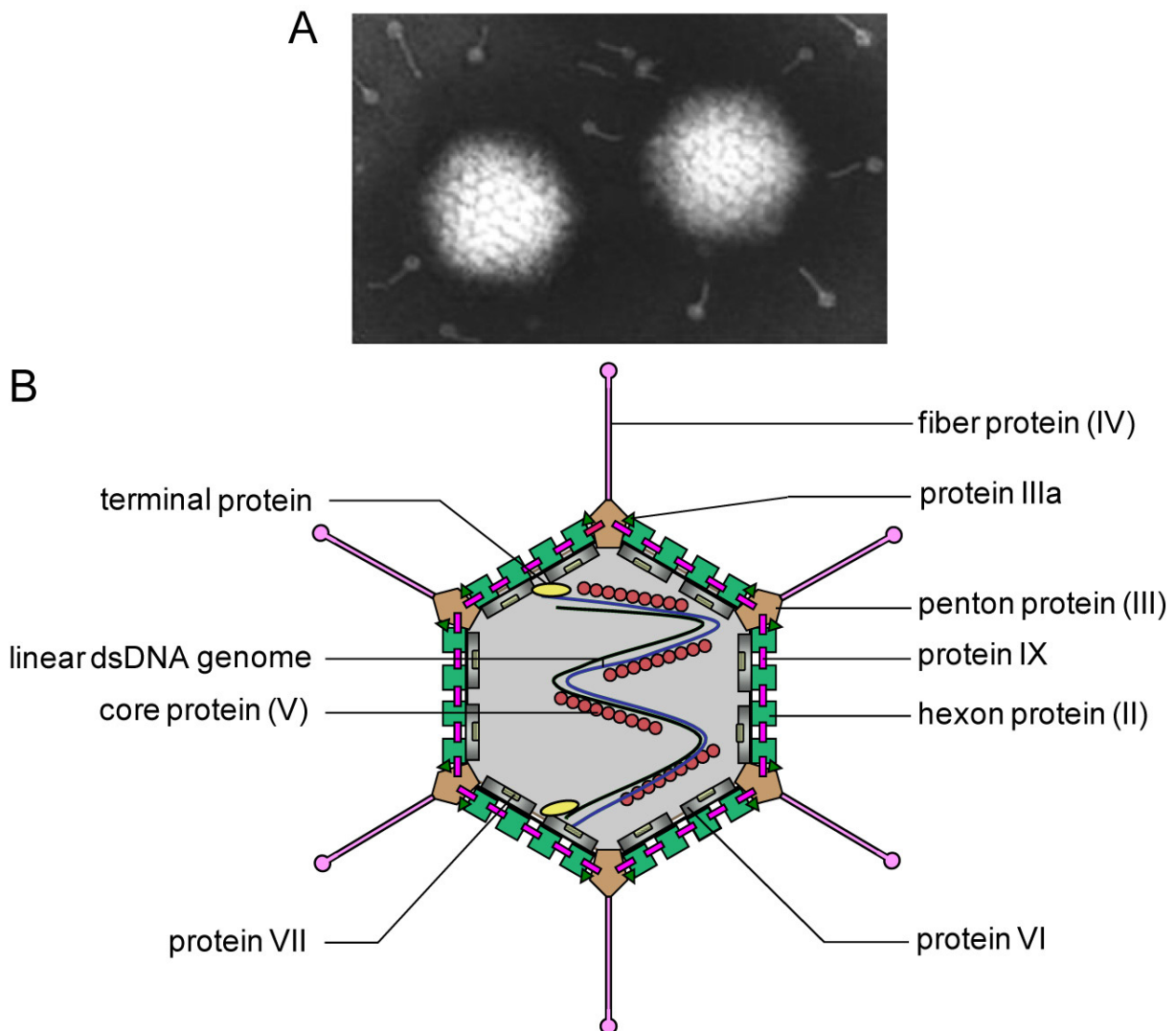


FIG 2 Electron micrograph and schematic representation of an adenoviral virion. (A) The icosahedral structure and spikes protruding from the capsids of adenoviruses can be seen in this electron micrograph (from Stewart et al., 1993). (B) Schematic representation of the structure of an adenovirus with detailed labeling of different proteins constituting the capsid shell as well as the inner organization.

Human Ad types have the same genomic organization and express a similar set of RNAs. The viral chromosome of the most widely studied subgroup C Ad types 2 and 5 have characteristic linear, double-stranded DNA genomes of 36 kb in length (Shenk, 2001). The genome of HAdV5 carries 9 different transcription units that encode 40 different polypeptides and two small RNAs (virus associated RNAs, VA RNAs). The genome of HAdV5 is organized into early and late genes. Early genes are named as E1-E4, and late genes, which are under the control of major late promoter (MLP), are named as L1-L5. In addition, two RNAs encoded from the IX and IVa2 genes are observed at intermediate times of infection (Fig. 3).

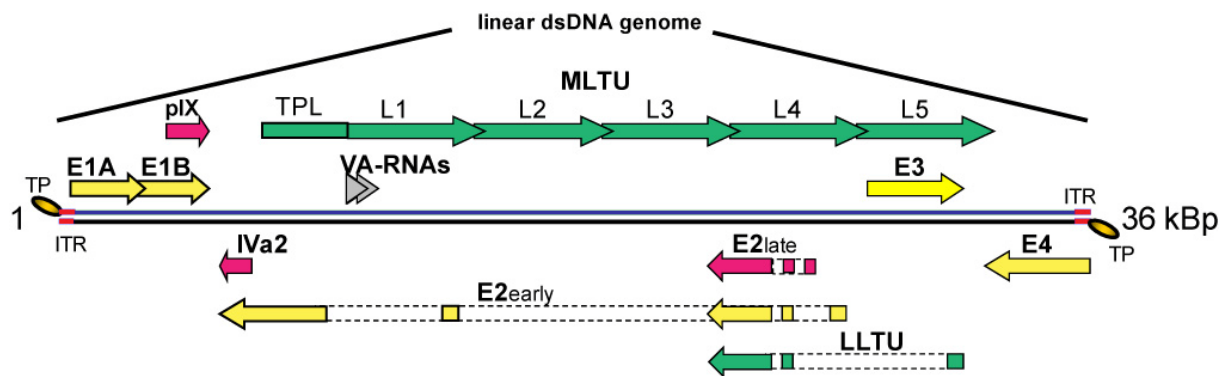


FIG 3 Schematic representation of a linear double-stranded DNA genome of HAdV5. The adenovirus genome includes nine transcription units and encodes approximately 40 proteins and two non-coding RNAs (VA RNAs: virus-associated RNAs). Arrows point to transcription direction. E: early. L: late. MLTU: major late transcription unit. VA RNAs: virus-associated RNAs. ITR: inverted terminal repeats. More details in Doerr and Gerlich, 2009.

### 1.1.4 Fundamentals of the productive infection cycle

Human adenoviruses infect a wide spectrum of different cells. Preferred target cells are post-mitotic resting and terminal differentiated epithelial cells of the pharynx as well as cells of the lung and of the intestinal tract. In tissue culture adenoviruses can be propagated in different tumor cell lines. While they pass in many human cells through a productive (lytic) cell cycle, the infection of cells of animal origin results in an abortive course of infection (Doerr and Gerlich, 2009; Shenk, 2001)

The productive course of infection is divided into an early and late phase. Both are separated by the initiation of the viral DNA synthesis. Per definition the early phase of infection begins with the adsorption of the virus to the cellular surface. After internalization and nuclear import of the viral DNA-protein-complex the transcription of the early viral genes by the DNA-dependant RNA polymerase II is initiated and the early proteins are expressed.

Ca. 20 regulatory proteins of the early transcription units E1A, E1B, E2, E3 and E4 are expressed in a temporally coordinated fashion. The function of the respective gene products is mainly to prepare the optimal conditions for production of viral structural proteins and viral DNA replication in the late phase of infection. For the viral replication, the passage of the resting cell from the G<sub>0</sub>- into S-Phase is essential as only in dividing cells there is sufficient material to support effective viral reproduction. This is mediated by the E1A proteins that, due to their interaction with the cellular pRB proteins and other mechanisms, initiate the expression of genes that are essential for S-Phase transition. Alongside this function, E1A expression also mediates a strong induction of cell cycle control mechanisms and apoptosis (Chakraborty and Tansey, 2009).

In addition, proteins of the E1- and E3- regions block different antiviral protective mechanisms of the host cell e.g. induction of apoptosis. Moreover, they modulate the immune response to prevent a premature recognition and elimination of the infected cell by the immune system of the host organism (Gooding and Wold, 1990; Mathews and Shenk, 1991; Burgert and Blusch, 2000). The gene products of the transcription unit E2 are responsible for the replication of the viral DNA. These include the viral DNA polymerase, the DNA binding protein DBP (E2A-72K) and the terminal protein, which is covalently bound to the 5'-ends of the viral genome (Shenk, 2001). The E4 region encodes at least six different polypeptides, which are generated from alternatively spliced forms of the primary E4 transcript. These are labeled according to the arrangement of the open reading frame (E4orf1, E4orf2, E4orf3, E4orf4, E4orf6 and E4orf6/7) within the transcription unit. The proteins of the E4 region have diverse essential functions for viral replication (Täuber and Dobner, 2001). The start of the viral DNA replication initiates the beginning of the late phase of the lytic infection cycle and the transcription of the late transcription unit (MLTU: major late transcription unit). Five groups of mRNA (L1-L5) with different lengths are generated due to the use of different termination signals as well as alternative splicing. These mRNAs mainly encode proteins that are responsible for structural proteins of the icosahedral capsid. An essential part of the late phase is the shutdown of the cellular protein synthesis (host shut-off), while viral proteins are further produced. Furthermore, the late phase is characterized by a reorganization of the nucleus (Puvion-Dutilleul et al., 1995) that is at least in part caused by the massive nuclear accumulation of viral DNA and proteins as well as by a restructuring of the cytoskeleton (Defer et al., 1990). The productive infection cycle ends in tissue culture after about 24 hours. Depending on the virus type and cells infected, the host cell releases up to 10000 virus particles.

### 1.1.5 Oncogenic potential of adenoviruses

Transformation by adenoviruses was first postulated in a hamster model in 1962 (Trentin et al., 1962). Since then, many HAdVs have demonstrated their potential in inducing tumors in rodents, but with varying efficiency (Tab. 2). Nevertheless, all human Ads are able to transform cells of newborn rodents *in vitro* (McBride and Wiener, 1964; Nevins and Vogt, 1996). Despite the transformation efficiency in rodent cells, transformation of human cells is a very rare phenomenon (Hahn et al., 1999). However, some reports exist stating the finding of HAdV DNA in human tumors: in small-cell lung carcinoma HAdV5 DNA was found (Kuwano et al., 1997), in more than two-thirds of brain tumor samples adenovirus DNA of species B, D and C was discovered (Kosulin et al., 2007) and in children with acute

lymphoblastic leukemia HAdV DNA was also found (Gustafsson et al., 2007). Therefore, oncogenesis in humans driven by HAdVs cannot be excluded.

**TAB 2 Oncogenicity of human adenoviruses in rodents.**

ONCOGENICITY IN RODENTS	SUBGROUP	SEROTYPE	TUMOR TYPE
<b>Highly oncogenic</b>	A	12, 18, 31	undifferentiated sarcomas
	D	9, 10	fibroadenomas
<b>Weakly oncogenic</b>	B	3, 7, 11, 14, 16, 21, 34, 35	undifferentiated sarcomas
<b>Non-oncogenic</b>	C - F	C (1, 2, 5, 6); D (8, 13, 15, 17, 19, 20, 22-30, 32, 33, 36-39, 42-49, 51); E (4); F (40, 41)	none

### 1.1.6 Adenovirus-encoded oncogenes

Most Ad tumors, tumor cell lines and transformed cell lines are characterized by the persistence of chromosomally integrated viral DNA, and the expression of specific viral antigens (Graham et al., 1984). However, Ad transformation follows the classical concept of viral oncogenesis where viral genes persist within the transformed cells. In contrast, it has also been reported that Ad DNA could not be detected in cells which were known to be transformed by Ads. This phenomenon is explained by a hit and run model, where adenoviral oncogenes induce a change of the cell (hit) which is kept after losing the oncogenes (run) (Nevins and Vogt, 1996).

In simple terms, adenoviral oncogene-mediated transformation involves only two viral proteins. The adenoviral E1A protein sequesters pRb thereby releasing and activating E2F transcription factor family members. This results in uncontrolled S-phase progression with subsequent induction of p53 accumulation and activation. To circumvent detrimental p53 activities like cell cycle arrest or premature apoptosis, E1B-55K binds and stably inactivates p53 transcriptional functions. As a net result, cells are “programmed” for unprogrammed cell proliferation leading to cell transformation (Berk, 2005).

More specifically, the E1 region of the genome is often sufficient for adenoviral-mediated transformation (Trentin et al., 1962; Graham et al., 1984; Nevins and Vogt, 1996; Endter and Dobner, 2004), but gene products of the E4 region are thought to foster the E1-mediated transformation processes (Ohman et al., 1995; Moore et al., 1996; Nevels et al., 1997, 1999a, 1999b). The early adenoviral genes E1A, E1B and E4 reorganize the cell for efficient viral replication. This is mainly done by inducing the S-phase and deactivating the cell cycle

checkpoints. Since the cell cycle is deregulated, transformation may occur. E1A is the first transcription unit to be expressed after virus entry into the host cell. Its transcription is regulated by a constitutively active promoter that requires no prior viral protein synthesis. The E1A gene products are responsible for transcription, activation of the other adenoviral early genes and for activation of cellular genes that induce entry of the infected cell into the S-phase of the cell cycle. The E1A proteins associate with a variety of cellular targets that are directly or indirectly responsible for activation of cell proliferation. One such target is the retinoblastoma tumor suppressor (pRb). E1A associates with pRb causing the dissociation and activation of the E2F family transcription factors that lead to unscheduled DNA synthesis and cell proliferation (Berk, 2007). The activities of E1A result in activation and stabilization of the tumor suppressor p53, which leads to activation of apoptosis, thus hindering virus replication. p53-dependent and independent apoptosis is efficiently inhibited by other early gene products encoded in the E1B and E4 units (Lowe and Ruley, 1993). The E1B transcription unit encodes two proteins that are directly involved in regulation of p53 activity and apoptosis inhibition. E1B-55K counters E1A-induced p53 stabilization by inhibiting p53 through binding its activator domain (Shen et al., 2001). The E1B-19K blocks p53-independent induction of apoptosis by binding two members of the proapoptotic BCL-2 family, BAK and BAX (Cuconati et al., 2003). Complexes of BAK and BAX activate apoptogenic proteins like caspase-9 and -3 and finally lead to apoptosis of the host cell (Berk, 2005).

### **1.1.7 Human *Adenovirus* type 5 E1B-55K**

The human *Adenovirus* type 5 (HAdV5) early region 1B 55-kDa protein (E1B-55K) is a multifunctional phosphoprotein (Malette et al., 1983; Teodoro et al., 1994; Teodoro and Branton, 1997; Wimmer et al., 2010) and regulator of adenoviral replication (Blackford and Grand, 2009). E1B-55K in complex with E4orf6, cellular factors cullin-5, Rbx1, or elongins B and C mediates the degradation of cellular proteins such as p53, Mre11, DNA ligase IV, integrin  $\alpha$ , and Bloom's helicase (Cathomen and Weitzman, 2000; Querido et al., 2001; Blanchette et al., 2004; Baker et al., 2007; Dallaire et al., 2009; Orazio et al., 2011). It has been shown that these functions are necessary to antagonize the DNA damage response that would eventually lead to concatenation of viral genomes (Stracker et al., 2002), as well as stress responses that would initiate cellular antiviral defense mechanisms (Weitzman and Ornelles, 2005; Lilley et al., 2007; Schreiner et al., 2010). Furthermore, E1B-55K, along with E4orf6, mediates the export of viral late mRNA transcripts (Dobner and Kzhyshkowska, 2001; Gonzalez and Flint, 2002; Flint and Gonzalez, 2003; Blanchette et al., 2008) and is

responsible for blocking cellular mRNA export (Babiss and Ginsberg, 1984; Babiss et al., 1985; Pilder et al., 1986). Moreover, E1B-55K alone can induce a decrease in protein levels of Daxx (death domain-associated protein), which was shown to be a restrictive factor for adenoviral replication (Schreiner et al., 2010). E1B-55K is known to be phosphorylated at amino acids serine 490, serine 491, and threonine 495 (Teodoro et al., 1994; Teodoro and Branton, 1997). Phenotypic analyses of a mutant virus lacking these sites point to an essential involvement of this posttranslational modification in E1B-55K functions and viral replication in general (Teodoro et al., 1994; Schwartz et al., 2008). For example, these modifications seem to be necessary for E1B-55K's p53-repression functions, i.e., the ability to bind p53 (Schwartz et al., 2008), inhibit its transactivational abilities (Teodoro et al., 1994; Teodoro and Branton, 1997) and induce the proteasomal degradation of p53 (Querido et al., 2001; Schwartz et al., 2008). Also, localization of the E1B-55K protein is affected by mutating the phosphosites (Schwartz et al., 2008). However, the kinase responsible for E1B-55K phosphorylation is still unknown. SUMO-1 conjugation is another posttranslational modification of E1B-55K and has been described to be important for subcellular localization, transformation processes, and p53 repression (Endter et al., 2001, 2005; Endter and Dobner, 2004). The respective amino acid to be modified is lysine 104. Interestingly, mutations in the neighboring nuclear export signal (NES) enhances SUMO-1 conjugation on lysine 104 together with nuclear retention. However, concomitant mutation of lysine 104 relieves E1B-55K from its strict nuclear localization. In this context, shuttling processes depending and not depending on the export factor CRM1 are discussed

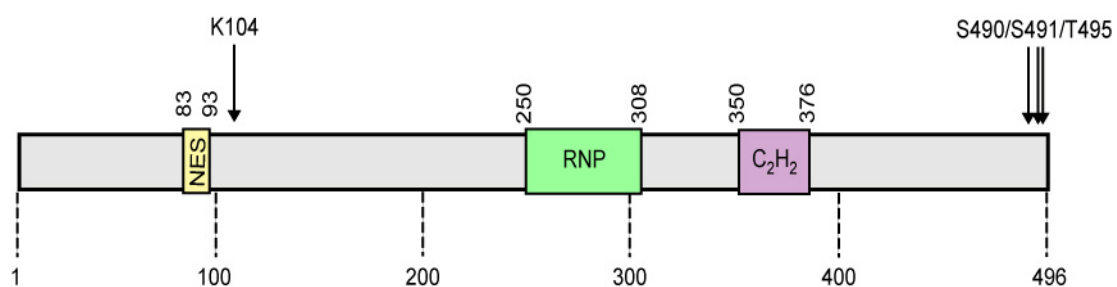


FIG 4 Schematic representation of the HAAdV5 E1B-55K protein. Arrows indicate residues known to be sumoylated (K104) or phosphorylated (S490/S491/T495). The colored boxes indicate functionally interesting regions on the primary amino acid sequence of E1B-55K. RNP, RNP motif; C<sub>2</sub>H<sub>2</sub>, putative zinc finger (modified from Blackford and Grand, 2009).

## 1.2 CK2

The cellular CK2 protein is a serine/threonine kinase known to be ubiquitously expressed, highly conserved in eukaryotic cells, and considered to be constitutively active (Pinna, 1990; Meggio and Pinna, 2003; St-Denis and Litchfield, 2009). Today, CK2 is known to phosphorylate more than 300 cellular and viral proteins, and yet the list is far from complete, as shown by comparative amino acid sequence screen analyses among putative CK2 phosphorylation motifs/sites (Meggio and Pinna, 2003; Salvi et al., 2009). Among these substrates are proteins involved in DNA replication (topoisomerase I [Pinna, 1990; Meggio and Pinna, 2003]), transcription (c-Myc [Pinna, 1990; Meggio and Pinna, 2003]), cell cycle control (cyclin H [Schneider et al., 2002]), ribosome biogenesis (L5 [Park and Bae, 1999]), apoptosis induction (Bid [Desagher et al., 2001]), and cell differentiation (HOXB7 [Yaron et al., 2001]), as well as numerous viral proteins (e.g., EB2 from Epstein-Barr virus [EBV] (Medina-Palazon et al., 2007), EBNA-2 from EBV [Grässer et al., 1992], NS2 from hepatitis C virus [HCV] [Franck et al., 2005], and ZEBRA from EBV [El-Guindy and Miller, 2004]), that comprise ca. 10% of the known CK2 substrates (Meggio and Pinna, 2003). Apart from its role in normal cellular signaling pathways and viral infections, CK2 is reported to be involved in tumorigenesis. For example, increased CK2 activity is linked to several kinds of malignancies such as breast cancer (Münstermann et al., 1990; Landesman-Bollag et al., 2001) or colorectal carcinoma (Pistorius et al., 1991), while reduced activity has been associated with limited cell viability (Wang et al., 2001; Slaton et al., 2004). Indeed, the large number of cellular substrates highlights the important role CK2 plays in maintaining cell homeostasis. Several studies have shown that knockout of the CK2 $\alpha$  or  $\beta$  subunit is lethal at the embryonic stage in mice (Buchou et al., 2003; Seldin et al., 2008; Trembley et al., 2009). CK2 $\alpha$  or CK2 $\alpha'$  can form homo- or heterodimers and assemble with a homodimer of  $\beta$  subunits to form the CK2 holoenzyme (Filhol et al., 1991; Graham and Litchfield, 2000; Pinna, 2002). Either the holoenzyme or  $\alpha$  and  $\alpha'$  subunits show constitutive activity, so CK2 activity is not regulated through a “classical” signal transduction cascade, as known, for example, for mitogen-activated protein kinases (Pinna, 1997) or cyclin-dependent kinases (CDKs [Pinna, 2002]). It is assumed that constitutive activity and ubiquitous expression are two of the reasons why CK2 is exploited by many different viral pathogens (Meggio and Pinna, 2003). Mechanistically, CK2 can use either ATP or GTP as phosphoryl donors (Niefind et al., 1999). Phosphorylation occurs specifically at serine or threonine residues on target proteins, although CK2 shows a higher propensity to phosphorylate serine residues

(Meggio and Pinna, 2003). The general consensus motif for a CK2 phosphorylation site was found to be S/T-X-X-E/D (Pinna, 2002; Meggio and Pinna, 2003; Salvi et al., 2009).

### 1.2.1 CK2 regulation

Although CK2 is considered to be constitutively active, several studies could demonstrate that a fine-tuning in CK2 activity exists. Due to CK2's involvement in numerous cellular pathways such as regulation of translation, it is not surprising that other cellular factors involved in translation processes can have an influence on CK2 substrate specificity and activity. The eukaryotic translation initiation factor  $\beta$  (eIF2 $\beta$ ) binds CK2 and this binding leads to eIF2 $\beta$  phosphorylation. Interestingly, eIF2 $\beta$  exhibits disparate binding affinities to the different subunits of CK2 ( $\alpha$  and  $\beta$ ) and the CK2 holoenzyme. In this regard, high affinity toward the  $\alpha$  and low affinity toward the  $\beta$  subunit exists, which leads to different functional outcomes. Binding to the CK2 $\alpha$  subunit leads to an inhibitory effect upon specific substrates whereas interaction with the holoenzyme does not lead to the inhibitory function (Llorens et al., 2003). As another example, for an inhibitory effect exerted upon CK2, p53 also interacts with the kinase. Schuster et al. demonstrated that p53 binds the  $\beta$  subunit of CK2, leading to decreased CK2 activity which can lead to cell growth suppression (Schuster et al., 2001). On the one hand, wt p53 conformation is necessary to exert this negative effect. On the other hand, mutations in p53 disturbing the proper structure lead to loss of inhibiting functions (Schuster et al., 2001). In the context of p53 regulation, it is interesting to point out that the C-terminal part of the tumor suppressor protein exerts growth promoting activities and is therefore known as a transforming peptide (Soussi et al., 1990). In connection with CK2, the C-terminal region of p53 (amino acid 264 to 393) inherits multiple basic amino acid clusters capable of enhancing CK2 activity (Guerra et al., 1997). This is well in line with the growth promoting activities of CK2 (Piazza et al., 2012). The (basic) charge nature of polyamines is well characterized as having positive effects upon cell growth and differentiation (Pegg and McCann, 1982). Therefore, it is not surprising that polyamines also positively affect CK2 activity. Spermidine is a polyamine known to increase CK2 activity. The role of spermidine in tumorigenic processes may be indirect but involves upregulation through enhanced Ornithine decarboxylase (ODC) activity, an enzyme which is frequently elevated in protein levels and activity in different cancers (Montenarh, 2010). These few examples highlight the complex involvement of protein kinase CK2 in different cellular pathways connected to its regulation.

### 1.2.2 CK2 structure and inhibition

As denoted above, the protein kinase CK2 consists in holo conformation of two  $\alpha$  (43 kDa) or  $\alpha'$  (38 kDa) and a homodimer of  $\beta$  (each 27 kDa) subunits (Fig. 5). The resulting hetero tetrameric form is build up of the two  $\beta$  subunits connected through zinc-finger-domains and each of the  $\beta$  subunits is linked to the subunit  $\alpha$  or  $\alpha'$ . However, the catalytic  $\alpha$  or  $\alpha'$  subunits are not connected with each other (Fig. 5B) (Pinna, 1990; Pagano et al., 2008; Piazza et al., 2012).

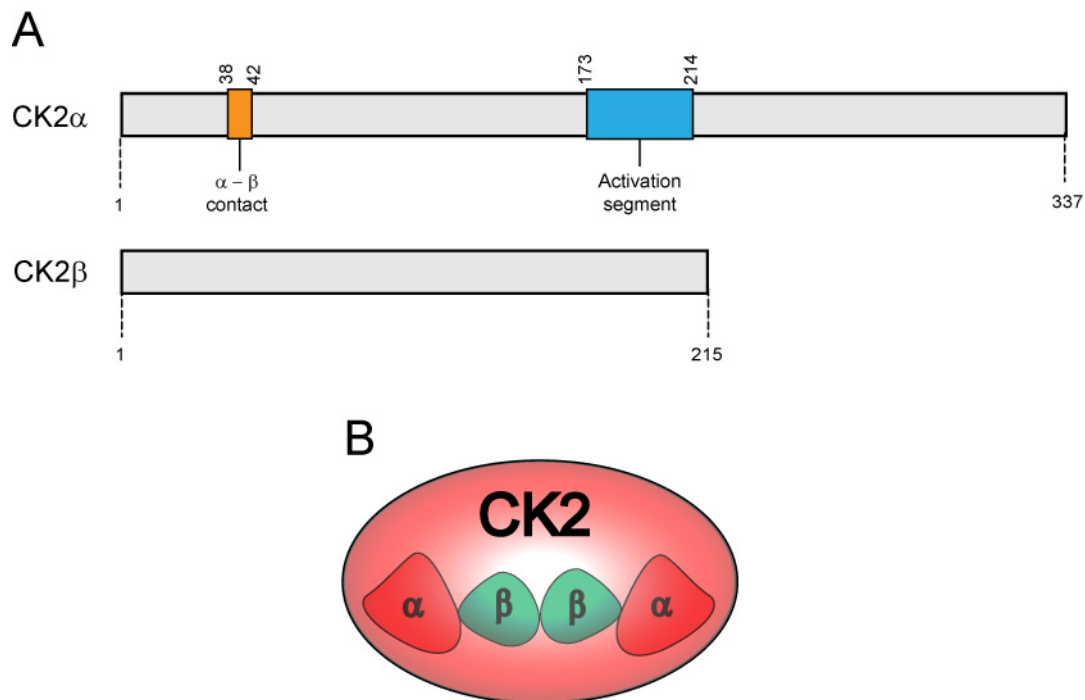


FIG 5 Schematic representation of CK2 $\alpha$  and CK2 $\beta$ . (A) Linear cartoon of the CK2 $\alpha$  polypeptide showing the contact region to the  $\beta$  subunit and the activation segment responsible for conformational activity. (B) This cartoon demonstrates the homodimeric form of two  $\beta$  subunits with attached  $\alpha$  subunits forming the CK2 holoenzyme.

Due to CK2's constitutive activity, its long half-life and high expression, several approaches in elaborating detailed functions in connection to cellular or potential substrate targets have faced difficulties. Especially, RNAi analyses or set-ups including dominant-negative kinase mutants experienced certain drawbacks (Seeber et al., 2005; Wang et al., 2005). However, structural insights into CK2 enhanced the development of several inhibitors or the improvement of pharmacological agents. Two of the most popular and widely used inhibitors are TBB (4,5,6,7-tetrabromobenzotriazole) and DMAT (2-dimethylamino-4,5,6,7-tetrabromo-1*H*-benzimidazole). TBB has been shown to have a narrower specificity than DMAT, whereas both compounds display inhibitory effects upon other kinases as well. At certain concentrations DMAT also inhibits PIM1 (provirus integration site for Moloney murine

leukaemia virus), PIM2, PIM3, PKD1 (protein kinase D1), HIPK2 (homeodomain-interacting protein kinase 2) and DYRK1a (dual specificity tyrosine-phosphorylated and -regulated kinase 1a). In contrast, TBB only inhibits PIM1 and PIM3 (Pagano et al., 2008). Therefore, to attenuate the effect of low specificity, more than one inhibitor could be used along with “phosphomutants” (proteins containing mutations abolishing phosphorylation) of the respective target. In principle, CK2 inhibitors bind with hydrophobic interaction a cavity which is smaller than in other kinases (Fig. 6B). This circumstance is being used to develop more high-specificity inhibitors against CK2.

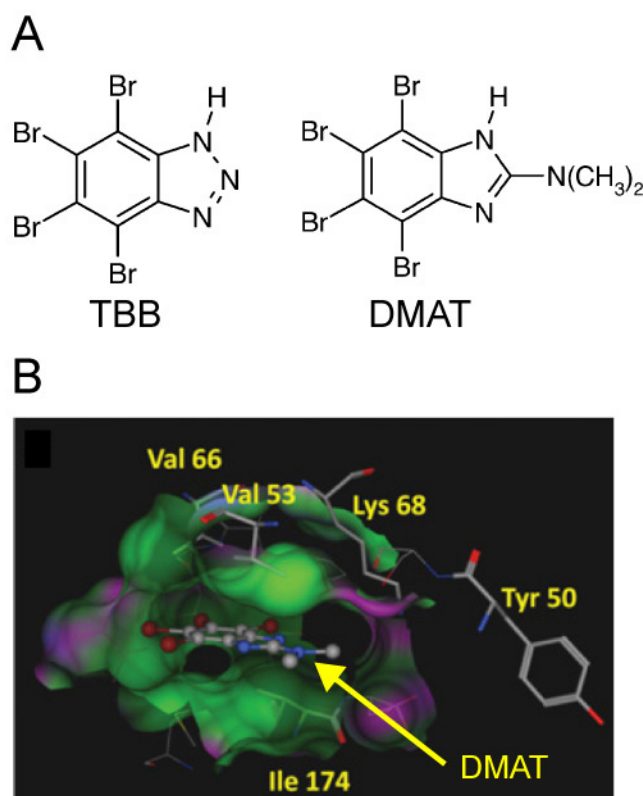


FIG 6 CK2 inhibitor TBB and DMAT. (A) The chemical structure of the two most widely used CK2 inhibitors. (B) Molecular docking of DMAT in the active site of CK2 (Pagano et al., 2008).

### 1.2.3 CK2 in specific pathways

The protein kinase CK2 is a remarkable protein with uncountable functions. This is, of course, caused by the extraordinary amount of CK2 substrates which are involved in every aspect of cell physiology. Among them, ca. 60 transcription factors involved in RNA synthesis and translation as well as ca. 80 proteins directly connected to signal transduction pathways represent only a certain part of CK2 substrates.

The elegant work from Stehmeier and Müller, demonstrated the intricate connection of CK2 phosphorylation and SUMOylation of PIAS1 which is a transcriptional coregulator and SUMO ligase (Stehmeier and Muller, 2009). Here, CK2 phosphorylation-dependent SUMO

interaction modules (phosphoSIMs) were defined, which connect two different posttranslational modifications on one molecule in a timely and spatial context. This adds another layer to the complexity of protein-protein interaction and demonstrates that phosphorylation can be directly connected to a second posttranslational modification. Interestingly, CK2-regulated phosphoSIM modules were also found in PML nuclear bodies (PML-NBs) (Stehmeier and Muller, 2009). As a matter of fact, this is not the only connection CK2 inherits in connection to these important nuclear protein complexes. Scaglioni et al. could nicely offer a new perspective in CK2-induced regulation. In this, a mechanism has been presented that demonstrates CK2-induced phosphorylation of Serine 517 on PML, which leads to polyubiquitination and degradation of this tumor suppressor (Scaglioni et al., 2006). This has many implications in cancer biology and in the understanding of infectious diseases. In example, Epstein-Barr virus EBNA1 has been demonstrated to exploit CK2 activity in order to enhance PML phosphorylation which, as stated before, triggers the degradation of PML-NBs that also inherit antiviral activities.

### 1.3 Usp7

The interest in deubiquitinating enzymes (DUBs) is increasing since the number of functions linked to this protein class is growing rapidly. Herein, cell physiologic processes like tumor-induction and -repression or regulation of gene transcription are involved. Moreover, it becomes obvious that several viruses exploit deubiquitination functions in order to promote viral replication. The cellular protein ubiquitin-specific protease 7 (Usp7, also known as herpesvirus-associated USP [HAUSP]) is a member of the largest group of DUBs and a critical component of the p53-Mdm2 stress response pathway, therefore implicated in tumorigenesis. Extensive studies on Usp7's physiological functions revealed its astonishing position in the molecular network of p53 regulation. Usp7 was shown to directly bind and deubiquitinate p53 and its negative regulator Mdm2 (Li et al., 2002). Under different stress conditions Usp7 has a greater propensity to bind p53 than Mdm2 which leads to increased p53 deubiquitination and Mdm2 auto-ubiquitination, resulting in overall p53 stabilization (Meulmeester et al., 2005; Ronai, 2006)

It is known that Usp7 is targeted at least by the three viral proteins HSV-1 ICP0, EBV EBNA1 and KSHV vIRF4 (a fourth viral protein, HCMV UL35, was recently found to interact with Usp7). Of those viruses, HSV-1 infection strongly relies on Usp7. A lack of Usp7's function and/or disturbed binding of ICP0 towards Usp7 results in destabilized ICP0, lower virus gene expression and subsequently reduced virus yield (Everett et al., 1997;

Canning et al., 2004; Boutell et al., 2005). Equally detailed studies were performed with the EBV protein EBNA1 and its relationship towards Usp7. Apart from binding to Usp7, EBNA1 facilitates recruitment of Usp7 to PML nuclear bodies, a prerequisite for disruption of these nuclear protein complexes, thereby, for example, promoting the development of nasopharyngeal carcinoma (Sivachandran et al., 2008; Sarkari et al., 2011). The third viral protein KSHV vIRF4 was recently shown to inherit peptide fragments which block the catalytic activity of Usp7 in order to suppress antiviral p53 functions (Lee et al., 2011). Overall, Usp7's deubiquitinating functions seem to play key roles during herpesviral infection with strong indication for cancer-related processes.

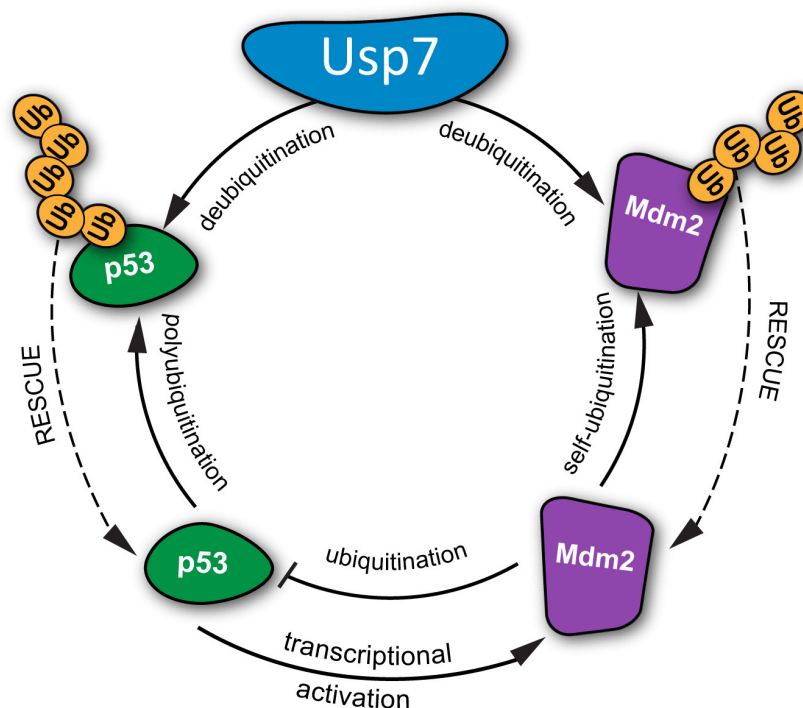


FIG 7 Usp7 at the center of p53 and Mdm2 regulation. Depending on the situation, Usp7 can deubiquitinate Mdm2 or p53. This activity can rescue both proteins from proteasomal degradation (modified from Cheon and Baek, 2006).

In general regard to tumor formation, it is noteworthy that Usp7 is involved in the negative regulation of PTEN (phosphatase and tensin homologue) and FOXO4. Both proteins are tumor suppressors acting in the nucleus upon monoubiquitination. Usp7 functions in removing the ubiquitin moieties and thereby promoting the nuclear exclusion/inactivation of the respective proteins. In this sense, it is believed that Usp7 inhibition would lead to nuclear accumulation of PTEN and/or FOXO4 resulting in antitumoral activities and apoptosis in cancer cells (Nicholson and Suresh Kumar, 2011).

### 1.3.1 Structure and function of Usp7

Usp7 has a molecular weight of approximately 135 kDa (1102 aa, 3309 bp). It has also been reported to be present in cells in a dimerized polyubiquitinated and polyneddylated form (Lee et al., 2005). Usp7 can be divided into three domains: N-terminal domain, protease core and C-terminal domain containing five ubiquitin-like domains (Ubl). The N-terminal domain of Usp7 shows sequence homology to the tumor necrosis factor (TNF) receptor associated factors (TRAFs) and was also shown to bind to several TNF proteins (Zapata et al., 2001) and is therefore also called TRAF-like domain. The N-terminal region has also been reported to be responsible for nuclear localization (Fernández-Montalván et al., 2007). By sequence analysis the protease domain was identified to have conserved Cys and His boxes and based on the crystal structure of the protease core a papain-like catalytic triad consisting of C223, H464 and D481 was identified (Hu et al., 2002). The C-terminal domain functions like the N-terminal domain as a platform for protein-protein interaction. Moreover, the C-terminal domain acts in activating mode of the catalytic domain and can raise activity by a 100-fold (Faesen et al., 2011).

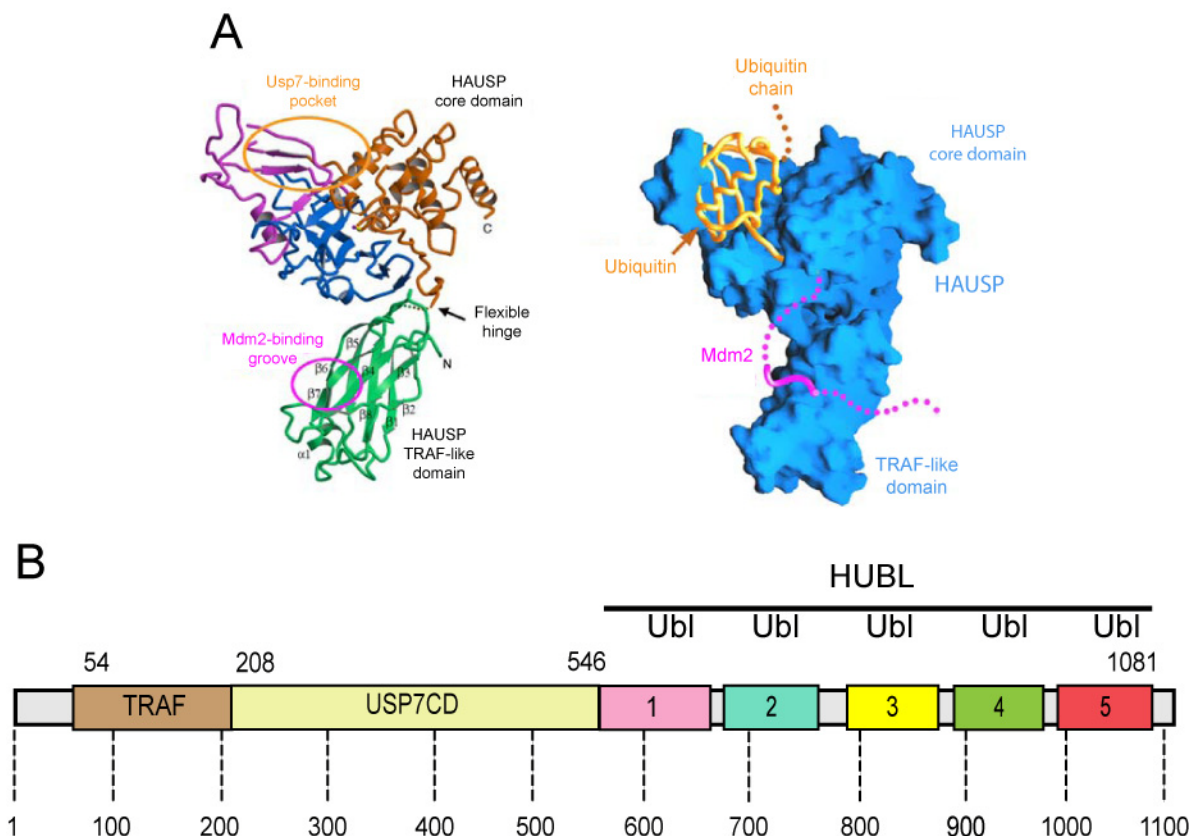


FIG 8 Functionally important domains of Usp7. (A) Substrate binding domains are highlighted (from Hu et al., 2006). (B) Usp7 is divided into several domains: TRAF substrate binding domain (brown), a catalytic domain (yellow), and five Ubl domains (ubiquitin-like; 1-5) forming the C-terminal HUBL domain (from Faesen et al., 2011).

## 2 Materials

### 2.1 Cell lines

#### 2.1.1 Prokaryotic cell lines

Bacterial strain	Specifications
<i>E. coli</i> DH5 $\alpha$	<i>supE44</i> , $\Delta$ <i>lacU169</i> , ( $\Delta$ 80 <i>dlacZ</i> $\Delta$ M15), <i>hsdR17</i> , <i>recA1</i> , <i>endA1</i> , <i>gyrA96</i> , <i>thi-1</i> , <i>relA1</i> (Hanahan, 1983)
<i>E. coli</i> XL2-Blue	<i>recA1</i> , <i>endA1</i> , <i>gyrA96</i> , <i>thi-1</i> , <i>hsdR17</i> , <i>supE44</i> , <i>relA1</i> , <i>lac</i> , (F' <i>proAB</i> , <i>lacI</i> <sup>q</sup> Z $\Delta$ M15, <i>Tn10</i> (Tet <sup>r</sup> ), <i>Amy</i> , <i>Cam</i> <sup>r</sup> ) (Bullock et al., 1987)
<i>E. coli</i> <sup>®</sup> TOPP <sup>™</sup> 3	<i>rif</i> <sup>r</sup> (F' <i>proAB lacI</i> <sup>q</sup> Z $\Delta$ M15, <i>Tn10</i> (Tet <sup>r</sup> )) <i>kan</i> <sup>r</sup>
<i>E. coli</i> <sup>®</sup> TOPP <sup>™</sup> 6-GST-E1B55(348-496)	<i>rif</i> <sup>r</sup> (F' <i>proAB lacI</i> <sup>q</sup> Z $\Delta$ M15, <i>Tn10</i> (Tet <sup>r</sup> ))
<i>E. coli</i> <sup>®</sup> TOPP <sup>™</sup> 6-GST-E1B55 (348-496;S490A, S491A, T495A)	<i>rif</i> <sup>r</sup> (F' <i>proAB lacI</i> <sup>q</sup> Z $\Delta$ M15, <i>Tn10</i> (Tet <sup>r</sup> ))

#### 2.1.2 Eukaryotic cell lines

Cell line	Specifications
2E2	HEK-293 derived inducible helper cell line expressing the E2 gene products and E4orf6 under control of a tetracycline-dependent promoter (Catalucci et al., 2005).
A549	Human lung carcinoma cell line expressing wild-type p53 (Giard et al., 1973).
Brk1	Spontaneously immortalized BRK-cells (stock of group).
H1299	Human lung carcinoma cell line, p53 negative (Mitsudomi et al., 1992).
HC2	H1299-derived empty shRNA vector expressing monoclonal cell line. This work.
HEK-293	HAdV5-transformed, human embryonic kidney cell line; the E1 region is integrated into the genome and the adenoviral E1A and E1B gene products are stably expressed (Graham et al., 1977). Helper cell line.
HEK-293T	HEK-293 derived cell line expressing the SV40 large TAg (DuBridgde et al., 1987).
hMSC	Human bone marrow-derived stromal mesenchymal stem cells (hMSCs) (Lange et al., 2005).
HU5	H1299-derived shUsp7 expressing monoclonal cell line. This work.
pBrk	Primary baby rat kidney cells prepared from 3-5 days old CD rats (Charles River, Kiblegg).

## 2.2 Adenoviruses

Adenovirus	Specifications
H5pg4100	Wild-type HAdV5 carrying a 1863 bp deletion (nt 28602-30465) in the E3 reading frame (Kindsmüller et al., 2007).
H5pm4149	HAdV5 E1B-55K null mutant carrying three amino acid exchanges in the CK2 consensus (S490/91A, T495A).
H5pm4174	HAdV5 E1B-55K mutant carrying four stop codons at the aa positions 3, 8, 86 and 88 of the E1B-55K sequence (Kindsmüller et al., 2009).
H5pm4230	HAdV5 mutant in the H5pm4149 background plus #1763 plasmid background results in $\Delta$ E1B-55K $\Delta$ E4orf3. This work.

## 2.3 Nucleic Acids

### 2.3.1 Oligonucleotides

#	Name	Sequence	Purpose
2156	XhoI-55K-fwd	5'-CTC AGA TCT CGA GCT ATG GAG CGA AGA AAC CC-3'	cloning
2157	55K-EcRI-rv	5'-CAG AAT TCT CAA TCT GTA TCT TCA TCG-3'	cloning
64	E1B bp2043 fwd	5'-CGCGGGATCCATGGAGCGAAGAAACCCATCTGAGC-3'	sequencing
110	E1B361-389rev:24	5'-CGGTGTCTGGTCATTAAGCTAAAA-3'	sequencing
111	E1B804-826 FW:23	GTT TAA CAA TAC CTG TGT GGA AG-	sequencing
112	E1B 1197-1215FW:19	5'-GGG TAA CAG GAG GGG GGT G-3	sequencing
162	T7	5'-TAA TAC GAC TCA CTA TAG GGA GA-3'	sequencing
528	USP7-1320-fwd	5'-TGGGGACAATAAATAC-3'	sequencing
635	pcDNA3 fw	5'-ATGTCGTACAACCTCCGC-3'	sequencing
642	USP7-2000-fwd	5'-CGCTTGCTGAGTTTGT-3'	sequencing
661	USP7-2700-fwd	5'-AATGTTGCTGCAGTTT-3'	sequencing
782	seqE1-Boxfwd2454 bp	5'-CAAGGATAATTGCGCTAATGAGC-3'	sequencing

1020	E1B del Phos.Ad5 fwd	5'-CGCGCTGAGTTTGGCGCTGCCGATGAAGATGCAGATTGAG GTACTG-3'	mutagenesis
1021	E1B del Phos.Ad5 rev	5'-CAGTACCTCAATCTGCATCTTCATCGGCAGCGCCAAACTC AGCGCG-3'	mutagenesis
1134	USP7-212-fwd-BamHI	5'-CGGGATCCGGCTACGTCCGGCTTAAAG-3'	sequencing
1318	Seq E1B bp978-999 fwd	5'-GGCCTCCGACTGTGGTTGCTTC-3'	sequencing
1447	GAPDH omni fwd	5'-CCTGCACCACCAACTGCTTA-3'	quantification
1448	GAPDH omni rv	5'-GCC ATG CCAGTG AGC TTC CCG-3'	quantification
2228	NheI-Usp7fw	5'-CGCTAGCATG-AACCACCAGCAGCAG-3'	cloning
2229	Usp7-AgeIrv	5'-GACCGGTGCACCTGCTCCGTTATGGATTTTAATG-3'	cloning
2230	2230 XhoI-Usp7fw	5'-CTCAGATCTCGAGCTATGAACCACCAGCAGCAG-3'	cloning
2231	Usp7-SalIrv	5'-CCGTGCGACTGCAGAATTCTCAGTTATGGATTTTAATGGCC TTTTC-3'	cloning
2358	Usp7 Seqrv pos627	5'-GCCGACGTAGCCTGTGTG-3'	sequencing

### 2.3.2 Vectors

#	Name	Characteristics	Reference
101	pGEX4T-1	Bacterial expression vector, GST-tag	PL-Pharmacia
136	pcDNA3	Expression vector for mammalian cells, CMV promoter	Invitrogen
208	pSuper.retro.puro	Expression vector for shRNAs, H1 promoter	OligoEngine
232	LeGO-iVLN2	Lentiviral expression vector containing a neomycine resistance as well as an IRES triggered ORF for Venus.	(Weber et al., 2008)
234	LeGO-iBLB2	Lentiviral expression vector containing a neomycine resistance as well as an IRES triggered ORF for BFP.	(Weber et al., 2008)
1153	pPG-S2	E1-region subcloning vector	stock of the group

x	pECFP-C1	Expression vector for CFP fusion proteins	(Banning et al., 2010)
x	pEYFP-C1	Expression vector for YFP fusion proteins	(Banning et al., 2010)

### 2.3.3 Recombinant plasmids

#	Name	Vector	Insert	Reference
x	pECFP-YFP	pECFP-C1	YFP	Banning et al., 2010
608	E1B pXC15	pXC15	HAdV5 E1 region	Stock of the group
737	pE1A	pML	HAdV5 E1A	Stock of the group
1319	pcDNA-E1B-55K	pcDNA3	HAdV5 E1B-55K	Stock of the group
1366	pGEX-APRIL	pGEX-5X2	human APRIL	(Brennan et al., 2000)
1520	pGEX-156R	pGEX-2T	HAdV5 E1B-156R	stock of the group
1521	pcDNA3-E1B S490/91/A T495A	pcDNA3	HAdV5 E1B-55K	Stock of the group
1642	pSuper-shRNA-Usp7	pSuper. retro.puro	shUsp7	Stock of the group
1696	Ad5pPG-S2 E1B 4xstop	pPG-S2	mutated HAdV5 E1-region	stock of the group
1763	E4-Box E4orf3- neu	pPG-S2	mutated HAdV5 E1-region	stock of the group
2024	GST-E1B55(348-496, S490/1A/T495A), DH5 $\alpha$	pGEX-2T	HAdV5 E1B-55K	Stock of the group
2025	GST-E1B55(348-496, S490/1A/T495A)TOPP <sup>TM3</sup>	pGEX-2T	HAdV5 E1B-55K	Stock of the group
2103	LeGo-iVLN2 E1A	LeGO-iVLN2	HAdV5 E1A	Stock of the group
2104	LeGo-iBLB2 E1B-55K	LeGO-iBLB2	HAdV5 E1B-55K	Stock of the group
2452	YFP-E1B-55K	pEYFP-C1	HAdV5 E1B-55K	This work
2467	GST-E1B55(348-496, S490/1A)TOPP <sup>TM3</sup>	pGEX-2T	HAdV5 E1B-55K	Stock of the group
2468	GST-E1B55(348-496, S490/1D)TOPP <sup>TM3</sup>	pGEX-2T	HAdV5 E1B-55K	Stock of the group
2615	Usp7-CFP	pECFP-C1	human Usp7	This work

## 2.4 Antibodies

### 2.4.1 Primary Antibodies

Name	Properties
2A6	Monoclonal mouse antibody raised against Ad5-E1B-55K protein, N-terminal (Sarnow et al., 1982)
3D8	Monoclonal rat antibody raised against Usp7 protein, N-terminal. Stock of the group
B6-8	Monoclonal mouse antibody raised against Ad5-E2A-72K protein (Reich et al., 1983).
$\beta$ -actin (AC-15)	Monoclonal mouse antibody against $\beta$ -actin (Sigma).
DO-1	Monoclonal mouse antibody against p53 (Santa Cruz).
M73	Monoclonal mouse antibody against E1A (Harlow et al., 1985).
6B10	Monoclonal rat antibody raised against HAdV5-L4-100K protein, N-terminal (Kzhyshkowska et al., 2004).
RSA3	Monoclonal mouse antibody raised against the N-terminus of E4orf6 and E4orf6/7 proteins of HAdV5 (Marton et al., 1990).
$\alpha$ -late (L133)	Polyclonal rabbit antiserum raised against HAdV5 late structural proteins (Kindsmuller et al., 2007).
7C11	Monoclonal rat antibody raised against HAdV5-E1B-55K protein, C-terminal (Kindsmuller et al., 2007).
1807	Monoclonal mouse antibody raised against the HAdV5 N-terminal of the E4orf6 E4orf6/7-proteins (Marton et al., 1990).
5E10	Monoclonal mouse antibody raised against the human PML protein (Stuurman et al., 1992).
anti-Mre11	pNB 100-142; Novus Biologicals, Inc, rabbit PAb.
anti-DNA ligase IV	NB110-57379; Novus Biologicals, Inc, rabbit PAb.
anti-CK2 $\alpha$	rabbit PAb anti-CK2 $\alpha$ , ab13410; Abcam.
anti-CK2 $\beta$	Catalog no. 51; Santa Cruz Biotechnology, Inc.
6D5	mouse MAb anti-CK2 $\beta$ , Sigma.
22a	mouse MAb anti-phosphoserine/phosphothreonine, BD Transduction.

### 2.4.2 Secondary Antibodies

Name	Properties
------	------------

HRP-Anti-Mouse IgG	HRP ( <i>horseradish peroxidase</i> )-coupled antibody raised against mouse IgGs in sheep (GE Healthcare or Jackson Immuno Research,INC)
HRP-Anti-Rabbit IgG	HRP ( <i>horseradish peroxidase</i> )-coupled antibody raised against rabbit IgGs in sheep (GE Healthcare or Jackson Immuno Research,INC)
HRP-Anti-Rat IgG	HRP ( <i>horseradish peroxidase</i> )-coupled antibody raised against rat IgGs in sheep (GE Healthcare or Jackson Immuno Research,INC)

### 2.4.3 Fluorophore-coupled secondary antibodies

Name	Properties
Alexa™ 488 Anti-Mouse IgG	Alexa™ 488 antibody raised against mouse IgGs in goat (H + L; F(ab') <sub>2</sub> Fragment; Molecular Probes).
FITC- Anti-Rabbit IgG	Fluorescein-isothiocyanate (FITC)-coupled antibody raised against rabbit IgGs in donkey; (H + L; Dianova) (H + L; Dianova).
FITC-Anti-Mouse IgG	Fluorescein-isothiocyanate (FITC)-coupled antibody raised against mouse IgGs in donkey; (H + L; Dianova) (H + L; Dianova).
FITC-Anti-Rat IgG	Fluorescein-isothiocyanate (FITC)-coupled antibody raised against rat IgGs in donkey; (H + L; Dianova).
<i>Texas Red</i> -Anti-Mouse IgG	<i>Texas Red</i> (TR)-coupled antibody raised against mouse IgGs in donkey; (H + L; Dianova).
<i>Texas Red</i> -Anti-Rabbit IgG	<i>Texas Red</i> (TR)-coupled antibody raised against rabbit IgGs in donkey; (H + L; Dianova).
<i>Texas Red</i> -Anti-Rat IgG	<i>Texas Red</i> (TR)-coupled antibody raised against rat IgGs in donkey; (H + L; Dianova).

## 2.5 Buffers, media and solvents

Description	Composition
0.5×TBE	0.045 M Tris base, 0.045 M sodium borate, 0.005 M EDTA
2xHBS	50 mM HEPES, 1.5 mM Na <sub>2</sub> , 280 mM NaCl, pH 7.12
5xTBE	0.45 M Tris, 0.45 M boric acid, 10 mM EDTA (pH 7.8) with CH <sub>3</sub> COOH
Ampicillin (500x)	50 mg/ml ampicillin, sterile filtered, stored at -20°C
Bacteria freeze Medium	1:1 LB-medium and glycerol (87%), autoclave, stored at 4°C
Coomassie-destaining solution	Methanol 40% (v/v), acetic acid 10% (v/v)
Coomassie-staining	brilliant <i>Blue</i> R-250 1 mg/ml, methanol, 45% (v/v), acetic acid 10% (v/v)
DNA loading dye	0.25% bromphenol blue (w/v), 0.25% xylene cyanol (w/v), 50% glycerol, 2% 50xTAE
FACS buffer	PBS/FCS, 5% (v/v)
Kanamycin (250x)	25 mg/ml kanamycin, sterile filtered, stored at -20°C

Kinase reaction mixture	0.1 mM Na <sub>3</sub> VO <sub>4</sub> , 2 mM DTT, 1 mM Pefabloc SC (AEBSF; Roche), 1 mM phenylmethylsulfonyl fluoride (PMSF), 1.2% aprotinin, 200 μM ATP
Laemmli (5x)	25% Tris-chloride pH 6.8 (v/v), 50% glycerol (v/v), 10% SDS (w/v), 500 mM DTT, 0.5% bromphenol blue (w/v), 1.4% 2-mercaptoethanol (v/v)
LB medium	10 g/l tryptone, 5 g/l yeast extract, 10 g/l NaCl, pH 7 with NaOH, autoclave
NP-40	50 mM Tris-chloride (pH 8.0), 150 mM NaCl, 1% NP-40, 1 mM PMSF, 2 mM dithiothreitol (DTT)
PBS	140 mM NaCl, 3 mM KCl, 4 mM Na <sub>2</sub> HPO <sub>4</sub> *7H <sub>2</sub> O, pH 7.4
PBS Tween	200 mM PBS, 0.1% Tween-20 (v/v)
PEI	dissolved in ddH <sub>2</sub> O to a concentration of 1 mg/ml, pH 7.2 with HCl, sterile filtered and stored at -80°C; working stock at 4°C for 1 month
Proteinase K solution	2% <i>N</i> -lauroylsarcosine (Sigma-Aldrich), 0.4 M EDTA (pH 8.0), and 2 mg of proteinase K (Sigma-Aldrich)/ml
RIPA	50 mM Tris-chloride (pH 8.0), 150 mM NaCl, 5 mM EDTA, 1% Nonidet-40 (v/v), 0.1% SDS (w/v), 0.5% sodium deoxycholate (w/v)
RIPA- <i>light</i> (pH 8,0)	Tris-chloride (pH 8,0) 50 mM, NaCl 150 mM, EDTA 5 mM, NP40 1% (v/v), SDS 0,1% (w/v), Triton X-100 0,1% (w/v)
STE buffer	10 mM Tris-chloride (pH 8.0), 150 mM NaCl, 1 mM EDTA
Storage buffer	0.5 M EDTA (pH 8.0)
TBS-BG	20 mM Tris-chloride (pH 7.6), 137 mM NaCl, 3 mM KCl, 1.5 mM MgCl <sub>2</sub> , 0.05% Tween-20, 0.05% sodium azide, 5 mg/ml glycine, 5 mg/ml BSA
TE50 buffer	10 mM Tris-chloride (pH 8.0), 50 mM EDTA
TGS	25 mM Tris, 200 mM glycine, 0.1% SDS (w/v)
Towbin	25 mM Tris-chloride (pH 8.3), 200 mM glycine, 0.05% SDS (w/v), 20% methanol (v/v)
Trypan blue	0.5% trypan blue, 0.85% NaCl

## 2.6 Standards and Markers

Size determination of DNA fragments on agarose gels was based on a 1 kb, 100 bp and low range PFG Marker (0.1-200 kb) DNA ladders (New England Biolabs), whereas the molecular weight of proteins on SDS-polyacrylamid gels was determined by *PageRuler™ Prestained Protein Ladder Plus* (Fermentas).

## 2.7 Animals

Primary baby rat kidney cells (BRK) were obtained from kidneys of 6-day-old Sprague Dawley rats (Charles River, Kisslegg).

## 2.8 Enzymes, reagents and consumables

If not mentioned otherwise, all chemicals and reagents were purchased from AppliChem, Biomol, Hartenstein, Invitrogen, New England Biolabs, Merck, Roche and Sigma. Cell culture materials were obtained from Falcon, Gibco BRL and Pan, other plastic materials and equipment were purchased from Falcon, Sarstedt, Whatman, Nunc, Biorad, Eppendorf GmbH, Brand, Protean, Schleicher and Schuell, Engelbrecht, Biozym, Hellma, VWR, Whatman and Greiner, Proteinkinase.de.

## 2.9 Commercial systems

Name	Company
CellTiter 96 AQueous One Solution Cell Prolifertation Assay	Promega
GeneJET Gel Extraction Kit	Fermentas
Plasmid Purification Mini, Midi und Maxi Kit	Quiagen
Protein Assay	BioRad
SuperSignal West Pico Chemiluminescent Substrate	Thermo Scientific Pierce
QuikChange™ Site-Directed Mutagenesis Kit	Stratagene
Lipofectamine™ 2000	Invitrogen

## 2.10 Software and databases

Digital program	Application	Source
BioEdit	sequence analysis	open source
GraphPad Prism 5.03	data analysis	GraphPad
Illustrator CS4	image processing	Adobe
Photoshop CS4	image processing	Adobe
PubMed/NCBI	literature search	PubMed/NCBI website
NCBI blast	sequence blast	NCBI
CLC Main Workbench 5.0	sequence data processing	CLC bio
Microsoft Office XP 2007	text processing	Microsoft
ImageJ 1.45s	image intensity quantification	open source
Leica Application Suite (also Lite)	image visualization, archive	Leica
Imaris 7.2.3	image visualization, colocalization analyses, quantification	Bitplane
ClustalW	sequence comparison	open source

## 3 Methods

### 3.1 Bacteriological techniques

#### 3.1.1 Cultivation of bacteria

##### Liquid culture:

Bacterial liquid cultures were grown in sterile LB medium supplemented with resistance-corresponding antibiotics (100 µg/ml ampicillin or 50 µg/ml kanamycin [LB agar plates]). Liquid cultures were incubated at 190-220 rpm for 16-30 h at 30°C/37°C in an incubator shaker (New Brunswick). Depending on experimental set-up and necessity, bacteria concentrations were determined by measuring the optical density (OD) at 600 nm wavelength against plain media (*SmartSpec™ Plus*; BioRad). Especially, bacteria containing E1B-55K or fragments of that gene in their plasmid were grown at 30°C.

##### Solid plate cultures:

Using an inoculating loop, bacteria (from liquid culture or glycerol stock) were spread on solid LB medium containing 15 g/l agar with the appropriate antibiotics (100 µg/ml ampicillin; 50 µg/ml kanamycin) and incubated at 30°C/37°C for 16-30 h. Plating of bacteria resulting from a transformation experiment was performed with a sterilized spreader rod. If necessary, solid plate cultures were sealed with *Parafilm* (Pechiney Plastic Packaging) and stored for several weeks at 4°C.

##### Glycerol storage:

To make glycerol stocks, 1 ml bacterial suspension was pelleted (3 min at 8000 rpm; Eppendorf 5417R), resuspended in 1 ml freeze medium and longterm-stored in cryotubes at -80°C.

#### 3.1.2 Transformation of *Escherichia coli* (*E. coli*)

##### Electroporation

5-10 min after thawing of electrocompetent DH5α cells, 1-10 µl of the ligation mixture (section 3.5.7) was added to the cells, cells were mixed gently and incubated on ice for 30 min. Afterwards, the cell-mixture was transferred to a precooled electroporation cuvette (BioRad). Electroporation was carried out in a *Gene Pulser* machine (Bio-Rad; 1,25 kV, 25 µF, 200 Ω). Immediately afterwards, bacterial cells were transferred with 1 ml room-temperature-warm LB medium into a new reaction tube. Depending on the plasmid used for

transformation, the whole mixture was incubated for 1 h at 30°C or 45 min at 37°C. Afterwards, 10 µl, 100 µl and rest of the suspension were spread on solid LB medium containing 15 g/l agar (see above). Next, over night (o/n) incubation at 30°C or 37°C followed.

#### Chemical transformation

The chemically competent cells stored at -80°C, were thawed on ice and then 100 µl of this suspension was transferred directly onto the bottom of a 15 ml round-bottom tube. Next, 1 µl or 100 ng of DNA were added to these cells and incubated 30 minutes on ice. Immediately after the 30 min incubation, the bacteria were heated at 42°C in a preheated water bath for 42 seconds (heat shock) and again incubated on ice for 2 min. Using this method the plasmid DNA can enter through the pores of the bacterial cell membranes that form due to the heat shock.

Directly after the transformation, the bacteria were mixed with 1 ml LB medium, which had been heated in a water bath at 30°C before, and transferred into a 1.5 ml reaction tube. In order to recover and adapt themselves to the new DNA, the cells were incubated at 30°C for 1 h and 30 min at 200 rpm. After the incubation, 10 µl were mixed with 90 µl LB medium (1:10 dilution). 100 µl (1:10) and 200 µl were plated onto LB agar plates. The rest of the suspension was centrifuged at 4000 rpm and 4 min at room temperature (RT). The supernatant was removed so that some residual volume remained. In the remaining supernatant, the cells were resuspended and uniformly distributed on an LB agar plate. Plates were incubated overnight at 30°C or 37°C.

#### **3.1.3 Expression and purification of recombinant fusion proteins**

Expression of GST-fusion proteins in *Escherichia coli* (TOPP3 or TOPP6) was induced for 2 to 4 h by adding IPTG (isopropyl-β-D-thiogalactopyranoside; PEQLAB) to a final concentration of 1 mM. The bacterial cells were centrifuged, and the pellets were washed with STE buffer (10 mM Tris-chloride [pH 8.0], 150 mM NaCl, 1 mM EDTA) and lysed by the addition of 1 mg of lysozyme (15 min on ice; Sigma-Aldrich), followed by the addition of DTT (5 mM) and *N*-lauroylsarcosine (10%; Sigma-Aldrich) and sonication twice with ultrasound (30 pulses, output 40, 0.5 impulse; Branson Sonifier 450). To precipitate insoluble cell parts, the lysate was centrifuged, and the supernatant transferred to a new 15-ml Falcon tube. Triton X-100 was then added (end concentration 1%), and the supernatant was vortexed and filtered using a 0.45-µm-pore-size filter. The samples were batch purified, and 100 µl of a 50% slurry (0.5 bed volume) of glutathione-Sepharose 4B beads (Amersham Biosciences) in

TBS was added to the filtered lysate supernatant. The mixture was incubated for 1 h at 4°C in an overhead incubator (GFL; Society for Laboratory Technology), and the beads were pelleted and washed six times with TBS. To analyze the protein content, the beads were boiled in Laemmli buffer and analyzed by SDS-PAGE. Proteins were visualized by safe stain (Coomassie) staining (Invitrogen).

### 3.1.4 Kinase assays

For *in vitro* phosphorylation, GST-fusion proteins (~1 µg) were incubated in kinase reaction mixture (0.1 mM Na<sub>3</sub>VO<sub>4</sub>, 2 mM DTT, 1 mM Pefabloc SC [AEBSF; Roche], 1 mM phenylmethylsulfonyl fluoride [PMSF], 1.2% aprotinin, 200 µM ATP) together with recombinant CK2α (170 U) or CK2 holoenzyme (340 U; both from proteinkinase.de) in the presence of [ $\gamma$ -<sup>32</sup>P]ATP (1 µCi). CK2 holoenzyme assays were performed with 340 U of kinase and 2 µg of substrate protein. Samples were incubated at 30°C for 0, 15, 30, or 60 min. *In vitro* phosphorylation was stopped by adding ice-cold TBS supplemented with fresh protease inhibitors (1% [vol/vol] PMSF, 0.1% [vol/vol] aprotinin, 1 µg of leupeptin/ml, and 1 µg of pepstatin/ml) to reaction mixtures. GST fusion proteins were washed three times with ice-cold TBS (as described above), resuspended in Laemmli loading buffer, and boiled at 95°C. The samples were separated via SDS-PAGE and SimplyBlue safe stained according to the manufacturer's instructions (Invitrogen). Phosphorylation signals were detected from dried gels via autoradiography. For inhibitor treatment in this setting, GST fusion proteins were incubated with 20 µM DMAT in a kinase reaction mixture for 30 min at room temperature before adding [ $\gamma$ -<sup>32</sup>P]ATP (1 µCi) to the samples.

## 3.2 Mammalian cell lines

### 3.2.1 Cultivation and passaging

Adhesive cells were cultured with corresponding medium (Gibco DMEM, PAN NCS/FBS, PAA penicillin/streptomycin) in cell culture dishes (Falcon/Sarstedt). Cells were incubated at 37°C and 5% CO<sub>2</sub> saturation (BBD 6220, Heraeus). Cells were passaged when they were subconfluent 1:2 to 1:20. To passage cells, medium was vacuumed off and cells were washed once with 1xPBS and then incubated at 37°C with trypsin/EDTA (PAA) solution until cells detached. To stop trypsin protease activity, 1 vol of culture medium (including serum) was added and then cell suspension was collected in a 15 or 50 ml tube (Falcon) and centrifuged at 2000 rpm for 3 min (Multifuge 3S-R, Thermo). Supernatant was vacuumed off and pellet was resuspended in medium and dispersed on new culture dishes.

### 3.2.2 Preparation of Primary Baby Rat Kidney Cells

To establish a primary BRK cell line, kidneys of 4-6 days old CD rats (Charles River) were extracted under semi-sterile conditions and mechanically shredded by scalpel. The cell mixture was incubated for 3 h at 37°C in PBS solution (1 ml/kidney) containing 0.05 mg/ml collagenase/dispase (Roche). The cells were vigorously shaken every 15-20 min to achieve homogenous dispersion. Next, the cell solution was washed three times in 50 ml of sterile PBS to remove the added enzymes. Afterwards, the cell pellet was resuspended in an appropriate volume and plated on 150 mm culture dishes distributing approximately four kidneys per dish. Due to the limited growth capacity of these primary cells, the culture media was changed every day to remove cell debris and keep the cells viable.

### 3.2.3 Mammalian cell counting

After trypsin incubation, cells were resuspended in growth medium containing FBS or NCS in an appropriate volume depending on the pellet size. 50 µl of this cell suspension was mixed with 50 µl trypan blue in a 1.5 ml reaction tube. The cell number was determined using a *Neubauer* cell counting chamber. The cells from four counting grids were counted within each of the four large squares. Hence, 16 counting grids were counted in total. The total number of cells per ml was determined by multiplying the dilution factor with  $10^4$ .

$$\text{cell number/ml} = \text{counted cells} \times \text{dilution factor} (2) \times 10^4$$

### 3.2.4 Storage of mammalian cells

Subconfluent cells were pelleted as described in 3.2.1. Depending on cell type, pellets were resuspended in FBS or NCS (same serum as in culture medium; PAN) containing 10% DMSO (Sigma). One milliliter of this suspension was transferred into a cryotube (Sarstedt), slowly cooled down with "Mr. Frosty" (Zefa Laborservice) and then stored at -80°C. For recultivation cells were rapidly thawed in a water bath (julabo U3) at 37°C and transferred to cell culture dishes (Falcon) containing prewarmed medium.

### 3.2.5 Mammalian cell harvest

Adherent growing mammalian cells were harvested using cell scrapers. The cells were scraped from the culture dishes and collected in a 15 ml or 50 ml reaction tube and pelleted (3 min, 2000 rpm, RT). After removing the supernatant, the cell pellet was washed once with PBS, again centrifuged and the supernatant removed. Cell pellets can be stored at -20°C for subsequent experimentation (several weeks) or can directly be processed.

### **3.2.6 Transfection of mammalian cells**

#### Transfection with PEI:

For most of the transfection experiments, polyethylenimine (PEI; Polysciences) was used. PEI is a 25 kDa polycationic polymer which builds complexes with DNA based on electrostatic interactions and therefore enables cell membrane penetration of DNA. Cells were seeded approximately 16 h before transfection onto plates. Prior to transfection medium was changed to DMEM (Gibco) including serum but excluding antibiotics. DNA was added to DMEM in tubes, incubated for 5 min and then PEI was usually added in a 1:5 to 1:10 ratio (1 µg DNA plus 5-10 µg PEI). The mixture was incubated for at least 10 min and then dropped onto 50 to 70% confluent cells. 4-8 h later medium was changed to culture medium.

#### Transfection with lipofectamine:

Lipofectamine is especially suitable for transfection of large DNA molecules like the HAdV5 genome. 15-17 h prior transfection, the mammalian cells were seeded with a cell number of  $3.6 \times 10^6$  cells per 60 mm cell culture dish. At the time of transfection cells should be 60-80% confluent. A mixture of DNA and lipofectamine in DMEM (1:1, 10 µl/ml) with a total volume of 1 ml, was incubated for 20 min at RT to allow the formation of complexes.

For the transfection, the old culture medium was removed, cells were washed once with 2 ml DMEM and replaced with 600 µl DMEM without antibiotics and NCS to ensure an optimum pH value for transfection. The mixture of DNA and lipofectamine was added and incubated for 6 h and slued every hour before the transfection medium was replaced by 4 ml DMEM with 10 % NCS supplemented with 8 µl tetracycline (8 µg).

Cells were harvested 24-72 h after transfection as described in section 3.2.5.

#### Generation of Usp7 knockdown cell lines

To establish stable monoclonal knockdown cell lines from H1299 cells, these cells were seeded onto 6-well plates (Falcon), and transfected with pSuper-shUsp7 or pSuper-shRNA vector (control; pSuper.retro.puro) by the PEI method. 2-3 days after transfection, fresh medium containing 3 µg/ml of puromycin (Sigma) was added to the transfected cells. If cells survived, they were transferred to 100 mm dishes (Falcon), and selected for plasmid containing cells with 1 µg/ml puromycin, and if they grew further, they were split 1:30-1:50 and reseeded onto 150 mm (Falcon). When cell foci were observable, several were scratched off with a pipette and transferred to 24-well plates (Falcon). Clones were propagated under puromycin, and then analyzed regarding knockdown using Western blot analyses.

### 3.2.7 Transformation of primary BRK cells

Primary baby rat kidney cells were seeded into 6-well plates or 100 mm dishes (Falcon) 1-2 days prior to transfection in a density of  $1 \times 10^6$  cells per well, so that they were 50-60% confluent on the day of transfection. Cells were transfected with 3  $\mu\text{g}$  DNA and 50  $\mu\text{g}$  PEI (Polysciences). Medium was changed to culture medium 6-8 h post transfection. After 2-3 days, cells were transferred to 150 mm dishes. Medium was changed according to experimental set-up, but at least every 8 days. When transformed cells formed foci, which were observable with the eye (3-4 weeks), cells were fixed and stained with crystal violet and foci were counted.

### 3.2.8 Transformation of hMSCs

hMSC cells were seeded into 12-well plates (Falcon) in a density of  $4 \times 10^4$  cells per well. 12-20 h post seeding, cells were transduced with lentiviral particles containing adenoviral oncogenes (0.3 particles per cell). Prior to transduction, culture medium was replaced by 400  $\mu\text{l}$   $\alpha$ -MEM (Gibco), 10% FBS (PAN), 1% P/S (PAA) and polybrene (1:1000, enhances lentiviral transduction; Sigma). 5-6 h later, medium was replaced by culture medium. After 2-3 days, cells were transferred to 100 mm dishes (Falcon), and transduced cells were selected with antibiotics (G418 200  $\mu\text{g}/\text{ml}$  and blasticidin 50  $\mu\text{g}/\text{ml}$ ; Sigma) in order to decrease cell background. Medium was changed according to experimental set-up, but at least every 8 days. When transformed cells formed foci, which were observable with the eye (3-4 weeks), cells were fixed and stained with crystal violet and cell foci were counted.

### 3.2.9 FACS-experiments

CFP- or YFP-tagged proteins were analyzed by FACS. For this  $7 \times 10^5$  cells were seeded per 6-well plate well (Falcon),  $2 \times 10^6$  for 100 mm dishes (Falcon) and transfected with corresponding plasmid DNA constructs 12-20 h post seeding. For transfection, medium was replaced by 1.5 ml (6-well plates) or 5 ml (100 mm dishes) culture medium without antibiotics and 100  $\mu\text{l}$  (6-well plate) or 500  $\mu\text{l}$  (100 mm dish) of DMEM (Gibco) containing 1-8  $\mu\text{g}$  of DNA and 1:4 or 1:5 PEI (1  $\mu\text{g}/\mu\text{l}$ ; Polysciences). The mixture was incubated for 20 min and then dropped onto cells. Cells were harvested for FACS analyses about 48 h post transfection. For harvest cells were detached as described in 3.2.1 and pellets were resuspended in 400  $\mu\text{l}$  (6 well plate) or 800  $\mu\text{l}$  (100 mm dish) pre-cooled PBS, 1% FBS (PAN), transferred to FACS tubes (BD), kept on ice, and were protected from light. Samples were analyzed via FACS with BD FACS Canto II according to manufacturer's instructions or as described in Banning et al., 2010 or Koppensteiner et al., 2012.

### 3.2.10 Experiments with Usp7 inhibitor HBX

Various experiments were performed with the Usp7 inhibitor HBX (synthesized by Christina Arbelo in Prof. Dr. Chris Meier's group, see Fig. 23A). Usually for all experiments HBX was added 1:2000 resulting in a final DMSO (Sigma) concentration of 0.05%.

### 3.2.11 MTS-based proliferation assay

$1.5 \times 10^3$  cells were seeded per 96-well plate well (Falcon) as described in 3.2.1 and 3.2.3 12-20 h later, culture medium with different compound concentrations (concentration series in triplicates) was added to cells, replacing the old medium. As controls untreated and compound solvent (DMSO) treated cells were used. For all compound and solvent treated cells, the final concentration of DMSO (usually 0.05%) was equal. Cells were incubated for different time points with compound, usually 24, 48 and 72 h and then cell proliferation was measured with the Promega CellTiter 96 AQueous One Solution Cell Proliferation Assay according to manufacturer's instructions. The resulting color reaction was measured with a plate reader (BioTek SynergyMx).

### 3.2.12 Determination of growth behavior

Mainly to investigate whether the Usp7 inhibitor HBX influenced cell growth, growth behavior of cells was determined under each experimental condition. Cells were seeded and treated according to performed experiments. The number of viable and dead cells was determined with trypan blue as described in 3.2.3.

## 3.3 Handling adenoviruses

### 3.3.1 Generating virus from DNA

To generate infectious virus particles out of recombinant bacmid DNA, the bacmid was linearized and released from the bacterial DNA part by *PacI* digestion. This linearized DNA was precipitated with 1/10 vol of 3 M sodium acetate and 1 vol of isopropanol and washed with 75% ethanol. 20  $\mu$ g of the linearized bacmid DNA was used to transfect subconfluent 2E2 cells in a 60 mm cell culture dish as described in 3.2.6. The transfected cells were cultivated until they started to detach from the surface of the culture dish (max. 5 days). Even if they did not detach after 5 days they were harvested as described in section 3.2.5.

The obtained cell pellet was washed with 5 ml PBS and lysed afterwards in 3 ml DMEM by three times freezing in liquid nitrogen and thawing at 37°C in a water bath. By this, virus particles were released into the supernatant and separated from cell debris by centrifugation (4500 rpm, 10 min, RT). This virus-containing supernatant was used to infect previously

seeded 2E2 or 293 cells (100 mm cell culture dish) and 3-5 days later these cells were frozen/thawed to obtain new infectious virus particles as described above.

### **3.3.2 Propagation and storage of high-titer virus stocks**

In order to establish a high titer virus stock, several 150 mm dishes (Falcon) were infected at an MOI of 5-15 FFU/cell with a given virus. After 3-5 days of incubation the medium turned to yellow color, cell morphology changed and cells were harvested and centrifuged at 2000 rpm for 5 min (Multifuge 3 S-R, Thermo). The virus-containing cell pellet was washed once with PBS and resuspended in DMEM (Gibco). After releasing the viral particles from the cells by 3x freezing in liquid nitrogen and thawing in the water bath (julabo U3) at 37°C, the cells were centrifuged for 15 min at 4500 rpm, virus-containing supernatant was mixed with 87% glycerol (sterile, 10% final concentration; Sigma) for preservation at -80°C.

### **3.3.3 Titration of adenoviruses**

To determine the concentration of virus particles, the amount of fluorescence forming units (FFU) was determined by staining the early adenoviral protein E2A with the antibody B6-8. At first, 15-17 h prior infection  $5 \times 10^5$ - $1 \times 10^6$  cells were seeded per well of a 6-well plate (6-well plates were treated with polylysine before). Next, the medium was removed and replaced with 1 ml of the virus-containing supernatant dilution (serial dilutions:  $1 \times 10^{-1}$ - $1 \times 10^{-5}$ ). 2 h post infection (h p.i.) 1 ml of 10 % DMEM (NCS) was added to the infected cells, which were incubated for another 22 h until the medium was removed and the cells were fixed with 1 ml ice-cold methanol for 15 min at -20°C. After removing the methanol, 6-well plates were dried at RT in the clean bench.

Before cells were stained for the immunofluorescence analyses, they were blocked 30 min with 1 ml TBS-BG. After removing the TBS-BG, the cells were incubated for 1 h at RT in 1 ml of a 1:10 dilution of the antibody B6-8 in TBS-BG. Three washing steps followed with 1 ml TBS-BG for 3 min each. Subsequently, the cells were incubated with 1 ml of the secondary antibody (Alexa<sup>TM</sup> 488 anti-mouse; 1:1000 in TBS-BG) for 1 h at RT in the dark. Afterwards, the secondary antibody was removed and the cells were washed twice for 3 min with TBS-BG and after the last washing step, they were covered with 1 ml TBS-BG. After this step, the cells could be stored at 4°C in the dark for 2-4 days without a loss of signal until FFU counting with the fluorescence microscope. The total infectious particle number of a virus stock was calculated according to the counted infected cell number (E2A-positive) and virus dilutions.

### Infection of mammalian cells with adenoviruses

Mammalian cells were seeded into appropriate dishes 12-20 h before infection, resulting in a confluency of 50-70%. Depending on the size of the dish, virus dilutions, usually with an MOI of 20 FFU/cell, were prepared in different volumes of DMEM (Gibco) and were given onto cells after removal of culture medium. Two h post infection, infection medium was replaced by culture medium. Cells were harvested (3.2.5) at different time points.

### Determination of virus yield

To determine the number of progeny virions, virus solutions were obtained from infected mammalian cells by freeze-thaw as described in 3.3.2, and FFUs were determined as described in 3.3.3.

## **3.4 Handling lentiviruses**

### **3.4.1 Titration of Lentiviral Particles**

Established lentiviruses were used in this study. To determine the exact virus titers,  $5 \times 10^4$  HEK-293T cells were seeded in 24-well dishes and infected with lentivirus after 6-10 h. Cells were infected with either 10  $\mu$ l or 100  $\mu$ l of lentivirus in a total volume of 500  $\mu$ l of standard culture media additionally supplemented with 8  $\mu$ g/ml polybren (Sigma-Aldrich) and the media was replaced after virus absorption 8 h post transduction or overnight. Cells were harvested by trypsination 48 h p.i. (3.2.1), resuspended in a volume of 500  $\mu$ l and stored on ice until subsequent analysis in a *FACS CantoII* (BD Biosciences). Since all of the LeGO constructs express different fluorescent markers via an IRES sequence, infected cells were determined by fluorescence against a mock-infected control. To ensure precise titer determination, all titrations were performed at least in duplicate with two different concentrations and calculated according to the formula shown below. Finally, the mean value of all settings was calculated and used in the respective experiments.

$$T = N \times P/100 \times V$$

T: titer [particles/ $\mu$ l]

N: seeded HEK-293T cells [number of cells]

P: fluorescence positive cells [%]

V: used virus supernatant [ $\mu$ l]

### **3.5 DNA techniques**

#### **3.5.1 Isolation of plasmid DNA from *E. coli***

The isolation of larger quantities of plasmid DNA from *E. coli* for the transfection and sequence analyses was performed with Qiagen Plasmid Midi und Maxi Kits according to manufacturer's protocol.

#### **3.5.2 Determination of DNA concentrations**

DNA concentrations were measured with the NanoDrop 1000 spectrometer according to manufacturer's instructions.

#### **3.5.3 DNA agarose gel electrophoresis**

An agarose gel was produced by boiling an appropriate amount of agarose in a microwave in 1xTBE buffer till it was solved completely. For the later staining of the DNA, 5 µg/µl ethidium bromide stock solution was added. At about 60°C the liquid agarose gel was poured into a flat base gel apparatus where the solution cooled down. 1/6 vol DNA loading dye was added to each DNA sample. The mixture was then loaded onto a solidified gel. Separation of DNA fragments was carried out at a voltage of 5 to 10 V/cm. Analytical gels were visualized using the G:box of Syngene at a wavelength of 312 nm and documented with the optical camera system. The DNA on preparative gels was detected by using long wave UV light (365 nm) on a UV table to avoid DNA damage. Additionally, the agarose gel solution as well as the running buffer was supplemented with guanosine (final concentration 1 mM) and MgCl<sub>2</sub> (final concentration 1 mM). DNA bands of interest, visualized on a UV table, were cut out and collected in 1.5 ml reaction tubes for further processing.

#### **3.5.4 Isolation of DNA fragments from agarose gels**

The probability of strand breaks by using anionic exchanger is higher if DNA fragments are larger than 10 kb. So, for the isolation of large bacmid DNA, a more gentle method was chosen. Hereby, the DNA band of interest was cut out of a preparative agarose gel, centrifuged for 1.5 h at 4°C and 20000 rpm. The DNA containing supernatant was precipitated with 1/10 vol 3 M sodium acetate and 1 vol isopropanol. Depending on the size of the DNA pellet, the volume of Tris-chloride pH 8.0 in which the DNA was dissolved, varied between 20 µl and 40 µl. The concentration and the quality of the DNA solution were detected with the NanoDrop spectrometer as described in 3.5.2.

### 3.5.5 Polymerase chain reaction (PCR)

#### Standard PCR Protocol

For standard amplification of a DNA template, a 50  $\mu$ l reaction mixture was prepared by mixing 25-50 ng of DNA template, 125 ng of forward primer, 125 ng of reverse primer, 1  $\mu$ l of dNTP mixture (dATP, dTTP, dCTP, dGTP; each 1 mM), 5  $\mu$ l of 10xPCR reaction buffer and 5 U of *Taq*-polymerase (Roche) in a 0.2 ml PCR reaction tube. The thermocycler (*Flexcycler*; Analytic Jena) was programmed as follows:

	2 min	95°C	preheating
20-30x	0.5-1 min	95°C	DNA denaturation
	0.5-1 min	55-70°C	primer annealing
	1 min/kbp	72°C	extension
	10 min	72°C	final extension
	forever	4°C	storage

To determine PCR efficiency 5  $\mu$ l of PCR reaction was analyzed by gel electrophoresis (3.5.3).

#### Site-Directed mutagenesis by PCR

The *in vitro* point mutagenesis in recombinant plasmids was performed using the instructions of the QuikChange<sup>TM</sup> Site-Directed Mutagenesis Kit. The *Pfu* turbo DNA polymerase was used for the amplification steps. PCR reactions were performed in 0.2 ml PCR tubes. Two complementary oligonucleotides containing the desired mutations were used to generate the mutated amplicon. Following cycle sequence was used:

	2 min	95°C	preheating
25x	30 s	95°C	DNA denaturation
	1 min	60°C	primer annealing
	7 min	68°C	extension
	10 min	68°C	final extension
	forever	4°C	storage

Amplified DNA products were then investigated by agarose gel electrophoresis to confirm if the PCR was successful. In the next step, the non-mutated template DNA was digested using the *DpnI* restriction enzyme. *DpnI* recognizes only methylated DNA, since *in vitro* produced

DNA is not methylated, only the “wild-type”-template is being digested. 50 µl of the PCR product and 1 µl of *DpnI* were mixed, and the reaction took place at 37 °C for at least 2 hours of incubation. Resulting mutant plasmids were then transferred into bacteria (DH5α or XL2-Blue cells) by heat shock transformation (3.1.2).

### **3.5.6 Cloning of DNA fragments**

#### Enzymatic restriction of DNA

Restriction endonucleases were purchased from New England Biolabs (NEB) and Roche and used together with the associated 10x buffers as specified by the manufacturer. If necessary, DNA was precipitated using 1/10 vol 3 M sodium acetate, 1 vol isopropanol and re-dissolved in sterile water. For analytical digestions, usually 0.5-1 µg of the DNA were used as well as 3-10 U restriction enzymes and, if not otherwise indicated, incubated for 1 h at 37°C. Preparative restriction cleavages contained 5-20 µg DNA and 50 U enzymes and were incubated for at least 2 h at 37°C. When necessary, the restricted fragments were separated by agarose gel electrophoresis (see 3.5.3) and isolated by gel extraction (see 3.5.4).

#### Ligation and transformation

After restriction digestions, linearized vectors were dephosphorylated with 1 U of alkaline phosphatase (New England Biolabs) for 30 min at 37°C in order to prevent religation of the vector. Incubation at 65°C for 20 min heat-inactivates the phosphatase. DNA fragments were purified by isopropanol precipitation as explained above. A standard ligation mixture was prepared with 20-100 ng of vector DNA and the 3-5 fold amount of insert DNA, 2 µl of 10x ligation buffer and 1 U of T4-DNA ligase (New England Biolabs). The mixture was incubated at 13°C o/n, 22°C 1 h and 37°C, 30 min before it was transformed into *E. coli* (3.1.2).

#### Identification of recombinant clones

Starting with transformed *E. coli* cells growing on LB agar plates with the appropriate antibiotics, single colonies were picked with a sterile pipette tip to inoculate LB medium with appropriate antibiotic. These cultures were incubated overnight at 30°C or 37°C and 220 rpm. Plasmid DNA was prepared as described in 3.5.1 and dissolved in 25 µl sterile water. 1 µl of each culture was analyzed by the cleavage with suitable restriction enzymes (3.5.6) and a subsequent agarose gel electrophoresis analysis. The resulting recombinant clones were identified and verified by DNA sequencing (Seqlab) and stored as a glycerine culture (3.1.1).

### DNA-sequencing

For DNA sequencing 0.5-1.0 µg of DNA and 20 pmol of sequencing primer were mixed with ddH<sub>2</sub>O to reach a total volume of 7 µl. Sequencing reactions were performed by Seqlab (Göttingen).

### **3.5.7 Analysis of viral DNA synthesis**

Adenoviral DNA replication was determined by PCR. At the indicated time points, infected cells were harvested and lysed in ice-cold lysis buffer containing protease inhibitors as described above. Then, 5-µg portions of total protein lysates were treated with 5 µg of proteinase K (Sigma) and Tween 20 (0.5%; Applichem). Next, 18 cycles of PCR (30 s at 95°C, 1 min at 55°C, and 2 min at 72°C) were performed with 24.5-µl portions of the lysates and 1.25 U of Dream*Taq* polymerase (Fermentas) in a 50-µl reaction volume. Two synthetic oligonucleotides - 64 (5'-CGC GGG ATC CAT GGA GCG AAG AAA CCC ATC TGA GC-3') and 110 (5'-CGG TGT CTG GTC ATT AAG CTA AAA-3') - were used to amplify a specific 399-bp DNA fragment from the E1B gene. As an internal loading control, the primers 1447 (5'- CCTG CAC CAC CAA CTG CTT A-3') and 1448 (5'-GCC ATG CCA GTG AGC TTC CCG-3') were used to amplify specific GAPDH (glyceraldehyde-3-phosphate dehydrogenase) DNA fragments. The reaction products were analyzed on 1% agarose gels containing 0.66 µg of ethidium bromide/ml.

### **3.5.8 Pulsed-field gel electrophoresis**

Samples were prepared as follows. First,  $1.2 \times 10^7$  A549 cells, mock-infected or infected with the indicated viruses, were treated with trypsin at 30 h p.i., and cell pellets were resuspended in 400 µl of PBS. Subsequently, 400 µl of molten low-melting point agarose (LMP agarose [Lonza]) was added. The mixtures were pipetted into mold plugs and incubated for 30 min at 4°C. Solid agarose plugs were incubated in proteinase K solution (2% *N*-lauroylsarcosine [Sigma-Aldrich], 0.4 M EDTA [pH 8.0], and 2 mg of proteinase K [Sigma- Aldrich]/ml) for 24 h at 50°C. After renewing the proteinase K solution, plugs were incubated additional 24 h, rinsed in double-distilled H<sub>2</sub>O several times, and incubated for 24 h in TE50 buffer (10 mM Tris-chloride [pH 8.0], 50mM EDTA) at 4°C. Afterward, the TE50 buffer was renewed, and PMSF was added (0.1 mM), followed by incubation at 4°C for 4 h with TE50/PMSF renewal after 2 h. Plugs were incubated in new TE50 buffer for an additional 24 h and transferred into storage buffer (0.5 M EDTA [pH 8.0]). The DNA in agarose blocks was analyzed by electrophoresis with a Biometra Rotaphor system through 1.5% agarose gel at 150 V with ramped pulse times from 10 to 90 s for 39 h at 15°C in 0.5xTBE (0.045 M Tris base, 0.045 M

sodium borate, 0.005 M EDTA). The gel was stained with ethidium bromide for 30 min at room temperature to visualize viral DNA.

### **3.6 Protein techniques**

#### **3.6.1 Preparation of total cell lysates**

Harvested mammalian cell pellets were resuspended in precooled RIPA buffer (100-600  $\mu$ l) containing protease inhibitors (1:100 PMSF, 1:1000 leupeptin, pepstatin and aprotinin; Sigma) and were incubated for 30 min on ice. Lysates were sonicated (4°C, 30 s, output 0.45-0.6 impulses/s; Branson Sonifier). Then cell debris were removed by centrifugation at 11000 rpm (Eppendorf 5417-R) and 4°C for 5 min and transferred to new 1.5 ml tubes.

#### **3.6.2 Quantitative determination of protein concentrations**

The concentration of soluble proteins in a sample was determined using the Bio-Rad Protein Assay. The assay is based on the protein quantification procedure of Bradford (Bradford, 1976) and measures the absorption at 595 nm using a spectrophotometer. With the help of a BSA-standard curve, unknown protein concentrations are determinable. To 800  $\mu$ l of PBS 200  $\mu$ l Bio-Rad reagent and 1  $\mu$ l of protein sample was added in polystyrene cuvettes, mixed by inversion and incubated for 5 min. The absorbance was measured with a Beckman Coulter DU800 spectrophotometer at 595 nm.

#### **3.6.3 SDS-polyacrylamide gel electrophoresis (SDS-PAGE)**

SDS-PAGE is used for separating proteins electrophoretically according to their molecular weights in the presence of denaturing SDS detergent. 1/5 vol of 5x Laemmli buffer was added and samples were denatured for 12 min at 55°C (thermal block Thermomixer comfort, Eppendorf) and then loaded on the gel. The gels were run (Biometra gel chambers) in TGS buffer with 3-5 mA per 1 cm gel height.

##### stacking gel (5%)

17% acrylamide (30%; Roth)

120 mM Tris-chloride, pH 6.8 (Sigma)

0.1% SDS (w/v; Sigma)

0.1% APS(w/v; Sigma)

0.1% TEMED (v/v; AppliChem)

#### seperating gel (10%)

33% acrylamide (30%; Roth)

250 mM Tris-chloride, pH 6.8 (Sigma)

0.1% SDS (w/v; Sigma)

0.1% APS(w/v; Sigma)

0.4% TEMED (v/v; AppliChem)

#### **3.6.4 Western blot**

Proteins can be detected specifically by Western blot analysis. For Western blots, proteins are immobilized on nitrocellulose membranes. The transfer of proteins from polyacrylamide gels to nitrocellulose membranes (Protran) was done with the help of the Biorad Trans-Blot Electrophoretic Transfer Cell according to manufacturer's instructions in Towbin buffer at 400 mA for 70-110 min, depending on the molecular weight of the protein. For blocking, membranes were incubated with PBS 5% skimmed milk powder (MP;Gluecksklee) for 1 h at room temperature (RT) or 4°C o/n. Then the membranes were washed 1x with PBS and 2x with PBS-Tween and incubated with primary antibodies (diverse dilutions in PBS-Tween with or without 1-4% MP) for 1 h at RT. After another 3 washes with PBS-Tween for 10 min, incubation with secondary antibodies (HRP-coupled, diverse dilutions in PBS-Tween with or without MP) followed for 3 hr at RT or o/n 4°C. For detection of secondary antibodies the Pierce SuperSignal West Pico Chemiluminescent Substrate (ECL-solution) was used, which results in a chemiluminescent reaction with the HRP-coupled antibodies. Before membranes were incubated with ECL-solution according to manufacturer's instructions, membranes were washed twice with PBS-Tween.

#### **3.6.5 Immunoprecipitation**

The principle of immunoprecipitation is based on the binding of a specific antibody to a matrix. This antibody binds specifically to its target protein, so that the isolation of specific proteins or protein complexes from a protein mixture becomes possible. The coupling of IgG antibodies from mice and rabbits was carried out to protein A-sepharose. Protein A binds to the Fc-region of any IgG antibody thus antibodies coupled to the matrix can isolate their corresponding antigen in an insoluble complex due to their high molecular weight by centrifugation. Bound proteins can be dissolved by denaturing the precipitate for 5 minutes at 95°C in an appropriate sample buffer, and can then be detected by Western blot analysis (3.6.4). The detection of proteins that are not directly recognized by the antibody, but which

bind to the detected protein, is called coimmunoprecipitation. In this way, it is possible to investigate protein-protein interaction.

**Procedure:** For each sample 2 mg lyophilized protein A-sepharose were rehydrated with 30  $\mu$ l RIPA-light buffer for 1 h rotating at 4°C. 500 ng-1  $\mu$ g antibodies per sample were added to the rehydrated protein A-sepharose and incubated for at least 1 h rotating at 4°C (antibody coupling). 500-600  $\mu$ g whole cell protein lysates were precleared with 50  $\mu$ l Pansorbin for at least 1 h rotating at 4°C. Afterwards, precleared lysates and sepharose-antibody-suspension were centrifuged at 6000 rpm for 5 min at 4°C. Supernatant from the protein preclearing was transferred into new 1.5 ml reaction tubes. Matrix-bound antibodies were subjected to another washing step with 500  $\mu$ l precooled RIPA-light, NP-40 or RIPA buffer containing protease inhibitors. After this, the sepharose-antibody pellet was resuspended in an appropriate volume depending on the number of samples. Then, 100  $\mu$ l of this suspension (2 mg protein A-sepharose coupled with 500 ng-1  $\mu$ g antibodies) were added to the precleared protein lysates, following over night rotation at 4°C.

After this precipitation step, the suspension was centrifuged (6000 rpm, 5 min, 4°C), washed three times with 500  $\mu$ l cooled lysis buffer and centrifuged (6000 rpm, 5 min, 4°C). Afterwards, 15  $\mu$ l 2x Laemmli buffer was added to each sample, boiled for 5 min at 95°C and then centrifuged 5 min at 13000 rpm. Later on, the samples were separated on SDS-polyacrylamide gel and analysed (3.6.3 and 3.6.4).

For CK2 $\beta$  immunoprecipitation studies, 0.8  $\mu$ g of anti-CK2 $\beta$  antibody (mouse MAb 51; Santa Cruz Biotechnology, Inc.) was added to 800-1,100  $\mu$ g of Pansorbin (Calbiochem)-precleared protein lysates and incubated overnight at 4°C. On the next day, 2-3 mg of protein A-Sepharose was added, followed by incubation for 2 h (while rotating). The immune complexes were washed three times, eluted from the Sepharose beads using 0.1 M triethylamine (pH 11.5), separated by SDS-PAGE, and analyzed by immunoblotting.

For inhibitor treatment, DMAT (2-dimethylamino-4,5,6,7-tetrabromo-1*H*-benzimidazole; Calbiochem) or TBB (4,5,6,7-tetrabromobenzotriazole; Sigma-RBI) was added to the cell culture at 4 h p.i. to a final concentration of 2.5 or 12.5  $\mu$ M, respectively.

### 3.6.6 Immunofluorescence

#### Methanol fixation

Adherent cells were cultured on coverslips in cell culture dishes (six-well plate) as described in 3.2.1 and infected the following day. To fix the cells, the medium was aspirated off and the coverslips were incubated for 15 min in ice-cold methanol at -20°C. Next, the fixed cells were

dried at RT and stored at -20°C or used immediately for the *in situ* staining and subsequent immunofluorescence.

#### Immunofluorescence staining

For immunofluorescence visualization, the coverslips were incubated 1 h in TBS-BG to saturate non-specific binding sites. After the buffer was removed, the slides were washed with TBS- Tween (0.05%) and once with TBS. Later on, the coverslips were incubated for 1 h at RT in 50 µl primary antibody solution in an appropriate dilution with TBS. In the next step, the coverslips were washed twice with TBS-Tween (0.05%), once with TBS, washing solution was removed and the cover slips incubated with the secondary fluorescent antibodies (1:100 dilution in TBS) in the dark for 1 h. For staining the DNA-chromatin-complex, 0.5 µg/ml DAPI (4', 6-Diamidin-2'-Phenylindol dihydrochlorid) was added. Unbound secondary antibodies were removed by three successive washing steps with TBS-Tween (0.05%). The coverslips were then dripped off slightly and fixed with Glow mounting medium (20 µl) placed with the cell layer face down onto a glass slide. The slides could be stored at 4°C for several days to a few weeks in the dark. Further analyses were performed with the help of an immunofluorescence microscope (Leica) and its supplied digital imaging processing system, Leica Application Suite Advanced Fluorescence.

# **Part I**

## **4 An investigation conducted to explore the role of CK2 for adenoviral infection – The connection between E1B-55K and CK2**

The first part describes a novel interaction partner of the HAdV5 E1B-55K protein, namely CK2. Apart from phosphorylating E1B-55K, CK2 seems to be an important cellular factor regulating a significant part of E1B-55K's interactome which has many significant implications for the adenovirus life cycle.

Protein functions, localization and stability are commonly controlled by different mechanisms like protein-protein interaction, protein structure and several posttranslational modifications. The most prevalent posttranslational modification is protein phosphorylation which is, in simple terms, the addition of phosphate to serine, threonine or tyrosine residues. The simple addition of a single phosphate can have profound effects on the structure of a protein, the propensity toward interaction partners and thus protein function in general. However, not only cellular proteins rely on phosphorylation as a regulation mechanism, also viral proteins evolved to use and abuse the cellular machinery of protein phosphorylation to boost their own functions and therefore viral replication.

### **4.1 E1B-55K is phosphorylated at highly conserved residues at the C terminus, which has similarity to the CK2 consensus phosphorylation motif**

Previous studies by Branton and coworkers have shown that the HAdV5 E1B-55K protein is phosphorylated at serine and threonine residues near the C terminus (S490/491, T495) within sequences characteristic of CK2 substrates (Fig. 9A, B and C) (Teodoro et al., 1994; Teodoro and Branton, 1997). Additionally, comparative ClustalW analyses of all known E1B-55K amino acid sequences are depicted to show the high conservation of the CK2 consensus sequence (Fig. 9B). To investigate the role of this cellular protein kinase in phosphorylating the adenoviral protein, the mutant virus H5pm4174 (E1B-P minus) was generated. This mutant contains three alanine substitutions at positions 490, 491 and 495 within the 496-amino-acid residue E1B-55K polypeptide (Fig. 9C). To test whether the amino acid changes abolish phosphorylation of E1B-55K, combined immunoprecipitation-immunoblotting assays were performed using total cell lysates from wt and mutant virus-infected A549 cells (Fig. 9D). As expected, wt E1B-55K (phospho-E1B-55K) was precipitated with an antibody

reactive for phosphoserine and phosphothreonine residues from H5pg4100 wt-infected cells (Fig. 9D, lane 4). In contrast, no E1B-55K protein was detected in the same immunoblots from cells infected with E1B mutants H5pm4149 lacking E1B-55K or H5pm4174 lacking the phosphorylation sites (S490/491A, T495A, and E1B-P minus; Fig. 9D, lanes 2 and 3).

A

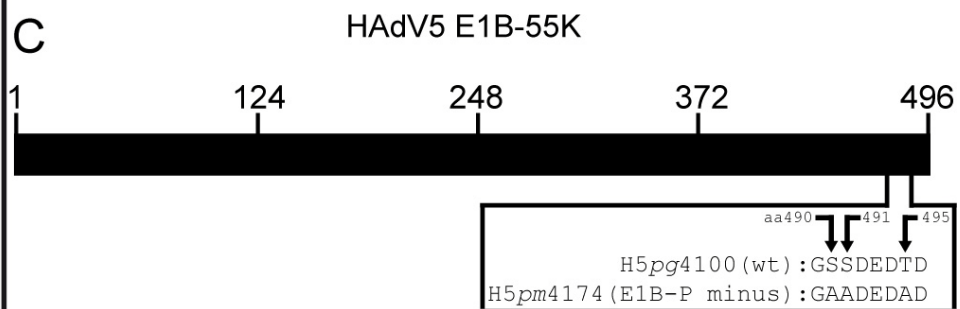
S/T-x-x-E/D

B

HAdV1	<b>GSS</b> <b>DE</b> DTD-
HAdV2	<b>GSS</b> <b>DE</b> DTD-
HAdV3	<b>GSS</b> <b>GE</b> ETD-
HAdV4	<b>GSS</b> <b>GE</b> ESD-
<b>HAdV5</b>	<b>GSS</b> <b>DE</b> DTD-
HAdV6	<b>GSS</b> <b>DE</b> DTD
HAdV7	<b>GSS</b> <b>GE</b> ETD-
HAdV8	<b>SSS</b> <b>GE</b> DTD-
HAdV9	<b>SSS</b> <b>GE</b> DTD-
HAdV11	<b>GSS</b> <b>GE</b> ETD-
HAdV12	<b>ESS</b> <b>DE</b> ---
HAdV14	<b>GSS</b> <b>GE</b> ETD-
HAdV15	<b>SSS</b> <b>GE</b> DTD-
HAdV16	<b>GSS</b> <b>GE</b> ETD-
HAdV17	<b>SSS</b> <b>GE</b> DTD-
HAdV18	<b>ESS</b> <b>DE</b> DGN-
HAdV19	<b>SSS</b> <b>GE</b> DTD-
HAdV21	<b>GSS</b> <b>GE</b> ETD-
HAdV22	<b>SSS</b> <b>GE</b> DTD-
HAdV28	<b>SSS</b> <b>GE</b> DTD-
HAdV29	<b>SSS</b> <b>GE</b> DTD-
HAdV31	<b>ESS</b> <b>DE</b> DN--
HAdV34	<b>GSS</b> <b>GE</b> ETD-
HAdV35	<b>GSS</b> <b>GE</b> ETD-
HAdV36	<b>SSS</b> <b>GE</b> DTD-
HAdV37	<b>SSS</b> <b>GE</b> DTD-
HAdV40	<b>ESS</b> <b>DE</b> ---
HAdV41	<b>ESS</b> <b>DE</b> ---
HAdV46	<b>SSS</b> <b>GE</b> DTD-
HAdV50	<b>GSS</b> <b>GE</b> ETD-
HAdV52	<b>ESS</b> <b>DE</b> ---
HAdV53	<b>SSS</b> <b>GE</b> DTD-
HAdV54	<b>SSS</b> <b>GE</b> DTD-
HAdV55	<b>SSS</b> <b>GE</b> DTD-
HAdV56	<b>SSS</b> <b>GE</b> DTD-
HAdV57	<b>GSS</b> <b>DE</b> DTD-
HAdV58	<b>SSS</b> <b>GE</b> DTD-
HAdV59	<b>SSS</b> <b>GE</b> DTD-
HAdV60	<b>SSS</b> <b>GE</b> DTD-
HAdV62	<b>SSS</b> <b>GE</b> DTD-

~100% conserved

C



D

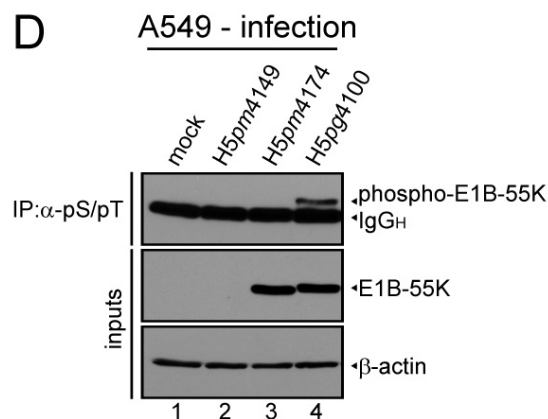


FIG 9 CK2 phosphorylation consensus motif of E1B-55K and E1B-55K phosphorylation. (A) Simplified CK2 consensus motif according to Meggio and Pinna, 2003. A serine or threonine in boldface denotes CK2-targeted amino acids in this motif. (B) Alignment of all currently available E1B-55K C-terminal amino acid sequences. Amino acids highly conserved (grey background) throughout different E1B-55K proteins and known to be phosphorylated in HAdV5 are boxed. Amino acids matching the general CK2 consensus motif are in bold. (C) Schematic representation of E1B-55K showing the amino acid sequence of the C terminus of E1B-55K in H5pg4100 (wt) and the H5pm4174 (E1B-P minus) mutant. (D) A549 cells were mock-infected or infected with H5pm4149 (E1B minus), the E1B-P minus mutant H5pm4174 and H5pg4100 wt virus at an MOI of 20 FFU/cell. Total cell lysates were prepared and subjected to immunoprecipitation using anti-phosphoserine/phosphothreonine (pS/pT) antibody. Proteins were separated by SDS-PAGE and detected by immunoblotting with anti-E1B antibody 2A6. Steady-state concentrations (inputs) of E1B-55K and  $\beta$ -actin were determined by immunoblotting of protein extracts with anti-E1B-55K (2A6) and anti- $\beta$ -actin (AC-15). The Western blot represents one experiment which had been independently repeated at least four times.

## 4.2 CK2 $\alpha$ interacts with E1B-55K

As mentioned above, E1B-55K phosphorylation sites S490 and S491 lie within a protein kinase CK2 phosphorylation consensus sequence, suggesting that this kinase is responsible for E1B-55K phosphorylation (Fig. 9A and B). Therefore, it was tested whether E1B-55K interacts with the cellular protein kinase CK2. For this, the focus was laid on the  $\alpha$  subunit, which confers kinase activity either alone or in complex with the  $\beta$  subunit as a holoenzyme (Niefind et al., 1999; Meggio and Pinna, 2003). In a first attempt to show interaction between E1B-55K and CK2 $\alpha$ , endogenous CK2 $\alpha$  was immunoprecipitated from p53-negative H1299 cells transfected with wt pE1B-55K or mutant pE1B-55K (pE1B-P minus) encoding plasmids (Fig. 10A). By using this approach, it could be excluded that either p53 or another adenoviral protein might mediate an interaction between E1B-55K and CK2 since both proteins are also p53 interaction partners (Meggio and Pinna, 2003; Schwartz et al., 2008). Next, A549 and H1299 cells were infected with H5pm4149 (E1B minus), H5pg4100 (wt), and H5pm4174 (E1B-P minus) viruses (Fig. 10B, C), and immunoprecipitation experiments were performed as described above. Immunoblotting revealed that wt E1B-55K coprecipitated with CK2 $\alpha$  after transfection or infection of either cell line (Fig. 10A, lane 2; Fig. 10B, lane 3; 10C lane 7). In contrast, mutant E1B-55K from E1B-P minus did not coprecipitate in the transient transfection assay and only inefficiently coprecipitated after infection of either cell line (Fig. 10A, lane 3; Fig. 10B, lane 4; 10C lane 8). Of note, initial E1B-P minus virus infections in H1299 cells resulted in considerably lower E1B-55K levels. In order to load the same amounts for the immunoprecipitation reaction, E1B-P minus virus infection was carried out at an MOI of 50 FFU per cell. This phenomenon will be tackled in Part III.

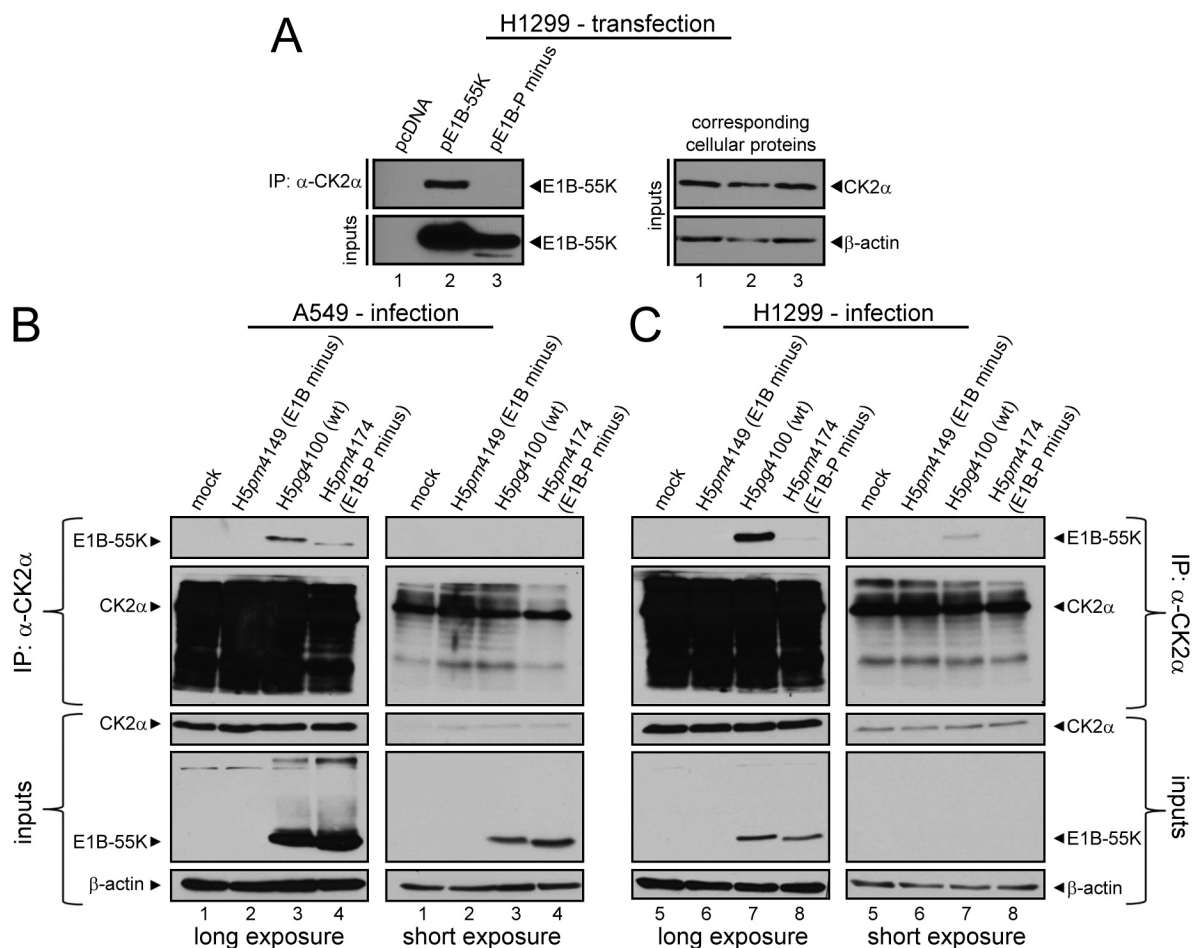


FIG 10 Coimmunoprecipitation to analyze E1B-55K and its interaction with CK2 $\alpha$  in infected cells. (A) CK2 $\alpha$  interaction with E1B-55K after transfection. H1299 cells transfected with empty plasmid vector (pcDNA) and vectors encoding E1B-55K (pE1B-55K) or mutant E1B-55K (pE1B-P minus) were subjected to immunoprecipitation with an anti-CK2 $\alpha$  antibody (ab13410). Proteins separated by SDS-PAGE were detected by Western blots with anti-E1B antibody (2A6). Western blot analyses of protein input levels are shown below for E1B-55K (2A6) and to the right for CK2 $\alpha$  (ab13410) and  $\beta$ -actin (AC-15). (B and C) CK2 $\alpha$  interaction with E1B-55K during infection A549 and H1299 cells either mock-infected or infected (MOI=20 FFU/cell) with H5pm4149 (E1B minus), H5pg4100 (wt), and H5pm4174 (E1B-P minus) virus were analyzed by immunoprecipitation assays using protein A-Sepharose-coupled anti-CK2 $\alpha$  antibody (ab13410). Proteins separated by SDS-PAGE were detected by immunoblotting with anti-E1B (2A6) and anti-CK2 $\alpha$  (ab13410) antibodies. Immunoblot analyses of protein input levels are shown below for CK2 $\alpha$ , E1B-55K (2A6), and  $\beta$ -actin (AC-15).

Taken together, these results clearly demonstrate that wt E1B-55K can interact with CK2 $\alpha$ . Whereas, the E1B-55K mutant from E1B-P minus exhibits significantly reduced or no binding to CK2 $\alpha$  in virus-infected A549 or H1299 cells, respectively (Fig. 10B and C) or in single wt E1B-55K/mutant E1B-55K H1299 transfection experiments (Fig. 10A). This indicates that the phosphorylatable amino acids S490, S491, and T495 contribute significantly to the CK2 $\alpha$  binding site on E1B-55K. Furthermore, the interaction between E1B-55K and CK2 $\alpha$  is apparently independent of p53 and other viral proteins, since both proteins can interact in pE1B-55K plasmid transfected p53-negative H1299 cells (Fig. 10A).

### 4.3 CK2 $\alpha$ is relocalized during adenovirus infection but in an E1B-independent manner

Souquere-Besse et al. previously demonstrated that CK2 $\alpha$  and  $\beta$  subunits are separated and relocalized during adenoviral infection (Souquere-Besse et al., 2002). To investigate the relative localization of CK2 $\alpha$  and E1B-55K in A549 cells, double-label immunofluorescence analyses were performed of cells infected with E1B minus H5 $pm$ 4149, wt H5 $pg$ 4100 or E1B-P minus H5 $pm$ 4174 virus. Similar CK2 $\alpha$  redistribution patterns could be observed in all infection settings. More specifically for wt and E1B-P minus, nearly 53% of wt-infected A549 cells ( $n=168$ ) displayed relocalization of CK2 $\alpha$  into nuclear ring-like structures, which showed specific CK2 $\alpha$ -positive foci at the periphery of these ring-like structures (Fig. 11B, panels I to L). Intriguingly, these ring-like structures form specifically around E1B-55K-positive nuclear regions (Fig. 11B, panels I to L), implicating that the interaction between CK2 $\alpha$  and E1B-55K might take place in these areas of the nucleus. In contrast, the remaining ~47% of cells largely revealed a CK2 $\alpha$ -staining with neither nuclear ring-like structures nor nuclear CK2 $\alpha$  foci (Fig. 11B, panels M to P). Here, CK2 $\alpha$  is found evenly distributed in the nucleus with some aggregates in the cytoplasm or directly at the periphery of the nucleus. Interestingly, a significant number of the cells showing this phenotype (almost 15 %) also displayed colocalization between CK2 $\alpha$  and E1B-55K in cytoplasmic aggregates (Fig. 11B, indicated by yellow arrows, panels M to P). Intriguingly, the relocalization pattern of CK2 $\alpha$  in E1B-P minus H5 $pm$ 4174-infected cells was very similar qualitatively and quantitatively to that displayed during wt infection (Fig. 11B, panels Q to T, 55.2% and U to X, 44.8%). This suggests that CK2 $\alpha$  relocalization is independent of E1B-55K's phosphorylation status or even E1B-55K interaction at all, as indirectly derivable from the coimmunoprecipitation studies (Fig. 10A, B, C) and directly shown by CK2 $\alpha$ -stainings after E1B minus H5 $pm$ 4149 infection (11B, panels A to H).

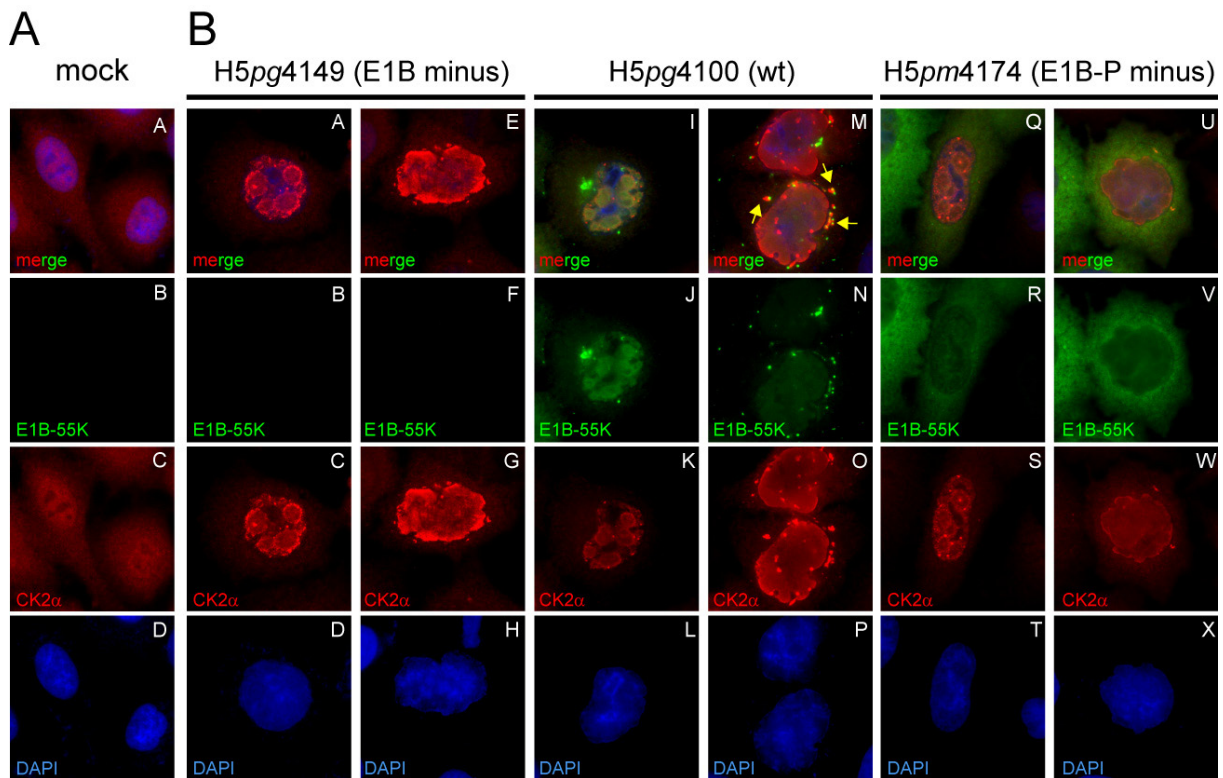


FIG 11 Indirect immunofluorescence to analyze E1B-55K and CK2 $\alpha$  in infected cells. A549 cells either mock-infected or infected with the indicated viruses (MOI=20 FFU/cell) were analyzed by *in situ* immunofluorescence staining for E1B-55K (2A6), CK2 $\alpha$  (ab13410), and DNA content (DAPI). Examples of the two major CK2 $\alpha$  relocalization patterns observed in this cell line are shown ( $n=168$ ).

In summary, data from the immunofluorescence analyses suggest that the location of interaction (if interaction takes place) between CK2 $\alpha$  and E1B-55K occurs mainly at the periphery of infection-induced CK2 $\alpha$ -positive ring-like structures in the nucleus, and to a lesser extent in cytoplasmic accumulations (Fig. 11B). It appears that phosphorylation at these carboxy-terminal sites regulates the subcellular distribution of E1B-55K as the mutant protein exhibits a substantially different localization pattern compared to the wt product (compare Fig. 11B, panels J+N with panels R+V).

#### 4.4 CK2 $\beta$ binds to E1B-55K and is relocalized during adenoviral infection in a phospho E1B-dependent manner

Association of CK2 $\alpha$  with CK2 $\beta$  can result in different functional outcomes. For example, association of the CK2 subunits into a stable holoenzyme reduces the amount of CK2 $\beta$  in the nucleus (Fillhol et al., 2003). Furthermore, substrate specificity can be altered by holoenzyme association (Meggio and Pinna, 2003). Interestingly, the results from infected A549 cells analyzed 24 h p.i. demonstrate that CK2 $\alpha$  is redistributed upon H5pg4100 (wt) and H5pm4174 (E1B-P minus) infection into nuclear areas, as well as cytoplasmic accumulations (Fig. 11B). To test whether CK2 $\beta$  also interacts with E1B-55K and to investigate its relative localization during wt and E1B-P minus virus infection in comparison to E1B-55K and CK2 $\alpha$ ,

coimmunoprecipitation and double-label immunofluorescence analyses were performed in A549 cells. The obtained results clearly show that wt E1B-55K interacts with endogenous CK2 $\beta$  and that this interaction also occurs with the phosphonegative E1B-55K, although this interaction is greatly weakened (Fig. 12A, lanes 3 and 4). Only in very rare cases a specific overlap in the staining of E1B-55K and CK2 $\beta$  accumulations could be detected (not quantifiable). Nevertheless, several different redistribution patterns of CK2 $\beta$  during adenoviral infection were detected, which strongly depend on the phosphorylation status of E1B-55K (Fig. 12B, C, D). In order to categorize those phenotypes, 4 general categories were defined (Fig. 12B and C). During wt infection (H5pg4100), 40.6% of CK2 $\beta$  relocated into small, mainly nuclear accumulations (Fig. 12B, panels E to H; category 1), whereas in the second largest cohort (33%, category 2) CK2 $\beta$  is more evenly distributed and concentrated in the nucleus (compare Fig. 12B, panels A to D and I to L and compare upper and lower cell in panel K; category 2). A total of 16.4% of the wt-infected cells showed a relocation of CK2 $\beta$  into mainly cytoplasmic bodies at the periphery of the nucleus (Fig. 12B, panels M to P, category 3), and 10% displayed no redistribution at all upon H5pg4100 infection (Fig. 12B, panels Q to T, category 4). In contrast, CK2 $\beta$  redistribution during H5pm4174 (E1B-P minus) infection revealed the same phenotypes but with mainly two different quantitative outcomes. Here, only 19.1% showed a CK2 $\beta$  relocation into small, nuclear accumulations (Fig. 12C, panels A to D, category 1). The largest cohort of H5pm4174-infected cells displayed no CK2 $\beta$  redistribution (Fig. 12C, panels M to P, category 4). However, no major differences could be observed between wt and mutant virus-infected cells in the amount of cells showing redistributed CK2 $\beta$  with phenotypes of categories 2 and 3 (compare 12B, panel K [33%] with 12C, panel G [34.1%] and 12B, panel O [16.4%] with 12C, panel K [9.9%]). These data suggest that phosphorylation of E1B-55K is important for proper CK2 $\beta$  relocation, although CK2 $\alpha$  reorganization displayed no major differences between wt and E1B-P minus infection (Fig. 11B). As illustrated in Fig. 12B and 12C, CK2 $\beta$  redistribution does not follow the same pattern as CK2 $\alpha$  relocation (compare with Fig. 11B). Costaining of CK2 $\alpha$  and CK2 $\beta$  in mock-infected, wt (H5pg4100)-infected or E1B-P minus (H5pm4174)-infected A549 cells revealed no significant overlap between both cellular proteins (Fig. 12D). However, infection with wt and E1B-P minus viruses resulted in redistribution of both CK2 subunits into the nucleus (Fig. 12D, panels E to H and I to L), indirectly supporting observations from Souquerre-Besse et al. (Souquerre-Besse et al., 2002) and Filhol et al. (Filhol et al., 2003).

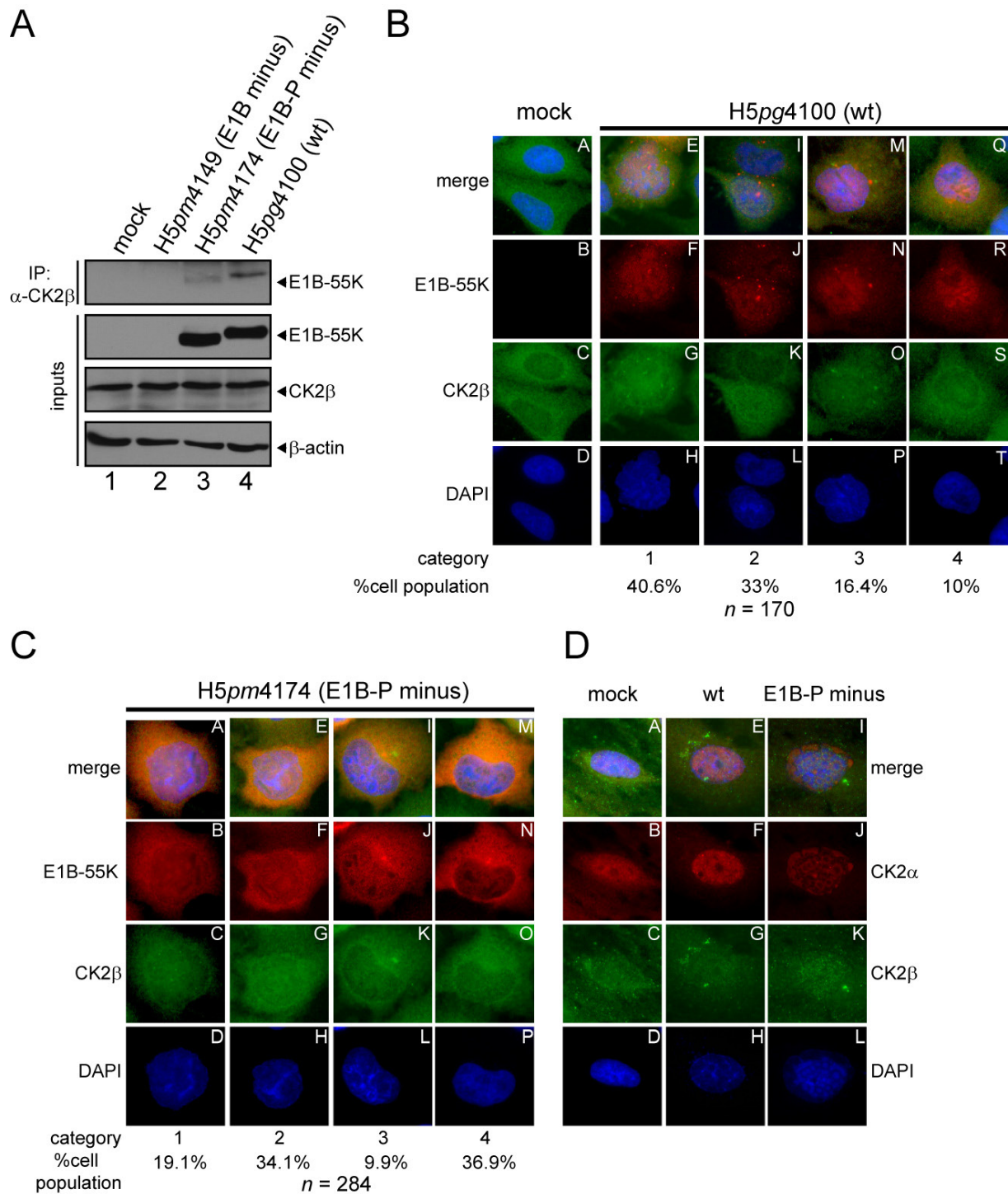


FIG 12 Coimmunoprecipitation and indirect immunofluorescence to analyze E1B-55K and its interaction with CK2 $\beta$  in infected cells. (A) CK2 $\beta$  interaction with E1B-55K during infection. A549 cells either mock-infected or infected (MOI=20 FFU/cell) with H5pm4149 (E1B minus), H5pg4100 (wt), or H5pm4174 (E1B-P minus) virus were analyzed by immunoprecipitation assays using protein A-Sepharose coupled anti-CK2 $\beta$  antibody (Santa Cruz, "51"). Proteins separated by SDS-PAGE were detected by immunoblotting with anti-E1B (2A6) antibody. Immunoblot analyses of protein input levels are shown below for CK2 $\beta$  (6D5), E1B-55K (2A6), and  $\beta$ -actin (AC-15). (B and C) CK2 $\beta$  is relocalized during adenoviral infection. A549 cells either mock-infected or infected with the indicated viruses (MOI=20 FFU/cell) were analyzed by *in situ* immunofluorescence staining for E1B-55K (7C11), CK2 $\beta$  (6D5), and DNA content (DAPI). Examples of the four major CK2 $\beta$  relocalization patterns observed in this cell line are shown (B, *n*=170; C, *n*=284). (D) Comparison of CK2 $\alpha$  and CK2 $\beta$  localization during adenoviral infection. A549 cells either mock infected or infected with the indicated viruses (MOI=20 FFU/cell) were analyzed by *in situ* immunofluorescence staining for CK2 $\alpha$  (ab13410), CK2 $\beta$  (6D5), and DNA content (DAPI). Presented are blots and immunofluorescence data which show results that have been reproduced in at least three independent experiments.

In conclusion, E1B-55K also binds to the  $\beta$  subunit of CK2, which is relocalized in a different manner than CK2 $\alpha$  during adenoviral infection. Moreover, this redistribution is probably dependent on the phosphorylation status of E1B-55K indicated by reduced binding of the phosphonegative E1B-55K and the increased number of cells showing no CK2 $\beta$  relocalization during H5pm4174 (E1B-P minus) infection.

#### **4.5 CK2 $\alpha$ , but not the CK2 holoenzyme, phosphorylates E1B-55K *in vitro***

These results clearly demonstrate that CK2 is interacting with E1B-55K. Next, it was necessary to find out whether this kinase can phosphorylate E1B-55K *in vitro*. GST-E1B fusion proteins (Fig. 13A) were incubated with recombinant CK2 $\alpha$  or the holoenzyme in the presence of [ $\gamma$ - $^{32}$ P]ATP, and the reaction products were analyzed by SDS-PAGE and autoradiography (Fig. 13B). Efficient phosphorylation was observed with GST-wt-E1B (Fig. 13B, lanes 1 to 3) but not with the triple mutant GST-E1B-P minus (Fig. 13B, lanes 10 to 12). Less efficient phosphorylation by CK2 $\alpha$  was also observed with mutant GST-E1B fusion proteins where both serine residues were changed to alanines (GST-E1B AAT) or aspartic acids (GST-E1B DDT) (Fig. 13B, lanes 4 to 6 and lanes 7 to 9, respectively), strongly indicating that T495 is also phosphorylated by CK2 $\alpha$ . Since at least one report (Arrigoni et al., 2004) defined a regulatory role for the  $\beta$  subunit of CK2, *in vitro* phosphorylation assays were also performed with recombinant CK2 (double  $\alpha$  plus double  $\beta$ ) holoenzyme (Fig. 13B, lanes 13 to 21). However, no signals were detected with either GST-wt-E1B (Fig. 13B, lanes 13 to 15) or the mutant constructs (Fig. 13B, lanes 16 to 21). Because double amounts of both kinase and substrate were included in the CK2 holoenzyme assays (Fig. 13B lanes 13 to 21), one can exclude the possibility that insufficient kinase and substrate amounts were responsible for the undetectable phosphorylation.

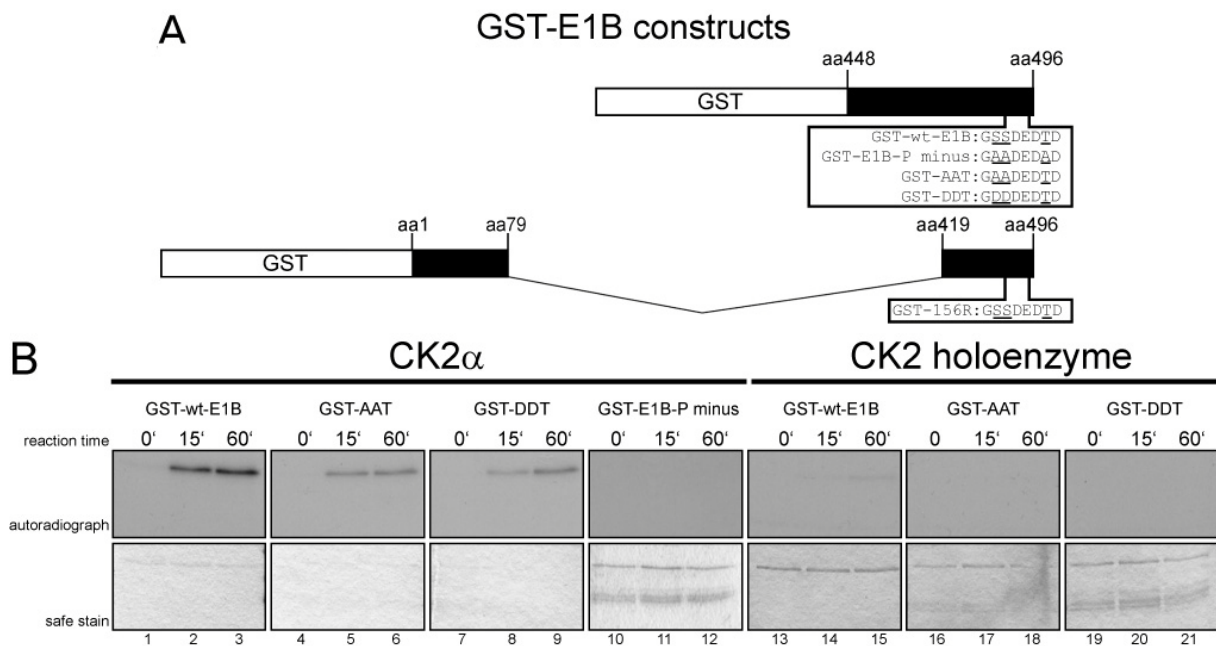


FIG 13 CK2 $\alpha$ , but not the CK2 holoenzyme, phosphorylates E1B-55K's C terminus *in vitro*. (A) C-terminal amino acid sequences of different GST-E1B fusion proteins used in the phosphorylation assays. Underlined are amino acids known to be phosphorylated and/or changed to the indicated amino acids. Numbers above the schematic drawing represent amino acid (aa) positions of E1B-55K from which the GST fragments are derived. (B) The indicated GST-E1B fusion proteins were incubated either with recombinant CK2 $\alpha$  or with CK2 holoenzyme together with radioactive [ $\gamma$ - $^{32}$ P]ATP for the indicated reaction times at 30°C. Kinase assays performed with the holoenzyme contained double the amount of substrate (GST-wt-E1B, GST-E1B-P minus, GST-AAT, and GST-DDT) and holoenzyme units compared to CK2 $\alpha$  assays. After extensive washing, kinase assay samples were separated by SDS-PAGE and Coomassie stained ("safe stain", lower panels), and the gels were vacuum dried for autoradiographic detection with X-ray films (upper panels). Autoradiographs represent one of at least four independent experiments.

Collectively, these results suggest that CK2 $\alpha$  not only interacts with E1B-55K and phosphorylates this protein at the C terminus but that the  $\beta$  subunit may mediate inhibitory effects on the phosphorylation of E1B-55K.

#### 4.6 The 156R splice product of E1B-55K is also targeted by CK2 $\alpha$ but not by the holoenzyme

A splice product of the full-length E1B mRNA, called E1B-156R (156R), shares 77 identical C-terminal amino acids (and 79 N-terminal amino acids) with the full-length protein (Sieber and Dobner, 2007) and has been shown to be phosphorylated (Fig. 13A) (Teodoro et al., 1994). To examine whether 156R is also a target for phosphorylation via protein kinase CK2, a GST-156R fusion protein was used in a similar *in vitro* phosphorylation assay as described above. Recombinant CK2 $\alpha$  efficiently phosphorylated GST-156R, the GST-wt-E1B and GST-April, an essential protein for HuR-mediated nucleocytoplasmic translocation of the CD83 mRNA, which has been shown to be a CK2 target (Chemnitz et al., 2009) and served as a positive control (Fig. 14, lanes 1 to 3). Moreover, the CK2 holoenzyme also phosphorylated

GST-April efficiently (Fig. 14, lane 8) but was not capable of phosphorylating GST-156R or GST-wt-E1B efficiently (Fig. 14, lanes 7 and 9). Preincubation with the CK2 inhibitor DMAT (Pagano et al., 2004, 2008) almost completely abrogated CK2 $\alpha$ -mediated phosphorylation, (Fig. 14, lanes 4 to 6). These data reveal that E1B-156R is also targeted by CK2 $\alpha$  but not by the CK2 holoenzyme *in vitro*.

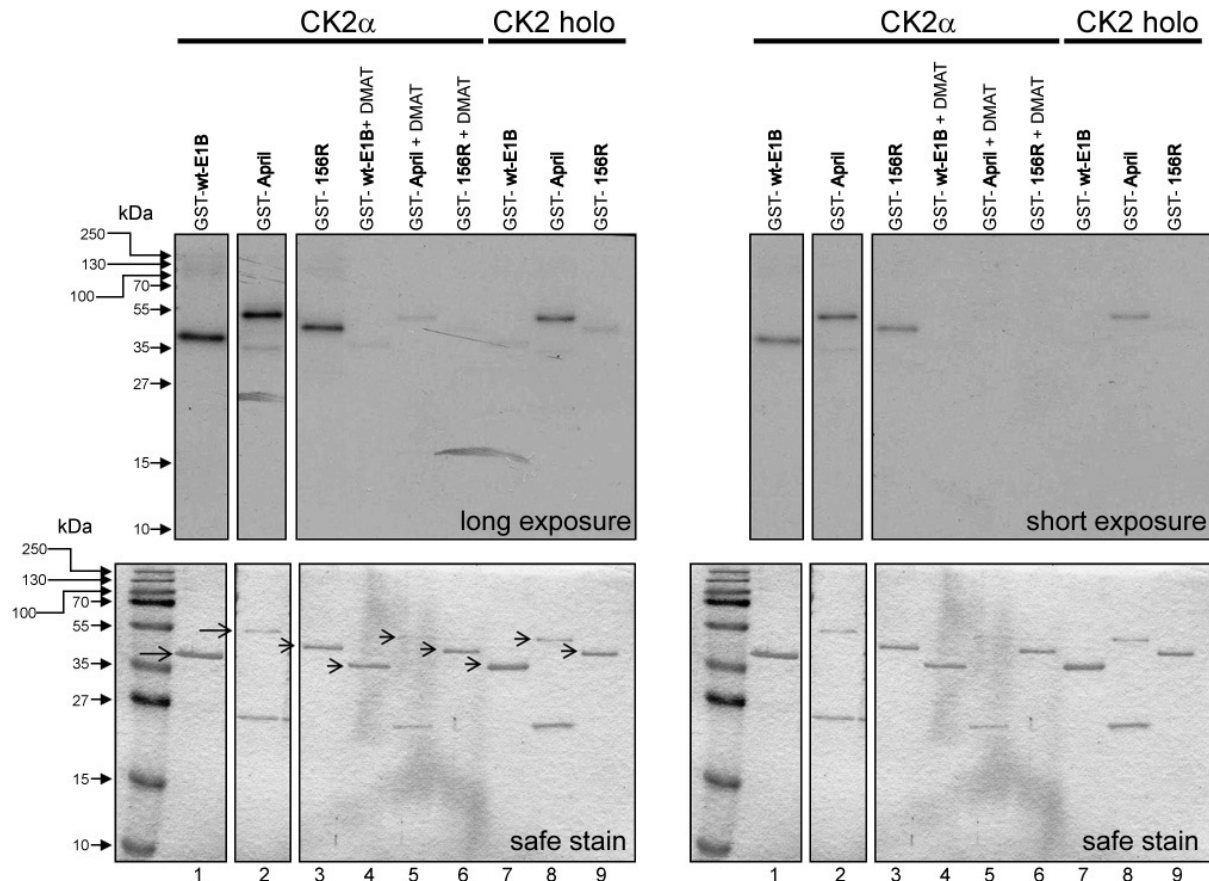


FIG 14 The 156R splice product of E1B-55K is also phosphorylated by CK2 $\alpha$  but not by the holoenzyme. The indicated GST-E1B and GST-April fusion proteins were incubated either with recombinant CK2 $\alpha$  or CK2 holoenzyme together with radioactive [ $\gamma$ - $^{32}$ P]ATP for 30 min at 30°C. Where indicated, CK2 $\alpha$  batches were incubated for 15 min in 20  $\mu$ M DMAT together with substrates at room temperature prior to starting the *in vitro* kinase reaction. Kinase assay products were analyzed by SDS-PAGE, and the gels were Coomassie stained (“safe stain”, lower panels) and then vacuum dried for autoradiography on X-ray films (top panels). Additional control lanes were omitted due to clarity. Segments are from the same autoradiograph. The autoradiograph represents one of at least three independent experiments.

#### 4.7 Inhibition of CK2 during adenovirus infection abolishes E1B-55K phosphorylation and interaction with diverse cellular proteins

Several coimmunoprecipitation experiments were performed to assess the involvement of E1B-55K phosphorylation for protein interaction.

To examine the binding capacity of the mutated E1B-55K from E1B-P minus towards Mre11, p53, and E4orf6, coimmunoprecipitation studies from infected lysates were performed. Fig. 15A, B and C, each lanes 3 and 4 illustrate reduced binding of the phosphonegative E1B-55K towards Mre11 (~80 to 90% reduction, ImageJ quantification), p53 (not quantifiable due to heavy chain band) and E4orf6 (~52% reduction, ImageJ quantification), which in turn might explain the delayed steady-state reduction of Mre11 or the increase in p53 protein levels during H5pm4174 infection as illustrated in Figure 16.

To test whether specific CK2 inhibition leads to reduced or completely abolished detection of phospho-E1B-55K in an infection set-up, the phosphorylation status of E1B-55K and its interaction with CK2 $\alpha$ , CK2 $\beta$  and Mre11 was determined after treatment with two specific CK2 inhibitors (DMAT and TBB). Resembling the results with mutant E1B-55K (E1B-P minus) from H5pm4174 and E1B minus from H5pm4149 infection (Fig. 9D, top panel, lanes 3, 4), it was only possible to detect severely reduced or no phosphorylation of E1B-55K after treatment with the DMAT or TBB inhibitors (Fig. 15D, E, F, top panels, lanes 4 to 6). Additionally, reduced or no coprecipitation of E1B-55K with endogenous CK2 $\alpha$ , CK2 $\beta$  and Mre11 was observed (Fig. 15D, E, F, second panels, lanes 4 to 6, respectively) after inhibitor treatment. Furthermore, cytotoxicity of DMAT and TBB was assessed and no increase in cell death could be detected compared to untreated cells, favoring the applicability of DMAT and TBB along with adenovirus infection (Fig. 15G).

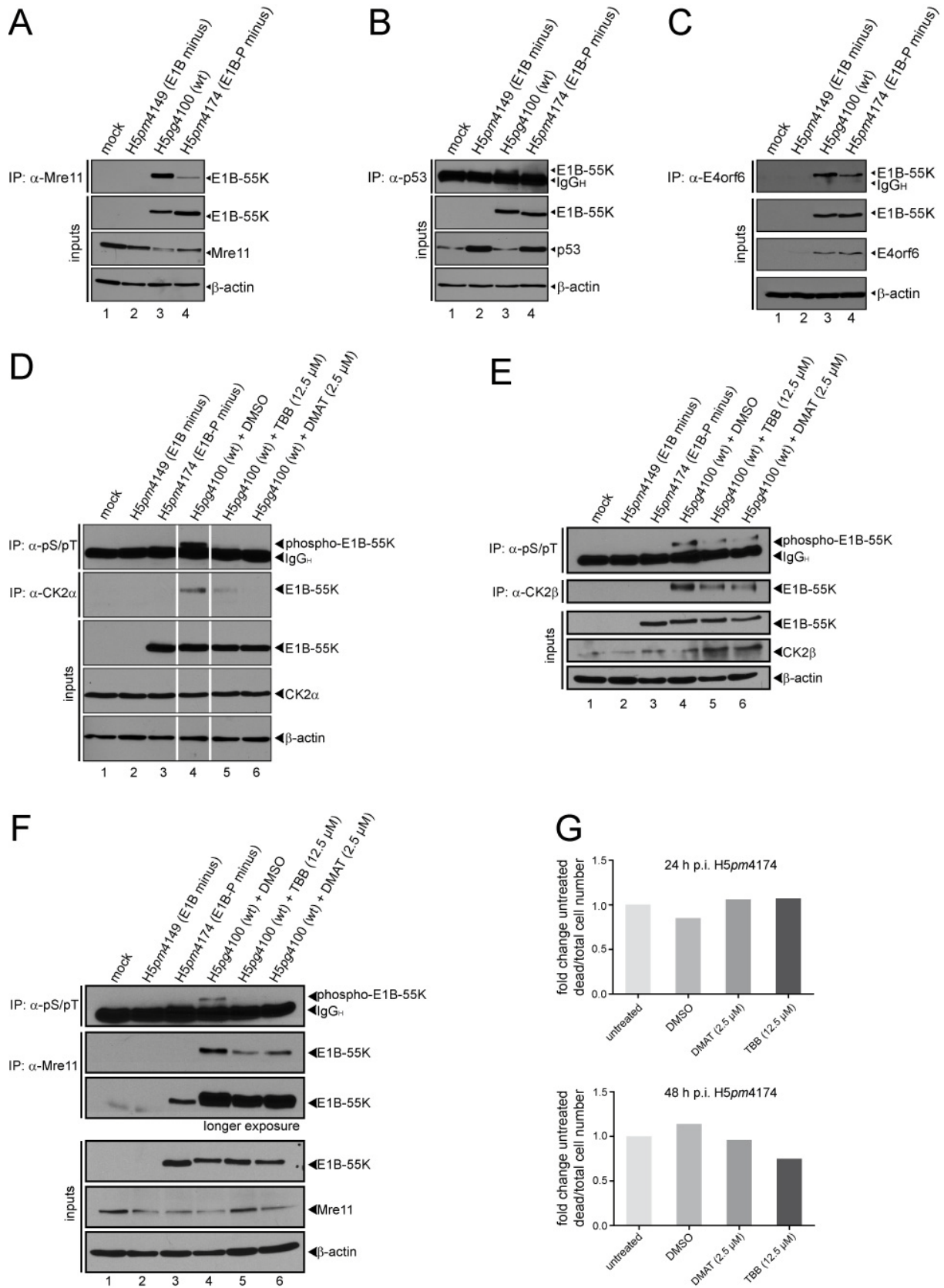


FIG 15 Phosphorylation of E1B-55K determines interaction with several proteins. (A, B and C) Coimmunoprecipitation with Mre11, p53 or E4orf6. A549 cells were mock-infected or infected with wt and mutant viruses at an MOI of 20 FFU/cell. Whole-cell lysates were subjected to immunoprecipitation with anti-Mre11 (pNB 100-142), anti-p53 (DO-1) or anti-E4orf6 (1807) antibodies. Proteins separated by SDS-PAGE were detected by immunoblotting with anti-E1B antibody 2A6. Steady-state concentrations (inputs) of E1B-55K (2A6), Mre11 (pNB 100-142),  $\beta$ -actin (AC-15), E4orf6 (1807), and p53 (DO-1) were determined by immunoblotting of protein extracts with the appropriate antibodies. Inhibitors TBB or DMAT reduce or abolish CK2 $\alpha$ , CK2 $\beta$ , and Mre11 binding and phosphorylation of E1B-55K. (D, E, and F) A549 cells were mock-infected or infected with H5pm4149 (E1B minus), H5pg4100 (wt), and H5pm4174 (E1B-P minus) virus at an MOI of 20 FFU/cell. As indicated, cells were also treated with DMSO, TBB, or DMAT 4 h p.i. until harvesting the cells at 24 h p.i. Immunoprecipitation assays were performed with anti-phosphoserine/phosphothreonine (pS/pT, 22a, D, E, and F), anti-CK2 $\alpha$  (ab13410 [D]; segments originate from one blot, and double control lanes were omitted due to clarity), anti-CK2 $\beta$  ("51" [E]) and Mre11 (pNB 100-142 [F]) antibodies. Proteins separated by SDS-PAGE were immunoblotted with anti-E1B antibody (2A6). Protein steady-state levels were detected by immunoblotting with antibodies specific for E1B-55K (2A6), CK2 $\alpha$  (ab13410 [D]), CK2 $\beta$  (6D5 [E]), Mre11 (pNB 100-142 [F]), and  $\beta$ -actin (AC-15 [D, E, and F]). (G) A549 cells were infected as indicated and treated as in (D, E and F). At indicated time points cells were counted and trypan blue positive cells determined along with total cell number. The Western blots represent one of at least three independent experiments.

In conclusion, CK2 $\alpha$  must bind to E1B-55K in order to phosphorylate the viral protein efficiently. Moreover, these data also suggest that CK2 $\alpha$ -mediated phosphorylation of E1B-55K determines the affinity of protein-protein interaction or substrate specificity toward Mre11, p53, E4orf6, CK2 $\beta$  and Mre11 (Fig. 15B, C, E and F respectively).

#### **4.8 Alanine substitution of E1B-55K's phospho-sites results in cell type-specific profound negative effects.**

Next, the effect of mutations on the ability of the Ad protein to promote viral early and late protein production was investigated. Since previous reports have shown that p53 accumulates upon infection with a phosphonegative E1B-55K virus (Schwartz et al., 2008), H1299 p53-negative cells were analyzed to exclude a possible negative effect exerted from p53-mediated antiviral responses like cell cycle arrest. In fact, viral early and late protein production was negatively affected during H5pm4174 virus (E1B-P minus) infection. Especially, for E1B-55K, L4-100K and the late structural proteins this reduction was well pronounced (Fig. 16B). Apart from that, protein steady-state levels were similar to wt infection. However, Mre11 reduction kinetics seemed to be slightly delayed, taking into account that during wt infection more Mre11 was loaded. Surprisingly, H5pg4100 (wt) and H5pm4174 (E1B-P minus) infection revealed almost identical adenoviral protein production in A549 cells (Fig. 16A, E1A, E2A, E1B-55K, E4orf6, L4-100K and HAdV5 capsid protein stainings). In contrast, Mre11 steady-state reduction was delayed and p53 degradation was impaired during E1B-P minus virus infection (Fig. 16A), indicating that the phosphonegative E1B-55K mutant exerts stability defects in H1299 but not in A549 cells (Fig. 16A and B). In past experiments, Teodoro et al. observed a severe defect in viral replication efficiency using a virus mutant lacking two of the three phosphosites in E1B-55K (pmS490/91A; [Teodoro et al., 1994]). To

test whether the mutant used in this study, lacking all three phosphosites (S490/491/T495A, E1B-P minus), also shows a defect in virus progeny production, virus yield was determined in H1299 and A549 cells 48 hours post infection (Fig. 16E). The following experiments revealed that H5*pm*4174 infection in H1299 p53-negative cells yielded undetectable virus progeny amounts at an MOI of 2 and 85% less viral particles at an MOI of 20 FFU per cell (Fig. 16E, H1299). These results indicate that other factors than, for example, p53 activation, are responsible for reduced progeny virion numbers. Moreover, reduced E1B-55K, L4-100K and late structural protein levels obviously explain the negative effect on virus replication at least in H1299 cells. Interestingly and similarly to H1299 cells, at an MOI of 2, 93% less viral particles were detected in H5*pm*4174 (E1B-P minus) infected A549 cells compared to wt-infected cells. To try to rescue this defect, similar experiments were performed with an MOI of 20 FFU per cell. However, the reduction was still a significant 65%, so that the defect could not be compensated completely (Fig. 16E, A549). Since defects in viral progeny production cannot be traced back to lower viral protein levels in general (in A549 Fig. 16A), the ability of the H5*pm*4174 (E1B-P minus) virus to synthesize DNA was investigated. Viral DNA replication efficiency during E1B-P minus infection was comparable to wt infection at both MOI of 2 or 20 FFU per cell in A549 cells (Fig. 16C), but reduced in H1299 cells (Fig. 16D).

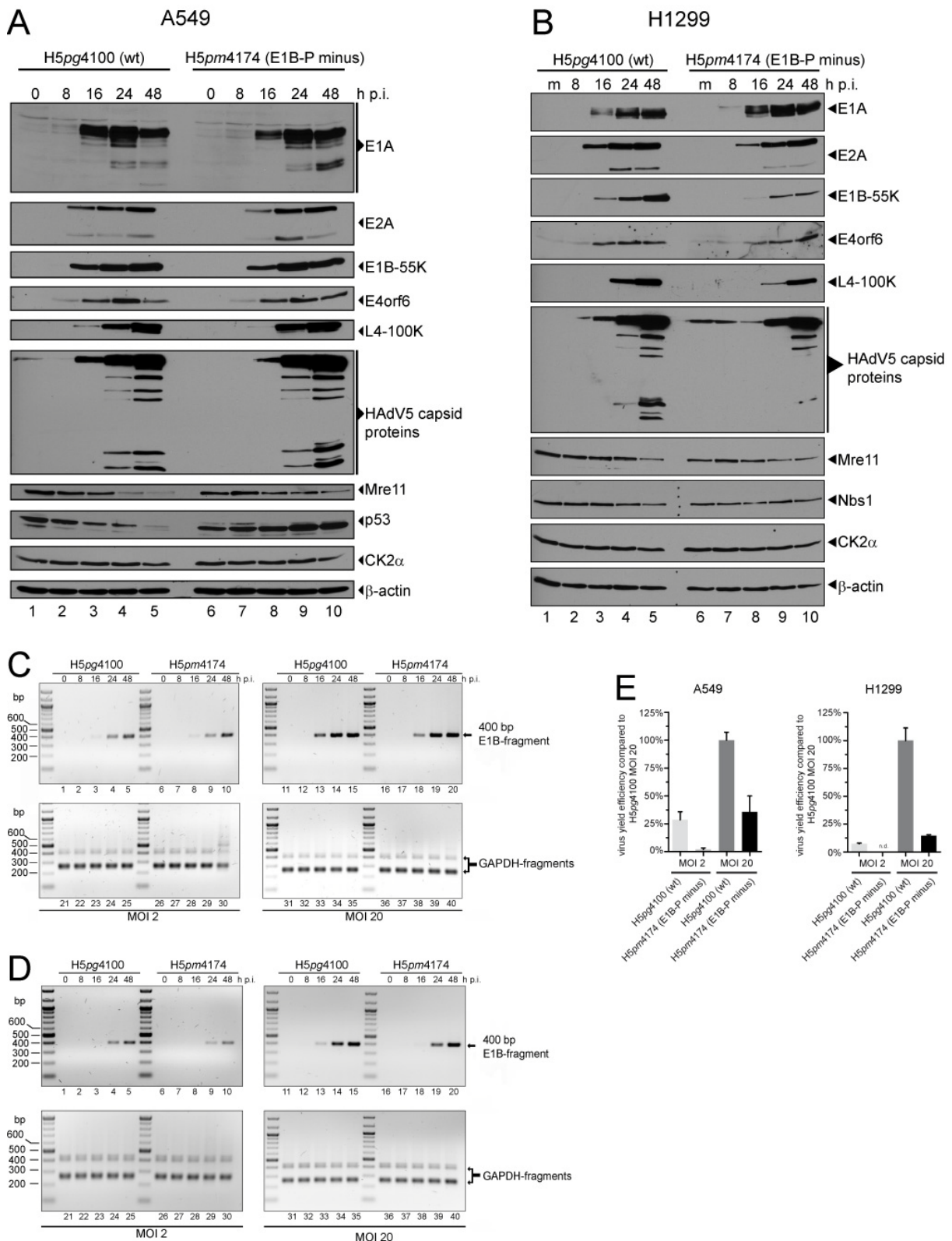
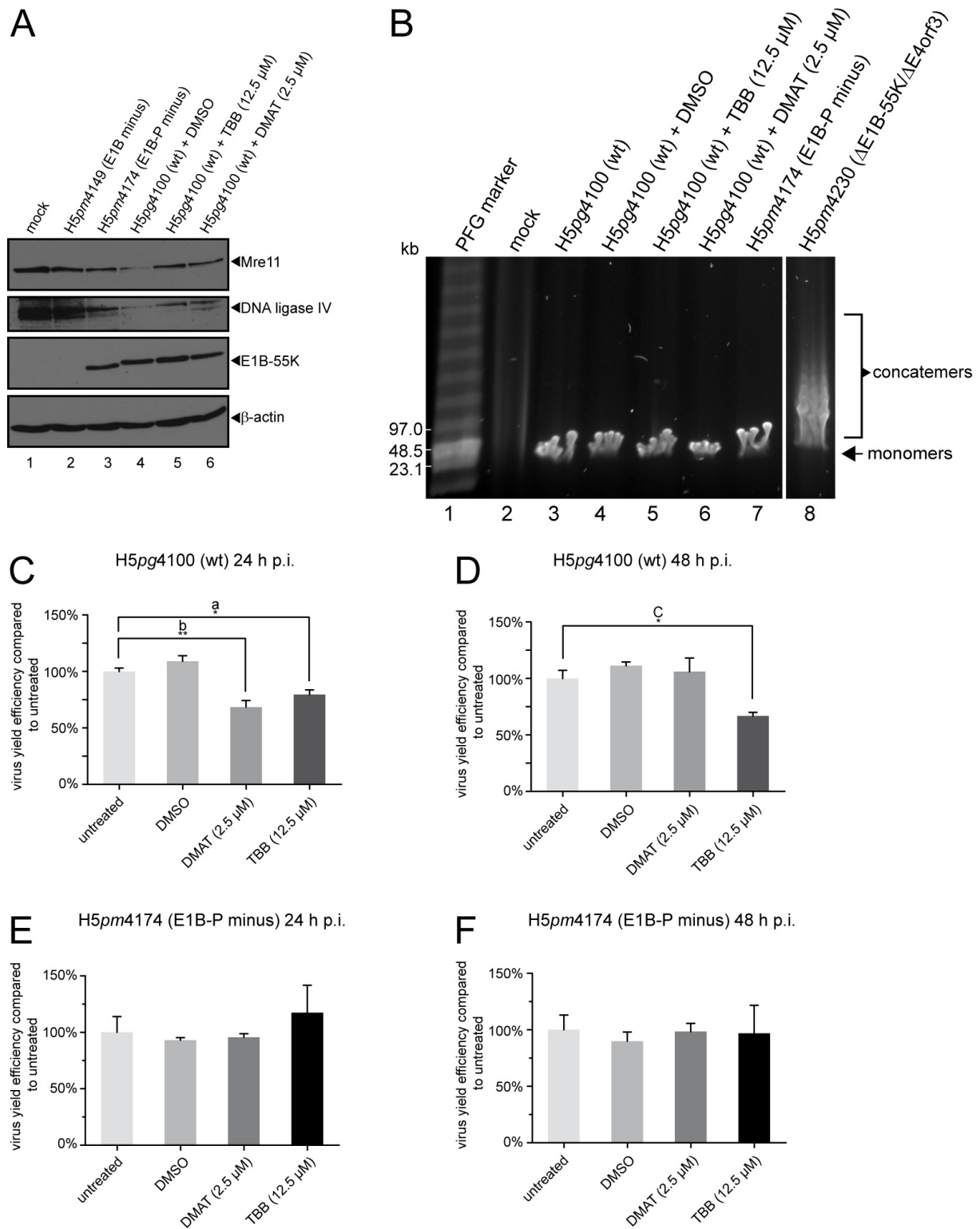


FIG 16 Phenotypic characterization of H5pg4100 (wt) and H5pm4174 (E1B-P minus) viruses. (A+B) Viral and cellular protein expression analyses. A549 and H1299 cells were mock-infected or infected with the indicated viruses at an MOI of 20 FFU per cell and harvested at the indicated time points. Total cell extracts were prepared, separated by SDS-PAGE, and immunoblotted for the indicated proteins. (C+D) Viral DNA synthesis. A549 and H1299 cells were infected with H5pg4100 (wt) or H5pm4174 (E1B-P minus) virus at an MOI of 2 or 20 FFU per cell. Total DNA was isolated at the indicated time points and subjected to PCR. PCR products were analyzed by agarose gel electrophoresis. PCR amplification of GAPDH (lanes 21 to 40) served as an internal control. (E) Virus growth. A549 and H1299 cells were infected with wt and E1B-P minus virus at an MOI of 2 or 20 FFU per cell and harvested at 48 h.p.i. The virus yield was determined by quantitative E2A-72K immunofluorescence staining (B6-8) on HEK293 cells. The results represent the average of at least three independent experiments. Bars indicate the standard error of the mean values. Virus yield efficiency is represented as a percentage of H5pg4100 (wt; MOI=20) yield efficiency.

These results suggest that decreased adenoviral progeny production is not solely due to reduced viral DNA synthesis. Especially, in A549 cells no obvious defect was visible which might explain the severely reduced virus yield, placing special emphasis on a cell-specific difference (p53-positive vs. p53-negative).

#### **4.9 Inhibition of CK2 during adenovirus infection limits down regulation of Mre11 and DNA ligase IV protein levels but does not induce adenoviral genome concatemerization although virus yield is significantly reduced.**

Specific inhibition of CK2 decreases binding efficiency of E1B-55K toward Mre11, CK2 $\alpha$ , and CK2 $\beta$  (Fig. 15). To evaluate the effect of CK2 inhibition during adenoviral infection more in detail, further approaches were used. First, degradation of Mre11 and DNA ligase IV was investigated by combined infection and CK2 inhibitor treatment in A549 cells. In fact, a phospho-E1B-55K-dependency on Mre11 and DNA ligase IV degradation was observed. Obviously, the phosphonegative E1B-55K mutant and CK2 inhibition after wt virus infection resulted in higher Mre11 and DNA ligase IV steady-state protein levels than after H5pg4100 (wt) infection with dimethyl sulfoxide (DMSO) control treatment (Fig. 17A, lanes 3 to 6). However, since degradation of Mre11 and (mainly) DNA ligase IV is mandatory to circumvent adenoviral genome concatemerization (Schwartz et al., 2008), pulsed-field gel electrophoresis was used to visualize adenoviral genomes in the context of H5pg4100 (wt) and H5pm4174 (E1B-P minus) infection and CK2 inhibitor treatment (Fig. 17B). Here, no assembly of adenoviral genome concatemers could be detected (Fig. 17B, lanes 3 to 7), only in the positive control after infection with H5pm4230 virus ( $\Delta$ E1B-55K/ $\Delta$ E4orf3, a similar virus mutant, was described previously). Therefore, lower virus yield cannot be explained by accumulation of viral DNA concatemers after H5pm4174 (E1B-P minus) infection. Intriguingly, and as expected, CK2 inhibition led to a modest reduction in virus yield after wt (H5pg4100) infection in A549 cells at 24 and 48 h p.i. (Fig. 17C, 32% DMAT and 21% TBB; Fig. 17D, 33% TBB), whereas CK2 inhibitor treatment had no effect upon H5pm4174 (E1B-P minus) virus yield at either 24 or 48 h p.i. (Fig. 17E and F).



**FIG 17** Inhibitors TBB and DMAT reduce Mre11 and DNA ligase IV degradation efficiency but have no effect on inducing viral genome concatemerization although virus yield is significantly decreased. (A) Mre11 and DNA ligase IV degradation upon CK2 inhibitor treatment. A549 cells were mock-infected or infected with H5pm4149 (E1B minus), H5pg4100 (wt), and H5pm4174 (E1B-P minus) virus at an MOI of 20 FFU/cell. As indicated, cells were also treated with DMSO, TBB, or DMAT at 4 h p.i. until harvesting the cells at 24 h p.i. Total cell extracts were prepared, separated by SDS-PAGE, and immunoblotted for Mre11(pNB 100-142), DNA ligase IV (NB110-57379), E1B-55K (2A6), and  $\beta$ -actin (AC-15). (B) Analysis of adenoviral genome concatemerization. A549 cells were mock infected or infected with the indicated viruses at an MOI of 30 FFU/cell. H5pm4230 ( $\Delta$ E1B-55K/ $\Delta$ E4orf3) infection was performed at an MOI of 100 FFU/cell. Cells were also treated with inhibitors as in panel A, but the cells were harvested for isolating total DNA at 30 h p.i. Adenoviral genome monomers and concatemers were visualized after pulsed-field gel electrophoresis by ethidium bromide staining

(segments originate from one agarose gel, and triple control lanes were omitted due to clarity). (C to F) Virus growth upon CK2 inhibitor treatment. A549 cells were infected with wt and E1B-P minus virus at an MOI of 20 FFU/cell and harvested at 24 or 48 h p.i. In addition, the cells were also treated with DMSO or CK2 inhibitors as described above (in panel A). Virus yield was determined by quantitative E2A-72K immunofluorescence staining (B6-8) on HEK293 cells. The results represent the average of at least three independent experiments. Two-tailed *t* tests (GraphPad Prism 5) were applied to calculate significance. Single and double asterisks indicate significant differences (\*  $P < 0.05$ , \*\*  $P < 0.01$ ). Bars indicate the standard error of the mean values. Virus yield efficiency is represented as a percentage of “untreated” virus yield efficiency.

Taken together, cellular substrates for adenoviral-mediated degradation like Mre11 and DNA ligase IV are inefficiently degraded in the context of a phosphonegative E1B-55K virus infection (H5pm4174) and upon CK2 inhibition. Additionally, other reasons than viral genome concatemerization are responsible for lower virus yield after H5pm4174 (E1B-P minus) infection or CK2 inhibitor treatment. Strikingly, the reduced production of progeny virions upon inhibitor treatment could not be further reduced in the E1B-P minus virus (H5pm4174) infection, stressing the specific positive effect of CK2 upon E1B-55K.

Consistent with previous work from different groups (Teodoro et al., 1994; Teodoro and Branton, 1997; Schwartz et al., 2008), the first part of this work shows that E1B-55K is phosphorylated at residues S490, S491 and T495 in virus-infected cells and confirm that mutations which convert these amino acids to alanines have profound negative effects on binding to and ubiquitin-dependent degradation of Mre11 and p53, and virus growth but, interestingly, neither affect viral early and late protein production nor viral DNA synthesis in A549 cells (Fig. 16A, C, E).

## 5 Discussion

### 5.1 The CK2 E1B relationship

It has long been speculated that E1B-55K might be phosphorylated by the protein kinase CK2. However, until now experiments have only concentrated on the properties of an E1B-55K phosphorylation-deficient mutant, which showed that phosphorylation regulates many E1B-55K functions, and therefore viral behavior in general, and is thus one of the most critical posttranslational modifications of E1B-55K (Teodoro et al., 1994; Teodoro and Branton, 1997; Schwartz et al., 2008). However, the kinase responsible was not identified, so the main goal for the first part of this work was to clarify this question.

It is known that many viruses and their gene products exploit the functions of CK2 for their own benefit, such as EBV protein ZEBRA (El-Guindy and Miller, 2004), Kaposi’s sarcoma-associated herpesvirus (KSHV) protein ORF57 (Malik and Clements, 2004), or herpesvirus protein ICP27 (Koffa et al., 2003). EBV ZEBRA is reported to require phosphorylation by

CK2 to turn the viral protein into a transcriptional repressor or activator and that this posttranslational modification contributes to ZEBRA's function in controlling viral lytic cycle gene expression (El-Guindy and Miller, 2004). CK2-mediated phosphorylation of ORF57 from KSHV is also necessary for controlling gene expression during the lytic infectious cycle (Malik and Clements, 2004). As another example, ICP27 requires CK2-mediated phosphorylation for correct subcellular localization and proper binding to several interaction partners (Koffa et al., 2003; Rojas et al., 2010).

In light of these reports and the fact that E1B-55K contains a highly conserved CK2 consensus motif (CKM-<sup>490</sup>SSDEDTD<sup>496</sup>; compare Fig. 9A and B), it is not surprising that the long suspected protein kinase CK2 is also involved in regulating E1B-55K activity. Indeed, this work demonstrates for the first time that E1B-55K binds to the catalytic  $\alpha$  and the regulatory  $\beta$  subunit of CK2 and is a substrate for CK2 $\alpha$  phosphorylation *in vitro* and in cell culture (Part I). The coimmunoprecipitation experiments in H1299 p53-negative cells transfected with E1B-55K alone demonstrated an interaction independent of the presence of p53 and other viral proteins. Furthermore, according to the *in situ* stainings, redistribution of CK2 $\alpha$  seems to be necessary for interaction with E1B-55K but not *vice versa*. In fact, although mutant E1B-55K from E1B-P minus does not efficiently bind to, and is not phosphorylated by CK2 $\alpha$ , almost the same CK2 $\alpha$  protein relocation could be observed during E1B-P minus infection, indicating that an as-yet-unidentified adenoviral protein may also participate in CK2 $\alpha$  redistribution (Fig. 11). This is further supported by the observation that CK2 $\alpha$  redistribution does not occur in cells transfected with wt pE1B-55K or pE1B-P minus alone (data not shown) or in infection with the E1B minus virus (H5pm4149). In fact, H5pm4149 infection resulted in the same phenotypic outcome of CK2 $\alpha$  redistribution as during infection with wt (H5pg4100) and E1B-P minus (H5pm4174) viruses investigated here.

It has been reported that a substrate's phosphosites make a significant contribution to the overall binding energy between a kinase and its substrate (Ubersax and Ferrell, 2007). Thus, it might be expected that mutating the phosphosites of E1B-55K, or blocking the active site of CK2 by its specific inhibitors DMAT or TBB, leads to inefficient or completely abolished binding. Indeed, DMAT or TBB treatment of adenovirus-infected A549 cells led to lower amounts of phospho-E1B-55K, which is probably due to the reduction of CK2 $\alpha$  binding toward E1B-55K (Fig. 15). In addition, it is possible that structural proteins such as the adenoviral fiber proteins play a role in CK2 subunit redistribution. Souquerre-Besse et al.

reported that infection with an adenovirus deleted of the fiber gene in its genome resulted in relocalization of both  $\alpha$  and  $\beta$  CK2 subunits into the same viral nuclear structures, in contrast to wt HAdV5 infection, where both subunits separate into two morphologically distinct virus-induced nuclear areas (Souquere-Besse et al., 2002). Indeed, CK2 $\alpha$  was also relocalized into the cytoplasm and not only in the nucleus. Furthermore, it was also possible to show that E1B-55K not only interacts with the  $\alpha$ , but also with the  $\beta$  subunit of CK2 and that phosphorylation of E1B-55K strongly determines the binding efficiency toward that subunit like for CK2 $\alpha$  (Fig. 10 and Fig. 12). Moreover, the phosphorylation status of E1B-55K is obviously also important for the outcome of CK2 $\beta$  redistribution (Fig. 12B and C). Importantly, in H5pm4174 infection (E1B-P minus) the amount of cells showing small nuclear CK2 $\beta$  accumulations decreases from 40.6 to 19.1% (Fig. 12C, category 1) and cell numbers showing no relocalization at all rise from 10 to 36.9%

(Fig. 12C, category 4).

From the immunofluorescence data it can be deduced that interactions between E1B-55K and CK2 $\alpha$  can take place partly in cytoplasmic accumulations or at the borders of specific ring-like structures precisely surrounding areas of nuclear E1B-55K regions after adenoviral infection in A549 cells (Fig. 11I), whereas deducing where CK2 $\beta$  and E1B-55K interaction takes place is more complicated since CK2 $\beta$  shows many different phenotypes with no significant overlap of E1B-55K and CK2 $\beta$  staining (Fig. 12B).

The fact that Souquere-Besse et al. observed a separation of CK2 subunits also fits very well with the *in vitro* observation that the holoenzyme phosphorylates the wt E1B-55K C terminus inefficiently. When combined with the *in vitro* phosphorylation and immunofluorescence data, a picture emerges suggesting that separation of the CK2 $\alpha$  and  $\beta$  subunits is necessary during the course of infection for efficient E1B-55K phosphorylation. Furthermore, though at this point only speculative but not improbable, it can be proposed that  $\beta$  subunits exert inhibitory effects upon E1B-55K C-terminal phosphorylation. There is one example where such an unusual regulatory mechanism for CK2 substrates is indeed described. Arrigoni et al. (Arrigoni et al., 2004) reported that calmodulin is a target for CK2 phosphorylation, which in turn is inhibited by CK2 $\beta$ . In light of these observations and knowledge owing to another study describing that dissociation of CK2 $\alpha$  and CK2 $\beta$  into separate subunits favors increased amounts of nuclear CK2 $\beta$  (Filhol et al., 2003), it can be assumed that E1B-55K is directly involved in CK2 $\beta$  redistribution in order to support its own phosphorylation by CK2 $\alpha$ . This hypothesis explains why E1B-55K binds to CK2 $\beta$ , although we assume at the same time an inhibitory effect of that subunit upon E1B-55K phosphorylation.

Since E1B-55K is reported to have several splice products, and at least one is also shown to be phosphorylated (Teodoro et al., 1994), E1B-156R was examined, which contains 77 amino acids of the full-length carboxy terminus. As anticipated, E1B-156R is also a target of CK2 $\alpha$  that similarly cannot be efficiently phosphorylated by the CK2 holoenzyme *in vitro*. This implies that CK2 $\alpha$  may regulate the functions of the full-length, as well as the E1B-156R splice product, and that the phenotypes observed during E1B-P minus infection can also be attributed at least in part to disturbed functioning of the similarly mutated E1B-156R peptide. Investigations into the role of E1B-156R phosphorylation are under way. In the present study wt and E1B-negative viruses originated from an HAdV5 genomic backbone. Thus, it was necessary to analyze E1B-55K phosphorylation with an E1B-55K phosphorylation deficient virus in the same genomic HAdV5 backbone. To confirm that the phenotype conferred by such a virus mutant located in this genomic backbone is comparable to previously reported viruses carrying the same mutations (Teodoro et al., 1994; Schwartz et al., 2008), several phenotypic analyses were conducted. Carried out in part previously, it was possible to confirm that under lytic infection conditions the newly generated virus mutant has similar characteristics, such as deficiency in p53 degradation and mislocalization of the mutated E1B-55K. Therefore, data obtained in the present study are to a great extent consistent and comparable to earlier data (Teodoro et al., 1994; Teodoro and Branton, 1997; Querido et al., 2001; Schwartz et al., 2008). Moreover, these data could be substantiated by CK2 inhibitor treatment of infected cells where a similar effect upon binding to and degradation of Mre11 could be observed (Fig. 15).

From the infection analyses in H1299 and A549 cells, strong differences became evident upon infection with the phosphonegative E1B-55K virus mutant (H5 $pm4174$ ). In H1299 cells, viral protein analyses demonstrated clearly reduced levels of E1B-55K, L4-100K and late structural proteins. Abolishment of CK2 phosphorylation has been shown to induce ataxin-3 instability and aberrant cytoplasmic localization, leading to malfunctioning of this protein (Mueller et al., 2009). In a very similar way to ataxin-3, phosphonegative E1B-55K displays aberrant cytoplasmic localization and instability in H1299 cells. In keeping with the late viral mRNA transport function of E1B-55K together with E4orf6, it is not surprising that L4-100K and structural proteins are also reduced in protein steady-state levels, though a concise mRNA analysis has to be performed. However, viral DNA replication also seems to be negatively affected during infection with E1B-P minus, supporting E1B-55K functions previously described in normal human foreskin fibroblasts (HFFs) (Chahal and Flint, 2012). These

defects easily account for the virus yield reduction in H1299 cells. Very intriguing in this context, significantly reduced levels of E1B-P minus virus progeny were also obtained in A549 cells, although neither a negative effect on viral DNA replication efficiency, nor on early or late viral protein expression was detected (Fig. 16A, C, and E). Hence, a defect in viral mRNA synthesis or transport can most probably be excluded. Furthermore, since p53 protein levels increase upon infection with E1B-P minus virus (Fig. 16A), it cannot be excluded that virus growth is decreased due to increased p53 activation with subsequent negative effects for the virus such as cell cycle arrest. However, several reports have stated the fact that p53 accumulation does not necessarily accompanies p53 activation and cell growth repressive or antiviral effects, due to heterochromatin silencing mechanisms executed by the E4orf3 protein (Goodrum and Ornelles, 1998; Soria et al., 2010; Chahal and Flint, 2012). Therefore, it is very likely that the defect in virus growth of E1B-P minus in A549 are independent of p53-mediated antiviral effects of whatever kind. Moreover, if so, then these defects would not be visible in H1299 cells, which is not the case. Under these circumstances, it may be deduced and speculated that either E1B-P minus exerts direct dominant-negative effects upon viral replication and stability of other adenoviral proteins (depending on the cell system) or a different cellular factor essential for virus growth and/or viral protein stability and connected to CK2-mediated phosphorylation of E1B-55K is differentially exploited in both cell systems. In this context, it would be very interesting to identify this factor since it probably represents the cellular factor responsible for correct virus growth. This subject will be further tackled in Part III.

To support the observations concerning the phosphonegative E1B-55K virus mutant, CK2 inhibitor studies were used and achieved a reduction of viral progeny at 24 h p.i., but at 48 h p.i. only with TBB treatment. It is possible that the DMAT inhibitor is not stable for a longer incubation period than 20 h and exerted no inhibitory effect anymore. Nevertheless, we were able to achieve up to 33% reduction of viral progeny virions upon CK2 inhibitor treatment (Fig. 17D, TBB). Probably, the remaining CK2 activity, as shown in Fig. 15D to F, is sufficient to support virus growth leading to this modest virus growth defect in comparison to virus growth defect after E1B-P minus virus infection. Strikingly, the CK2 inhibitors added no further negative effect on production of progeny virions upon E1B-P minus (H5pm4174) infection, clearly supporting the notion that specifically the phosphorylation of E1B-55K by CK2 is crucial for proper virus growth. Another possible explanation for the reduced production of progeny virions can be deduced from the observed delay in Mre11 degradation during E1B-P minus infection (Fig. 16A) or the inhibited degradation of DNA ligase IV (Fig.

17A). Mre11, which forms with Rad50 and Nbs1 the MRN complex, is responsible, among others, for DNA double-strand break repair and has been shown to mediate adenoviral genome concatenation, like DNA ligase IV, if not disturbed in its functions (Stracker et al., 2002). Thus, it cannot be excluded that a delayed Mre11 or DNA ligase IV degradation during E1B-P minus infection might give the MRN complex more time to exert negative effects such as viral genome concatenation (Stracker et al., 2002) and in effect hinder the appropriate assembly of virions with genome content. However, analyses on viral genome concatemerization during E1B-P minus infection or during wt infection with subsequent CK2 inhibitor treatment, revealed no production of viral concatemers (Fig. 17B). Thus, the reason for reduced viral progeny production during E1B-P minus (H5pm4174) infection or CK2 inhibitor treatment remains obscure.

Of note, considering the fact that E1B-55K's phosphosites at the C terminus also roughly fit the criteria for glycogen synthase kinase-3 (S-X-X-X-pS [Doble and Woodgett, 2003; Meggio and Pinna, 2003]) and CK1 (pS-X-X-S/T [Meggio and Pinna, 2003]) consensus phosphorylation sites, it is far too early to say that CK2 is the sole kinase phosphorylating E1B-55K. Experiments are under way to clarify potential specific roles of these other two kinases in E1B-55K regulation by phosphorylation. Nevertheless, the data demonstrate for the first time that CK2 $\alpha$  plays a significant part in phosphorylation of E1B-55K and is also involved in threonine 495 phosphorylation *in vitro*.

## Part II

### **6 The cellular protein Usp7 interacts with E1B-55K, promotes adenoviral replication and transformation processes**

This part intensively elaborates the subject of Usp7 exploitation by HAdV5 E1B-55K to lay the ground for the third and last part of this work. Here, new and more detailed information is added to this subject by using combined Usp7 knockdown and small-molecule inhibitor assay approaches. Eventually, Usp7 not only regulates the stability of E1B-55K, but also of other adenoviral proteins. Consequently, virus growth is negatively affected. Interestingly, the defects in adenovirus progeny production after Usp7 knockdown or inhibition are quantitatively similar to those observed after phosphonegative E1B-55K virus mutant (H5pm4174) infection described in Part I.

#### **6.1 Usp7 interacts with E1B-55K**

The deubiquitinating enzyme Usp7 is known to be targeted by different viral proteins. For example, HSV-1 ICP0 and EBV EBNA1 were both shown to exploit Usp7's function in order to promote important viral functions (Boutell et al., 2005; Sivachandran et al., 2008).

In previous investigations, Usp7 was established as a new binding partner and essential factor for viral replication and oncogene-mediated transformation (Koyuncu, 2009).

To expand and substantiate those findings, further analyses were employed. First, endogenous Usp7 was immunoprecipitated from p53-negative H1299 cells transfected with a plasmid encoding wt pE1B-55K and stained for coprecipitated E1B-55K (Fig. 18A, lane 2). Additionally, H1299 and A549 (p53-positive) cells were mock infected and infected with H5pm4149 (E1B minus) or H5pg4100 (wt) virus. Subsequent Usp7 immunoprecipitation experiments confirmed Usp7-E1B-55K interaction in both cell lines (Fig. 18B, lanes 3 and 6). To verify this interaction in a life-cell setting, flow cytometry-based FRET (Foerster's Resonance Energy Transfer) analyses were employed as described by Banning and colleagues (Banning et al., 2010) with Usp7-CFP serving as a donor chromophore and YFP-E1B-55K as an acceptor chromophore (schematic Fig. 18C). By using this assay, it was possible to detect ca. 17% FRET-positive cells (FRET+; Fig. 18D), indicating an interaction of Usp7 and E1B-55K also in living cells. However, the relatively low amount of FRET+ cells compared to the positive control can be explained by CFP/YFP-tag interference and/or competition between

endogenous and exogenous Usp7. Nevertheless, FRET+ cells scored significantly more than the negative controls (CFP in cotransfection with YFP; Fig. 18D first FACS panel).

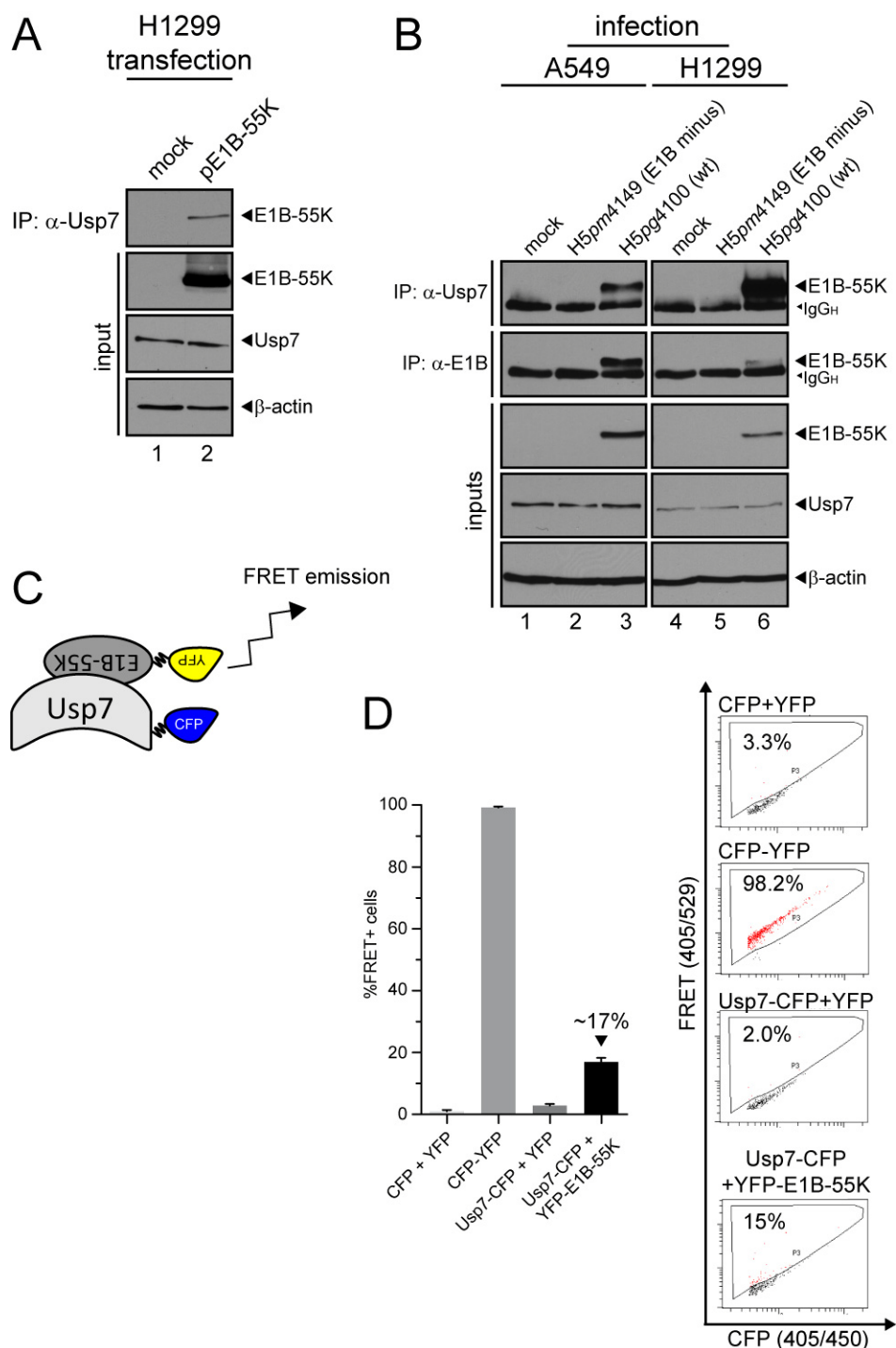


FIG 18 Usp7-E1B-55K interaction in different set-ups. (A) H1299 cells were transfected with vector pcDNA3 and vector encoding E1B-55K (pE1B-55K). 48 hours post transfection (h p.t.) cell lysates were subjected to immunoprecipitation with a Usp7 antibody (3D8). Proteins separated by SDS-PAGE were detected by Western blots with anti-E1B antibody (2A6). Western blot analyses of protein input levels are shown below for E1B-55K (2A6), Usp7 (3D8) and  $\beta$ -actin (AC-15). (B) A549 and H1299 cells either mock-infected or infected (MOI=20 FFU/cell) with H5pm4149 (E1B minus) and H5pg4100 (wt) were harvested 24 hours post infection and subjected to coimmunoprecipitation as described in (A). (C) Cartoon showing FRET emission after interaction of N-terminal YFP-tagged E1B-55K and C-terminal CFP-tagged Usp7. (D) H1299 cells were transfected with 1-8  $\mu$ g of pEYFP/pECFP, pECFP-YFP, Usp7-CFP or YFP-E1B-55K and PEI (1  $\mu$ g/ $\mu$ l) in a ratio 1:4 or 1:5, harvested 48 hours post transfection (h p.t.) and analyzed via FACS. S.e.m. from a minimum of six independent experiments are summarized. Representative primary FACS-plots are presented on the right.

Taken together, these and previous results unambiguously establish Usp7 as a novel interaction partner of E1B-55K.

## 6.2 Usp7 is relocalized during adenoviral infection

To determine whether adenoviral infection affects Usp7 subcellular localization in a time-dependent manner, extensive time course immunofluorescence studies were performed. A549 (and H1299 cells; data not shown) cells were mock infected or infected at an MOI of 20 FFU per cell with wt HAdV5 virus (H5pg4100) and then methanol-fixed at indicated hours post infection (h p.i.; Fig. 19A to E). Usp7 and E1B-55K (E1B) were probed with specific monoclonal antibodies (3D8 and 2A6 respectively) and visualized with double-label immunofluorescence microscopy. In uninfected cells (mock), Usp7 localizes diffusely in the nucleus with a few prominent dot-like structures (Fig. 19A, panels A to D). However, upon wt adenoviral infection (H5pg4100), Usp7 localization was dramatically changed. Several different relocalization patterns of Usp7 were observed which were categorized for each investigated time point with respect to E1B-positive cells. At 8 h p.i. (Fig. 19B, panels A to H), the majority of Usp7 showed no change, and only ca. 17% displayed a modest change in the redistribution pattern with more small dot-like structures in the nucleus compared to mock-infected cells (compare Fig. 19B, panel C [category 1] with Fig. 19B panel G [category 2]). In contrast, a heterogeneous Usp7 redistribution pattern could be observed at 16 h p.i. Due to different staining patterns, five categories were introduced for this time point. As indicated in Fig. 19C, panels A to D, 12% of E1B-positive cells appeared to have no relocalization of Usp7 at all (category 1). However, in 7.1% of the cells, Usp7 was diffusely distributed in the nucleus with large circular Usp7 structures accompanied by few prominent Usp7 foci (Fig. 19C, panels E to H, category 3). 12.2% of the cells displayed minor Usp7 ring-like structures (Fig. 19C, panels I to L, category 4) with an overall smaller diameter than in category 3. Additionally, these Usp7 rings were found throughout the nucleoplasm and did not exhibit significant overlap with the E1B-staining. The next two categories displayed a similar redistribution pattern among each other, but showed one striking difference: On the one hand, 31.6% of the E1B-positive cells were found to have numerous small disc-like Usp7 structures which can completely colocalize with nuclear E1B-55K (category 5, Fig. 19C, panels M to P). On the other hand, 36.7% of the E1B-positive cells were characterized by larger ring-like E1B-overlapping Usp7 structures (category 6, Fig. 19C, panels Q to T [36.7 %]).

With further progression into the late stage of infection (Fig. 19D, 24 h p.i.), Usp7 relocalization showed a new type of altered localization pattern, strictly following and overlapping with nuclear E1B-reticular network/ring-structures (Fig. 19D, panels U to X, category 7 [14.4%]). Of note, similar structures were previously described and shown to interconnect viral replication centers (Gonzalez et al., 2006). However, with the occurrence of the new phenotype, the other characteristic changes in Usp7 relocalization experienced different quantitative distribution. Phenotypes of category 1, 5 and 6 visualized at 24 h p.i., displayed no significant quantitative change in comparison to 16 h p.i. (compare Fig. 19C, panel A [12%] with Fig. 19D, panel A [9.6%]; Fig. 19C, panel M [31.6%] with Fig. 19D, panel M [28%]; Fig. 19C, panel Q [36.7%] with Fig. 19D panel Q [28%]). Changes in the quantitative distribution were only detected for category 3 and 4. The percentage of cells with one large circular Usp7 formation and several smaller Usp7 foci increased two-fold (category 3, compare Fig. 19C [7.1%] with Fig. 19D [14.4%]), whereas the amount of cells from category 4 showing smaller Usp7 rings dropped more than 50% at 24 h p.i. (category 4, compare Fig. 19C [12.2%] with Fig. 19D [5.6%]).

These changes probably reflect the progress of Usp7 redistribution throughout the course of infection, but also the asynchronous infection stages of the different cells. According to the phenotypic quantification at 16 and 24 h p.i., relocalization patterns of category 5 and 6 predominate, indicating that functional exploitation of Usp7 by E1B-55K (assuming there is one) might take place in viral replication center-resembling structures in the nucleus at the start of the late phase of infection.

Interestingly, at the very late phase of infection (48 h p.i.), several profound changes could be observed. Here, almost all E1B-positive cells displayed changes in Usp7 distribution. The already known phenotypes of the categories 3 and 5 were observed again (Figure 19E, panels A to H). However, at 48 h p.i., the cells showing numerous small ring-like Usp7 structures with E1B-overlap constituted only 11.4% of the E1B-positive cell population (category 5, compare Fig. 19D, panels M to P [28%] with Fig. 19E, panels E to H [11.4%]), whereas almost no quantitative change in the amount of cells representing category 3 could be detected (category 3, Fig. 19D and E, 14.4% and 14.9% respectively). Additionally, probably owing to the general nuclear morphological changes and the late stage of infection, the majority of the cells exhibited two types of new relocalization patterns (Fig. 19E, category 8 and 9). A considerable amount of 28.1% of the E1B-positive cells displayed a Usp7 staining with long, dense structures. These seemed to be interconnected Usp7 foci significantly overlapping with

E1B-staining. The largest cohort of the E1B-positive cells (45.6%, category 9) formed one or more larger, discrete Usp7 ring-like formations also overlapping with E1B-staining (Fig. 19E panels M to P).

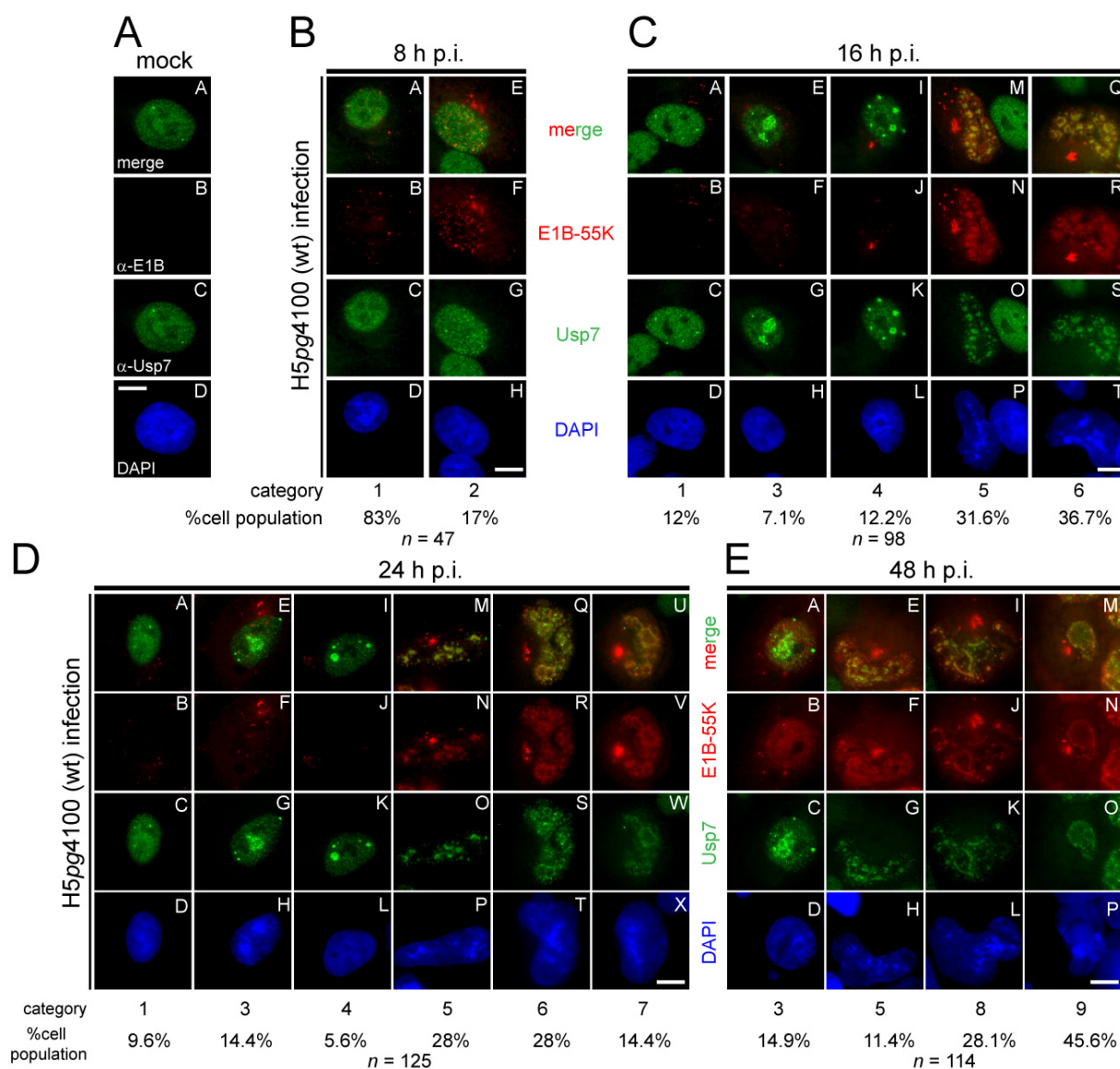


FIG 19 Indirect immunofluorescence to analyze Usp7 localization during adenoviral infection in comparison to E1B-55K. (A) Mock-infected A549 cells were analyzed by *in situ* immunofluorescence staining for E1B-55K (2A6), Usp7 (3D8), and DNA content (DAPI). (B-E) A549 cells infected with H5pg4100 (wt; MOI=20 FFU/cell) were analyzed by *in situ* immunofluorescence staining for E1B-55K (2A6), Usp7 (3D8), and DNA content (DAPI). Represented are the major phenotypes observed in A549 cells and which were categorized as indicated. Scale bar=10  $\mu$ m.

Taken together, at 16 h p.i., most of the E1B-positive cells occurred to have Usp7 relocalization in the nuclear compartment accompanied by E1B costaining probably indicating sites of interaction which resemble viral replication centers. Nevertheless, considering Usp7 redistribution occurring in the absence of apparent E1B costaining, (Fig.

19C, panels E to L), it can be speculated that another viral protein is involved in Usp7 relocalization.

### **6.3 Qualitative and quantitative assessment of Usp7-E1B colocalization**

To assess whether the observed colocalization between Usp7 and E1B-55K was qualitatively and quantitatively significant, the immunofluorescence data sets were additionally examined with the Imaris software analysis tool.

As a negative gating control, mock-infected cells were analyzed, which showed no R-correlation (Fig. 20A, panels A to C). An R value of 1 indicates a perfect correlation.

In general, the R values at the different infection time points provide a reliable estimation of the positive linear correlation between red and green staining indicating strong colocalization (Fig. 20B, C and D, each panels A to C).

As shown in sections 6.2 for 16 h p.i., 68.3% of E1B-positive cells were found to have Usp7 relocalized into category 5 and 6 (Fig. 19C, panels M to T). Of those two categories, ca. 25.4% of the cells displayed Usp7-E1B colocalization with a mean Pearson's correlation coefficient  $R^2$  value of 0.31 (Fig. 20B), indicating a good and reliable colocalization. Following the progress of infection at 24 h p.i., the amount of total Usp7-E1B colocalization found in categories 5, 6 and 7 (Fig. 19D, panels M to X [70.4%]) colocalizing with E1B-55K was modestly increased to ca. 34.1% with an almost equal mean  $R^2$  value of 0.39 (Fig. 20D). Finally at 48 h p.i., the amount of colocalized Usp7-E1B-55K further increased up to 49.5% (Fig. 19E, categories 5, 8 and 9) with a mean  $R^2$  value of 0.22. Different  $R^2$  values of several images were plotted and showed no significant difference except for 24 and 48 h p.i. (Fig. 20E).

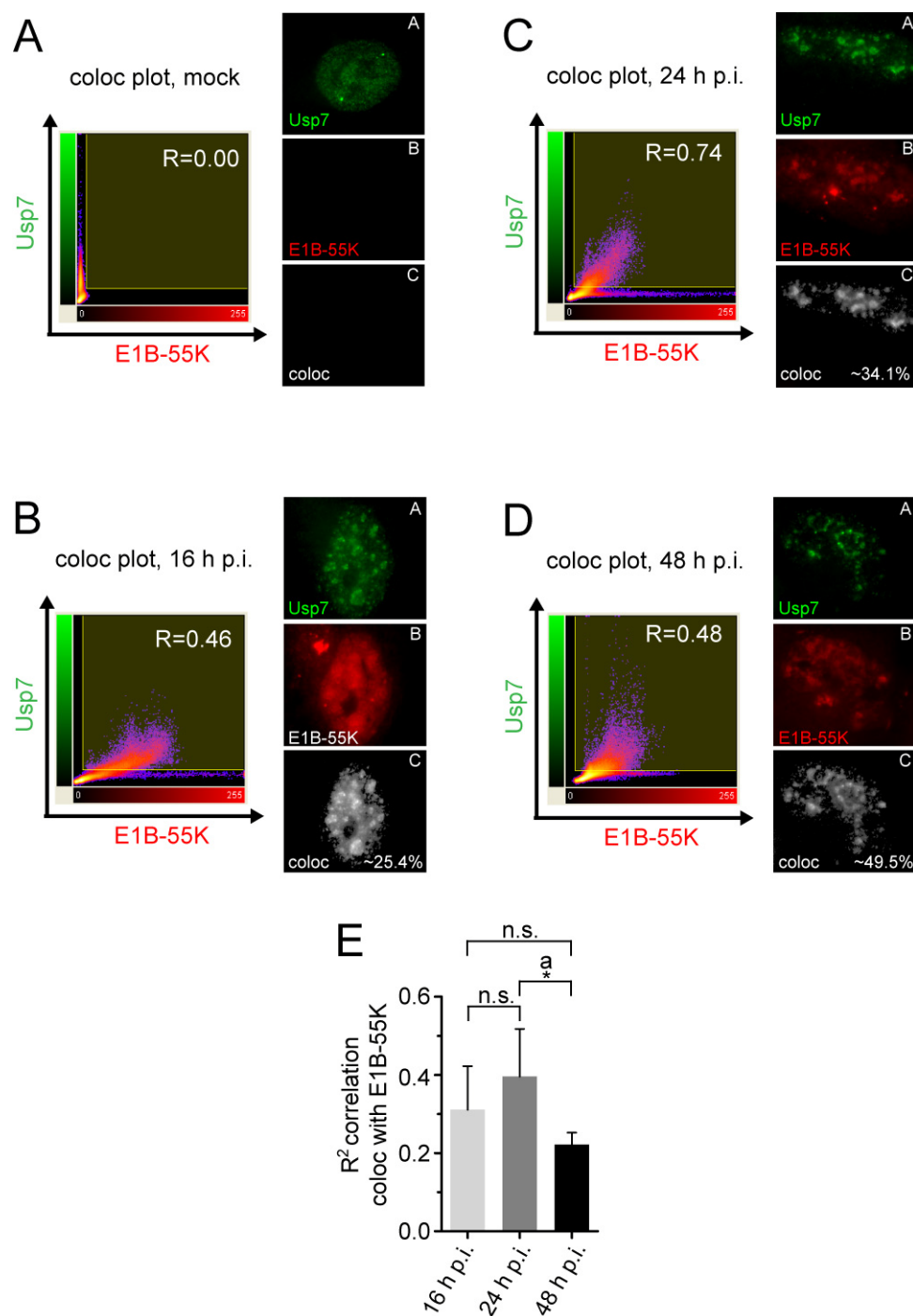


FIG 20 Image processing of immunofluorescence data from Usp7-E1B-55K costainings. (A) Immunofluorescence image data from mock-infected A549 cells were used as a negative gating control. (B-D) Immunofluorescence image data sets from infected A549 cells at different time points were analyzed for quality of colocalization. (E) All images were analyzed with Imaris 7.2.3. (Bitplane) to obtain the Pearson's correlation coefficient and the  $R^2$  values were plotted in the presented graph. A Student  $t$  test was done to assess statistical significance (GraphPad Prism 5). At least six images were analyzed for each time point. \*  $P < 0.05$ . n.s.=not significant.

In conclusion, these results demonstrate that Usp7 relocalization leads to increased costaining with E1B-55K which, was further substantiated with the software-based colocalization analyses. Together with the data from biochemical binding assays, it can be suggested that Usp7-E1B-55K interaction takes place in the nuclear compartment in structures resembling viral replication centers.

#### **6.4 Usp7 is relocalized to viral replication centers during adenoviral infection**

Strikingly, the relocalization pattern of Usp7 during wt adenoviral infection (H5pg4100) strongly resembled staining patterns of the adenoviral E2A protein (also called DBP, Fig. 21A, [Doucas et al., 1996]). E2A is a single-stranded DNA (ssDNA) binding protein not only colocalized with sites of viral ssDNA but also surrounding sphere-shaped sites of double-stranded DNA and is thus a marker for sites of both transcription and replication (Weitzman et al., 1996).

To test whether Usp7 is relocalized to sites of viral DNA replication and transcription, *in situ* costainings of E2A and Usp7 were prepared to detect significant colocalization of both proteins also in a time-dependent manner. In a similar approach as above (Figure 19), A549 cells were infected at an MOI of 20 FFU/cell and methanol-fixed at indicated time points. By analyzing the staining patterns of Usp7 in E2A-positive cells, it became evident that nearly all the cells displayed Usp7 staining patterns tightly bound to the E2A-stained structures. However, large and ring-like E2A centers, representing cells in the late phase of infection, partially colocalized like it could be seen with E1B-55K (Fig. 21F, blue arrow and dotted lines), but to a certain extent also surrounded Usp7 structures (Fig. 21C, panels Q to T and 21D, panels M to T; Fig. 21F, indicated by a yellow arrow and dotted lines).

In general, the phenotypes here can be assigned to those observed in Figure 19. Therefore only the different phenotypes of Usp7 relocalization in connection to E2A staining are shown and no further quantification was assessed.

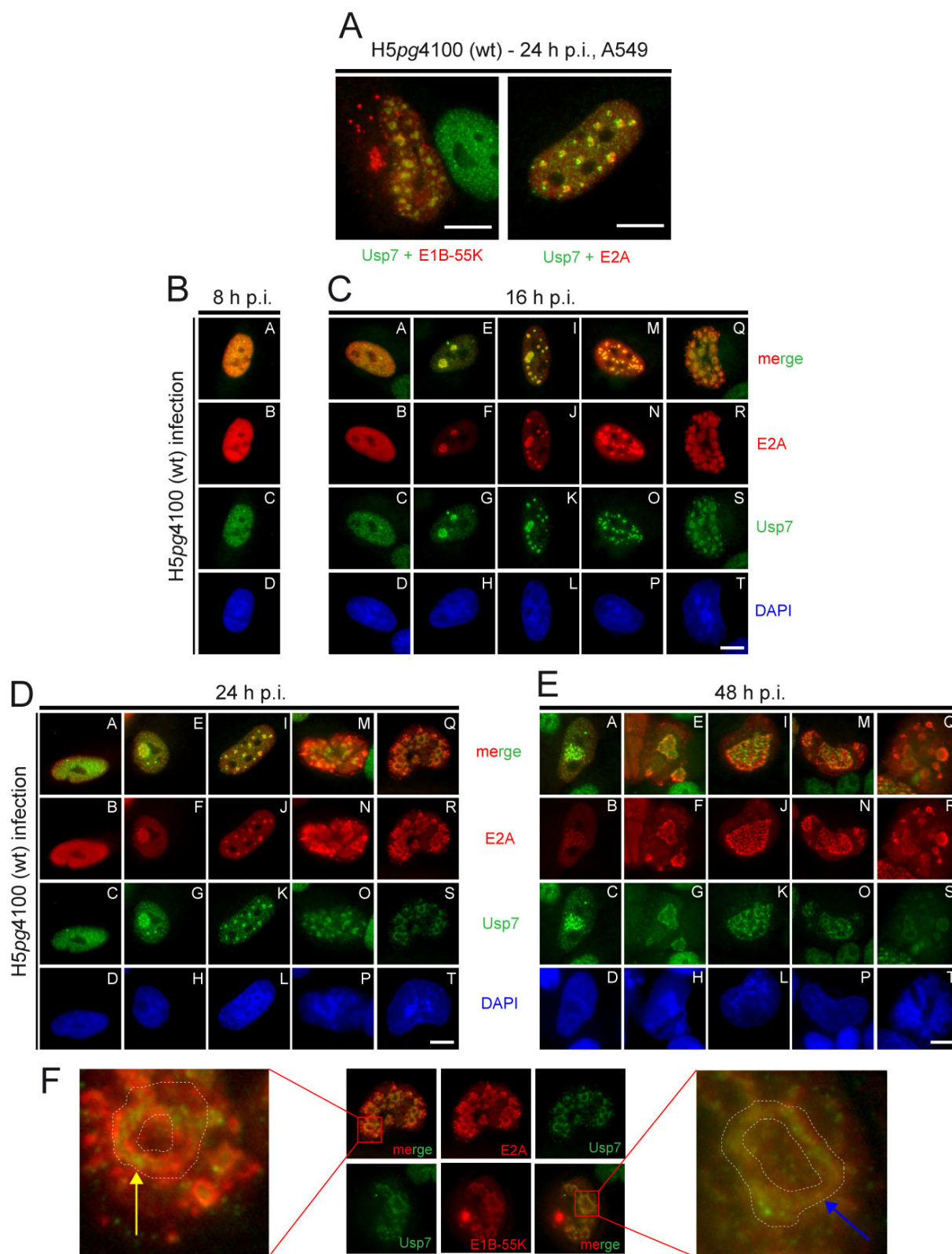


FIG 21 Indirect immunofluorescence to analyze the Usp7 localization during adenoviral infection in comparison to E2A. (A) H5pg4100-infected A549 cells 24 hours post infection (h p.i., MOI=20, FFU/cell) costained for Usp7 (3D8) and E1B-55K (2A6) (left) or Usp7 (3D8) and E2A (B6-8) (right) in direct comparison. (B-E) A549 cells infected with H5pg4100 analyzed at indicated time points (wt; MOI=20 FFU/cell) were analyzed by *in situ* immunofluorescence staining for E2A (B6-8), Usp7 (3D8), and DNA content (DAPI). Represented are the major phenotypes observed in A549 cells. (F) wt-infected A549 cells at 24 h p.i. (MOI=20 FFU/cell). Specific sections are enlarged, outlined with dotted lines, and indicated with a yellow or blue arrow as referred to in the text. Scale bar=10  $\mu$ m.

Taken together, from these observations, it can be concluded that the time-dependent Usp7 relocalization is strictly related to the formation of viral replication centers represented by the E2A staining.

### **6.5 Qualitative and quantitative assessment of Usp7-DBP colocalization**

To further foster the findings on the Usp7-E2A immunofluorescence data set, the Imaris software analysis tool was used to qualitatively evaluate colocalization (as described in section 6.3). Mock-infected cells served as negative gating control and no R-correlation existed (Fig. 22A). The following analyses provided a strong R correlation of Usp7-E2A colocalization among all investigated time points (Fig. 22B to 22E). Furthermore, a quantitative assessment of the  $R^2$  values supported the colocalization correlation between Usp7 and E2A (Fig. 22F).

Next, the interaction of Usp7 with E2A was examined. For this, combined immunoprecipitation-immunoblotting assays were carried out using total cell lysates from wt (H5pg4100) and E1B-55K-negative (H5pm4149) virus-infected A549 and H1299 cells (Fig. 22G). As anticipated, E2A coprecipitated with Usp7 after infection of either cell line. Infection with the E1B minus virus and subsequent coimmunoprecipitation revealed that E2A interacts with Usp7 in the absence of E1B-55K (Fig. 22G, A549 cells, lane 2) to the same extent as during wt (H5pg4100) infection in A549 cells. In contrast, in H1299 cells, Usp7-E2A interaction could only be detected in wt virus-infected cells, and was generally much weaker in comparison to A549 cells. This was probably due to the lower input levels of E2A in H1299 cells (compare E1B-55K input Fig. 22G), but might also indicate differences between both cell lines in their ability to promote viral protein production. Since the infection and coimmunoprecipitation experiments were performed in parallel with the same infection masters, the comparison of both cell lines was legitimate.

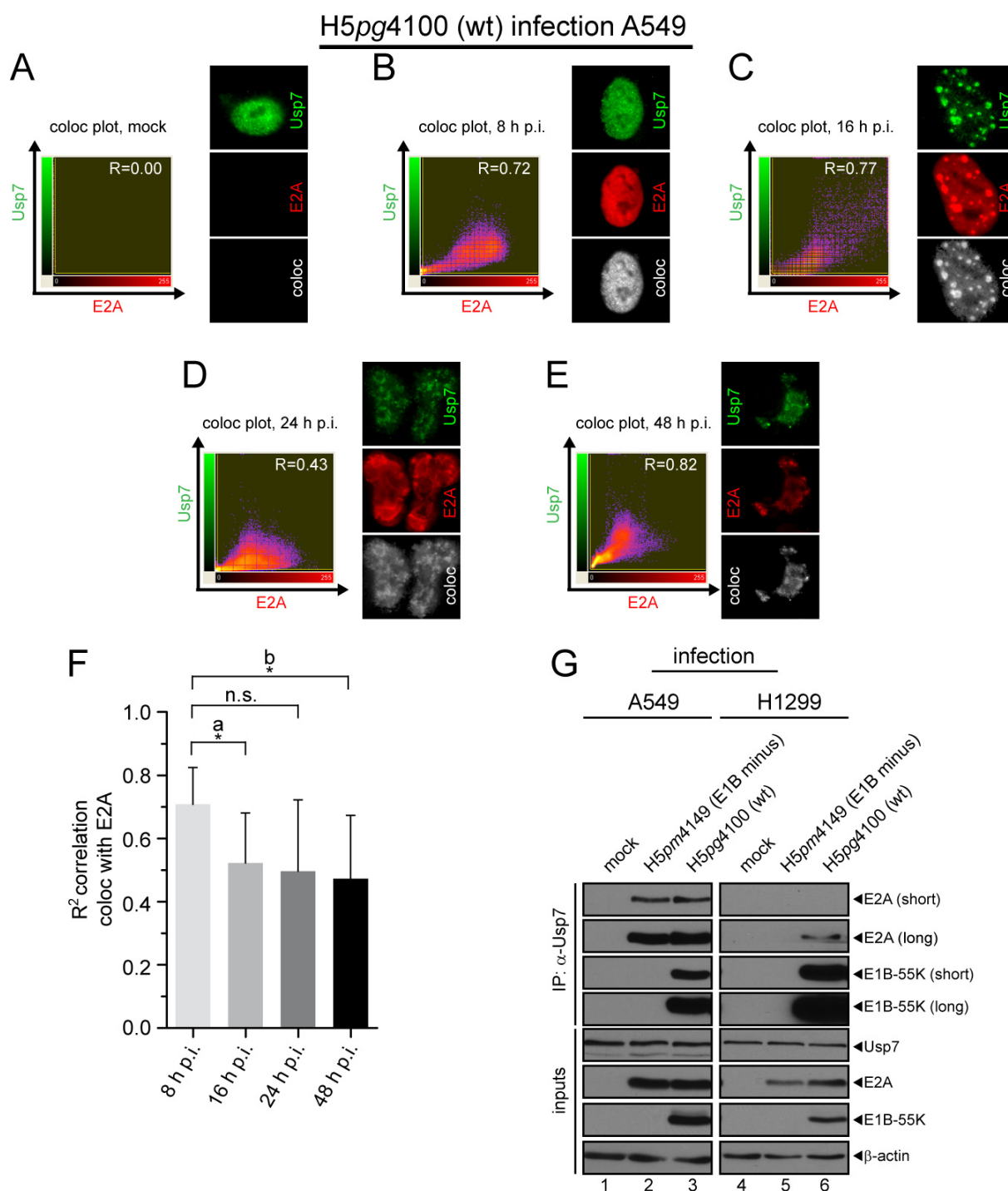


FIG 22 Image processing of immunofluorescence data from Usp7-E2A costaining to underline Usp7-E2A interaction. (A) Immunofluorescence image data from mock-infected A549 cells were used as a negative gating control. (B-E) Immunofluorescence image data sets from infected (H5pg4100) A549 cells at different time points were analyzed for quality of colocalization. (F) All images were analyzed with Imaris 7.2.3. (Bitplane) to obtain the Pearson's correlation coefficient and the  $R^2$  values were plotted in the presented graph. A Student  $t$  test was performed to assess statistical significance (GraphPad Prism 5). At least 10 images were analyzed for each time point. \*  $P < 0.05$ . (G) A549 and H1299 cells either mock-infected or infected (MOI=20 FFU/cell) with H5pm4149 (E1B minus) and H5pg4100 (wt) were harvested 24 hours post infection and subjected to coimmunoprecipitation with a Usp7 antibody (3D8). Proteins separated by SDS-PAGE were detected by Western blots with anti-E1B antibody (2A6) and anti-E2A (B6-8) antibody. Western blot analyses of protein input levels are shown below for E1B-55K (2A6), E2A (B6-8), Usp7 (3D8) and  $\beta$ -actin (AC-15).

Nevertheless, these findings present E2A as a new interaction partner of Usp7 in A549 and H1299 cell systems independent of E1B-55K. These findings also support the idea of E2A being involved in Usp7 relocalization since significant colocalization was found to be present as early as 8 h p.i. (Fig. 21B).

## 6.6 Introduction into a new class of inhibitors

Inhibition of enzymatic activity is a strong tool to investigate the functional roles of protein activity in a given system. Since Usp7 is a cysteine protease, it was of great interest to find an inhibitor against Usp7. Eventually, in 2006 Guedat and colleagues (Guedat et al., 2007) released a patent describing a substance class of novel cysteine protease inhibitors. Specifically, one compound and several derivatives were found to efficiently inhibit deubiquitinating enzyme activity, among them Usp7. However, those chemical substances were not commercially available. Hence, the collaboration partners Prof. Chris Meier and Christina Arbelo (Department of Chemistry/Organic Chemistry at the University of Hamburg) resynthesized one compound described in the patent (Guedat et al., 2007; example 1), in the following referred to as “HBX” (Fig. 23A). With this inhibitor at hand, it was possible to conduct further analyses concerning the role of Usp7 in adenoviral infection and transformation processes which is tackled in the next sections.

In a first attempt to characterize HBX, MTS-based (3-(4, 5-dimethylthiazol-2-yl)-5-(3-carboxymethoxyphenyl)-2-(4-sulfophenyl)-2H-tetrazolium) proliferation assays were carried out on cell lines used for the studies in this work. As shown in Fig. 23C to F, sigmoidal dose response curves were generated for three inhibitor treatment durations (24, 48 and 72 h) with several dilution rows at least in triplicate. The summarized  $GI_{50}$  values are represented in Figure table 23B.

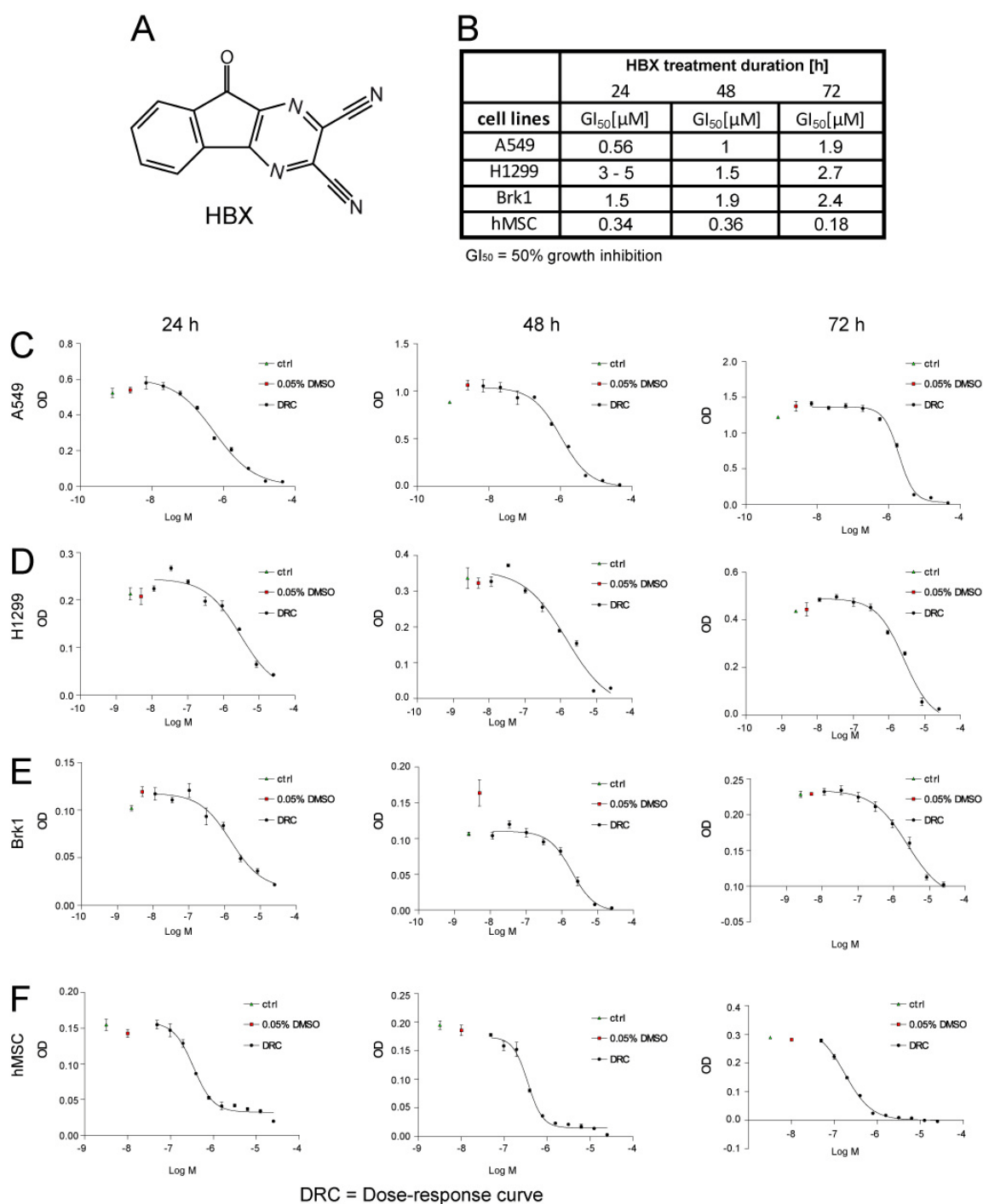


FIG 23 Assessing Dose-response curves of different cell lines upon Usp7 inhibitor HBX treatment. (A) Chemical structural formula of the Usp7 inhibitor HBX. (B) Several growth inhibitory 50 (GI<sub>50</sub>) values are summarized for the indicated cell lines. (C-F) A549, H1299, Brk1 and hMSC cells were seeded into 96-well plates ( $1.5 \times 10^3$ /well). Treatment of cells with a series of HBX concentration was performed for 24, 48, 72 h or cells were DMSO treated or left untreated (ctrl). S.e.m. values from a minimum of three independent experiments (3.2.11).

The three tumor cell lines A549, H1299 and Brk1 showed acceptable and similar tolerance to the inhibitor in the micromolar range (Fig. 23C, D and E). In contrast, the primary hMSC cells tolerated lower concentration of HBX (Fig. 23F), possibly owing to their primary cell characteristics.

Altogether, these results could be used for an estimation of inhibitor concentrations for subsequent experiments.

### **6.7 Analyses of the HBX effect on cell growth and viability**

Next, optimal conditions for infection experiments with subsequent inhibitor treatment were assessed along with cell growth and viability. Previous reports demonstrated that loss of Usp7 through knockout leads to decreased proliferation of the respective cell line (Cummins and Vogelstein, 2004). Therefore, with Usp7 having critical roles in cell proliferation, it was necessary to determine inhibitor treatment conditions in which cell growth was not significantly inhibited. Otherwise it would be difficult to distinguish between cell growth defects or specific compound-mediated effects leading to a negative outcome on virus yield. In the following, time-of-addition experiments after mock infection were performed to determine acceptable cell growth inhibition (data not shown). In effect, it turned out that 15 hours of inhibitor treatment prior to cell harvest worked the best for all investigated cell lines. As shown in Fig. 24A A549 cells exhibited no (statistically) significant decrease in cell number compared to untreated cells 24 hours post mock infection (h p.m.i.) at both HBX concentrations. However, a significant reduction of the cell number was observed 48 h p.m.i. (Fig. 24A) after HBX application at both concentrations (~25% reduction). Nevertheless, trypan blue exclusion to determine the number of viable cells displayed no significant cytotoxic effect on A549 cells either 24 or 48 h p.m.i., meaning that cell cytotoxic effects could be excluded in subsequent experiments (Fig. 24B). Similarly, H1299 cells experienced no cell growth defect after HBX treatment 24 h p.m.i., but underwent ca. 25% reduction 48 h p.m.i. (Fig. 24C). But again, no negative change in the ratio of viable to dead cells in comparison to untreated cells could be observed (Fig. 24D).

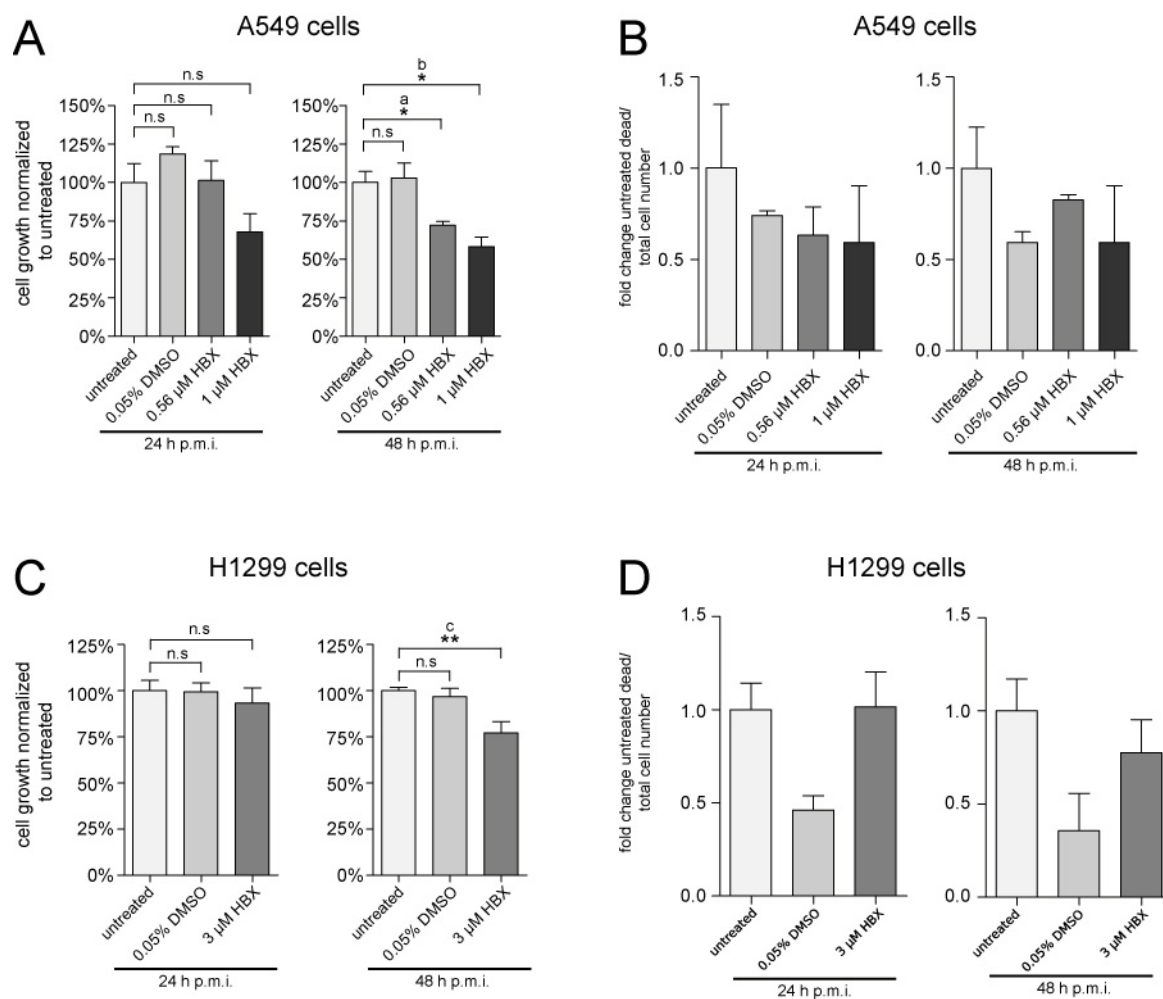


FIG 24 Analyses of the growth behavior of A549 and H1299 cells upon HBX treatment. (A+C)  $1.5 \times 10^6$  cells were seeded 15-20 h before HBX treatment start. Cells were treated with HBX or DMSO for a total of 15 h and harvested 24 or 48 hours post mock infection (h p.m.i.) and counted. S.e.m. of at least 3 independent experiments. \*  $P < 0.05$ , \*\*  $P < 0.01$ . (B+D) The number of dead cells was divided by the total cell number and then normalized to untreated. Trypan blue positive cells were counted after same experimental conditions as in (A+C). n.s.=not significant.

In summary, it was possible to find suitable conditions for HBX treatment in infection experiments where cell growth and viability were not significantly affected. Nonetheless, a particular cell growth defect after Usp7 inhibition was obtained at later stages of mock infection which first corresponds to previously performed experiments and was therefore expected and second will be considered in following experiments.

## 6.8 HBX does not affect Usp7 relocalization during adenoviral infection

In the preceding sections, the conditions for further experiments with HBX were defined. At first, the effect of inhibitor treatment upon cell morphology and/or redistribution of Usp7

during adenoviral wt infection (H5pg4100) were examined. Therefore, immunofluorescence analyses on HBX-treated and wt-infected A549 and H1299 cells were conducted.

Morphological changes or changes in the Usp7 re- and/or E1B-distribution could not be detected in A549 or H1299 cells after inhibitor treatment, and neither in uninfected nor infected cells at both investigated time points (compare Fig. 25A to 25D each panels A to R). Interestingly, Usp7 inhibitor treatment affected the amount of E1B-positive cells in both cell lines. Here, 37.4% (A549) or 95.6% (H1299) reduction could be observed and quantified 24 h p.i. (Fig. 25A and 25C). However, no decrease in the number of E1B-positive cells could be detected 48 h p.i., indicating that the inhibitor cannot diminish E1B-55K levels at the very late stage of infection.

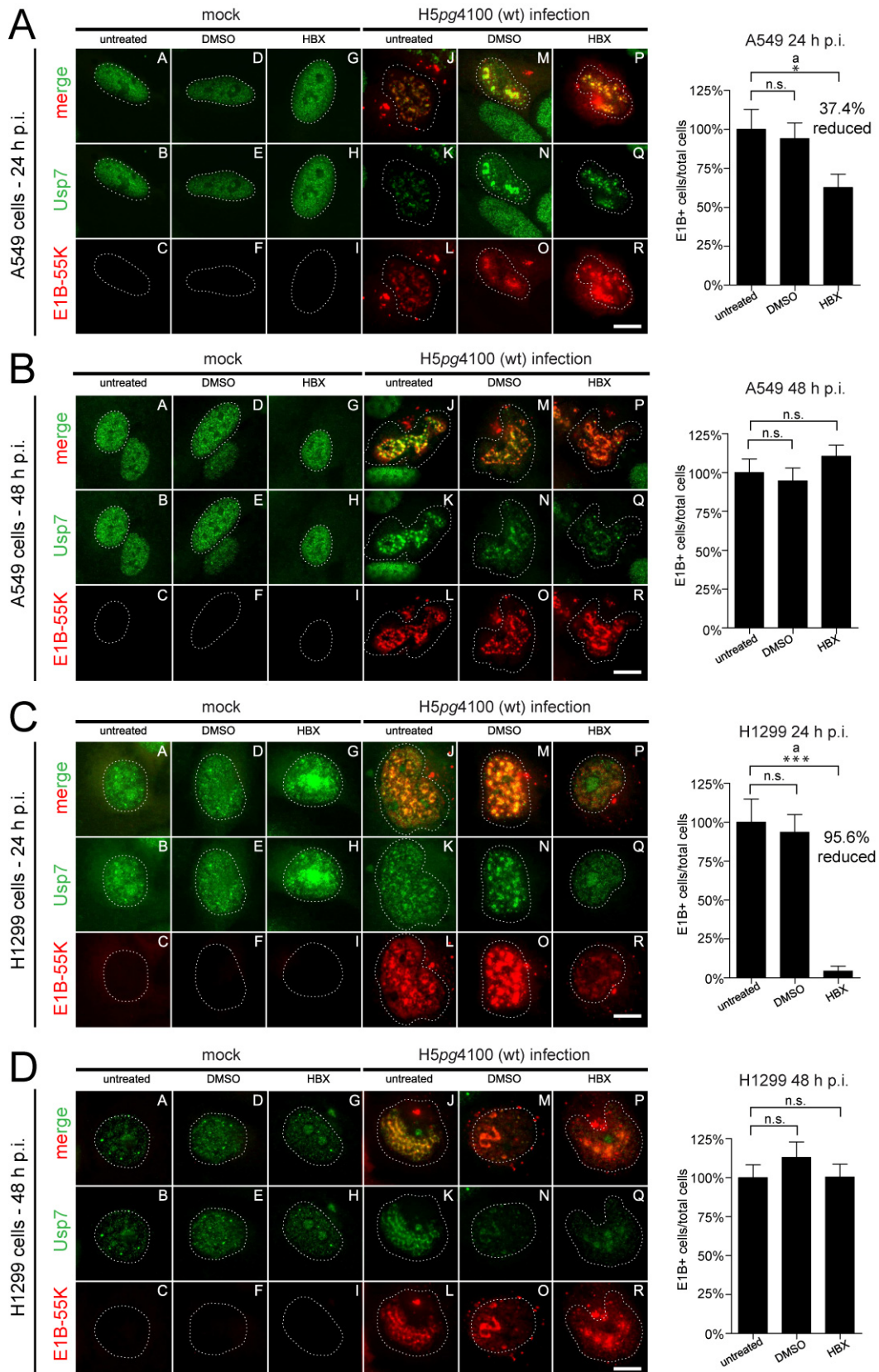


FIG 25 HBX treatment causes no change in the localization patterns of Usp7 and E1B-55K in infected cells but reduces the amount of E1B-positive cells. (A to D) A549 and H1299 cells were infected with H5pg4100 virus (MOI=20 FFU/cell) and analyzed by *in situ* immunofluorescence staining for E1B-55K (2A6) and Usp7 (3D8). Additionally, cells were subjected to DMSO or HBX treatment as described in Fig. 24. E1B-positive cells were quantified and normalized to total cell number. S.e.m. of at least three experiments. \*  $P < 0.05$ , \*\*\*  $P < 0.001$ . Border of nuclei are represented by dotted lines. Scale bar=10  $\mu\text{m}$ . n.s.=not significant.

Taken together, these results demonstrate that Usp7 inhibitor treatment does not affect subcellular localization of Usp7 and E1B-55K, but negatively affects E1B-55K appearance in the cell population.

### **6.9 Usp7 knockdown or inhibition reduces E1B-55K steady-state levels**

The obtained data from the E1B immunofluorescence quantification are suggestive of a functional consequence for the Usp7-E1B-55K interaction. To examine the relationship of this interaction more in detail, the consequences of reducing Usp7 steady-state levels and Usp7 inhibition for E1B-55K were analyzed. For this, a Usp7 knockdown cell line was generated using shRNA-mediated stable knockdown in H1299 cells.

The cell clones stably transfected with shRNA against Usp7 or empty vector shRNA were tested for altered growth behavior, which might influence virus replication. In effect, the H1299-derived Usp7 knockdown cell line HU5 (up to 86.6% knockdown efficiency, Fig. 27A, lanes 6 to 10) and its corresponding control cell line HC2 (stably transfected with shRNA vector control, Fig. 27A, lanes 1 to 5) exhibited almost identical growth rates compared to H1299 cells, indicating that HC2 and HU5 can be compared in regard to effects resulting from Usp7 knockdown (Fig. 26A) and that growth defects would not apply for possible negative effects observed in HU5.

Transfection of E1B-55K encoding plasmid into the Usp7 knockdown cell line HU5 demonstrated severely reduced E1B-55K protein steady-state levels although 1.5 times more protein lysates were loaded (Fig. 26B, lane 3). Accordingly, Usp7 inhibitor treatment led to the same effect in A549 and H1299 cells (Fig. 26C, lanes 6 and 9) and at the same time did not affect Usp7 levels (Fig. 26C, Usp7 stainings). Same lysates subjected to Usp7-IP, consequently demonstrated reduced precipitation of E1B-55K with Usp7 in the inhibitor-treated sample (Fig. 26C, lane 9 Usp7 IP short and long exposure).

In summary, knockdown of Usp7 or inhibitor treatment led to severely reduced E1B-55K steady-state levels, indicating a stabilizing role of Usp7 for E1B-55K and underlining the specific effect of the inhibitor used in the assays. Furthermore, these results support the immunofluorescence quantification data (Fig. 25).

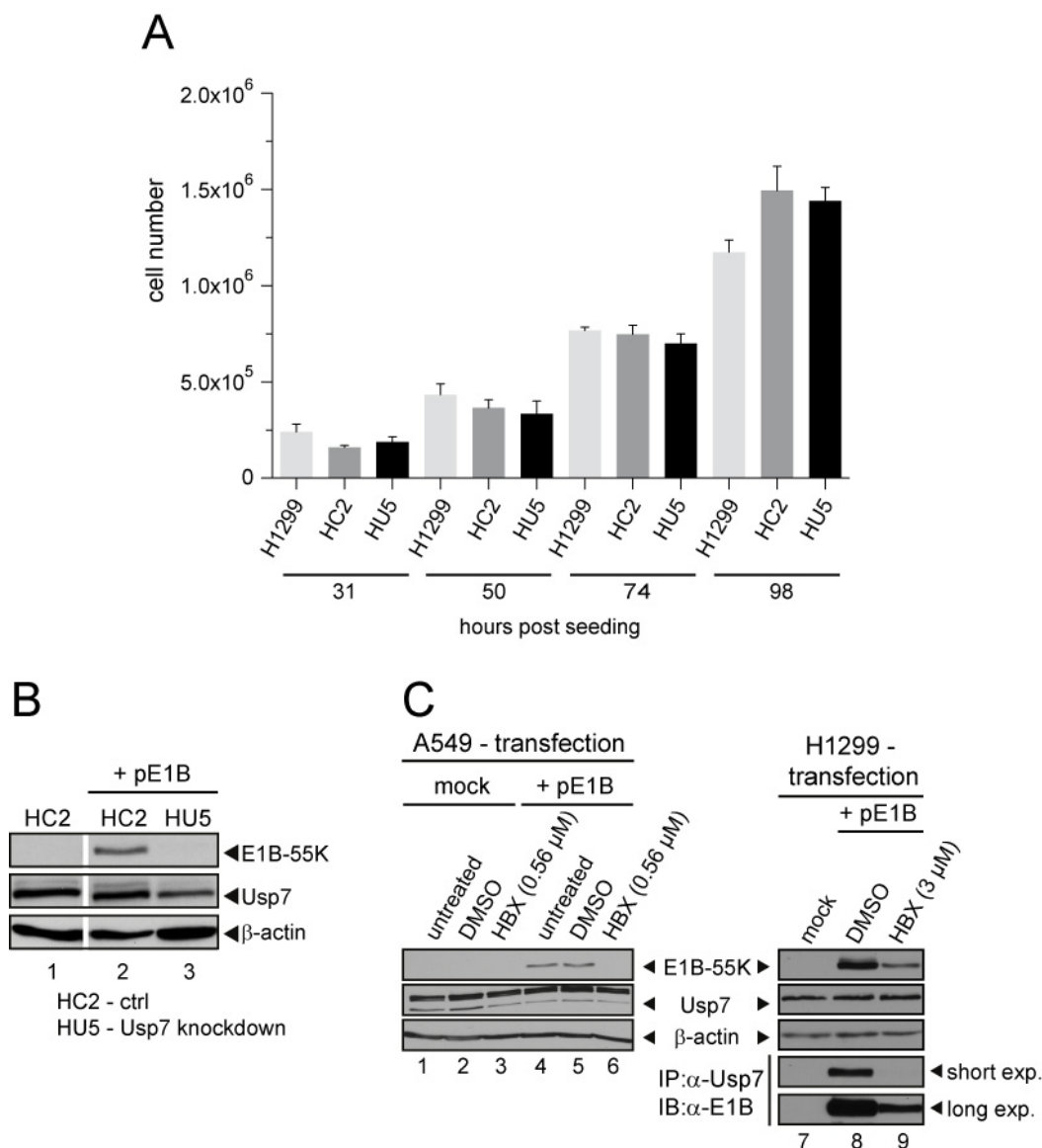


FIG 26 Usp7 knockdown and its effect on E1B-55K. (A)  $1.5 \times 10^5$  cells (indicated) were seeded into 6-well plates and cell number was determined at the indicated times post seeding. Three independent experiments were conducted and results plotted. (B) Equal numbers of the indicated cells were seeded, transfected using PEI with pcDNA3 or plasmid vector containing E1B-55K. 30 hours post transfection, cells were lysed and immunoblotted. Antibodies detecting E1B-55K (2A6), Usp7 (3D8) and  $\beta$ -actin (AC-15) were used. (C) A549 or H1299 cells were transfected with 2  $\mu$ g plasmid vector pcDNA3 (mock) or with 2  $\mu$ g pE1B-55K (wt E1B-55K) using 20  $\mu$ g PEI as transfection reagent. Cells were treated with DMSO, HBX (0.56  $\mu$ M, 6 h p.t. addition) or left untreated. Cells were harvested 30 hours post transfection (h p.t.), lysed and immunoblotted. Antibodies detecting E1B-55K (2A6), Usp7 (3D8), and  $\beta$ -actin (AC-15) were used. Additionally, H1299 cells were subjected to coimmunoprecipitation with Usp7 antibody 3D8 as described in Fig. 18A.

## 6.10 Impact of Usp7 knockdown on adenoviral replication

Subsequently, it was necessary to determine whether Usp7 knockdown or inhibition affected other adenoviral proteins during the course of time in infection and whether replication efficiency was affected. For this, the effect of Usp7 knockdown on the ability of wt adenovirus (H5pg4100) to promote viral early and late protein production was investigated.

Strikingly, adenovirus infection in the Usp7 knockdown cell line HU5 revealed that early protein steady-state levels (Fig. 27A, lanes 6 to 10, E1A, E1B-55K, E2A) and late structural protein levels (capsid proteins) were negatively affected by Usp7 knockdown in the H1299 background. Additionally, virus yield experiments performed in HC2 and HU5 at an MOI of 20 FFU/cell demonstrated up to 72.5% reduced viral progeny numbers 24 h p.i. in HU5 and still 26% reduction 48 h p.i. (Fig. 27B).

In conclusion, Usp7 probably exerts global positive effects upon adenoviral protein steady-state levels which can be made visible using artificial decrease of Usp7 levels. As expected, those general decreases in protein steady-state levels led to severely reduced progeny virion production.

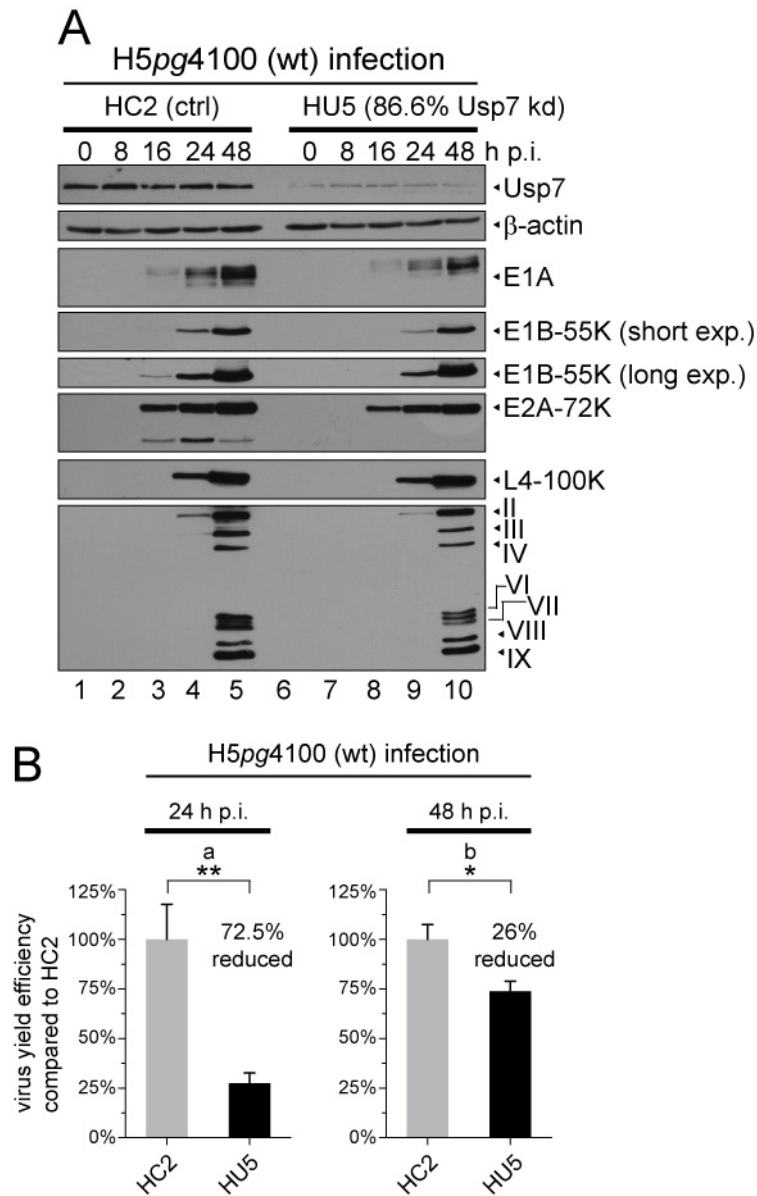


FIG 27 Usp7 knockdown in H1299 cells has a negative effect on adenoviral proteins and virus growth. (A) HC2 and HU5 cells were mock infected or infected in parallel with H5pg4100 (wt) (MOI=20 FFU/cell) and harvested at the indicated time points. Total cell extracts were prepared, separated by SDS-PAGE, and immunoblotted for the indicated proteins. (B) Same procedure as in (A), but here virus was extracted at indicated time points. The virus yield was determined by quantitative E2A-72K immunofluorescence staining (B6-8) on HEK293 cells. The results represent the average of at least three independent experiments. Bars indicate the standard error of the mean values. Virus yield efficiency is represented as a percentage of H5pg4100 (wt; MOI=20) in HC2 yield efficiency. \* P<0.05, \*\* P<0.01.

## 6.11 Impact of Usp7 inhibition on adenoviral replication

In order to investigate whether Usp7 inhibition leads to similar effects as Usp7 knockdown, infection experiments in H1299 and A549 cells were performed with subsequent inhibitor treatment. Usp7 protein steady-state levels were not affected after inhibitor treatment either in infected or mock-infected cells in both cell lines (Fig. 28A to D, lanes 1 to 6 Usp7 staining). Similar to the knockdown experiments, a reduction of E1B-55K and structural capsid proteins could be detected after HBX treatment in both cell lines (Fig. 28A and B, lane 3). However, E1B-55K decrease could only be observed 24 h p.i., but not 48 h p.i., consistent with the immunofluorescence quantification data (compare Fig. 25B and D with Fig. 28A and B, lane 6). This may suggest that functional inhibition of Usp7 cannot overcome the probably high transcription-translation activity at this stage of infection (at least for the early protein E1B-55K). Interestingly, E1A levels seemed to increase whereas E2A levels did not change in both cell lines and L4-100K levels displayed a modest decrease after HBX incubation (Fig. 28A and B, lane 3). It can be assumed that differences between both approaches (knockdown vs. inhibition) may reflect variances in efficiency of functional inhibition.

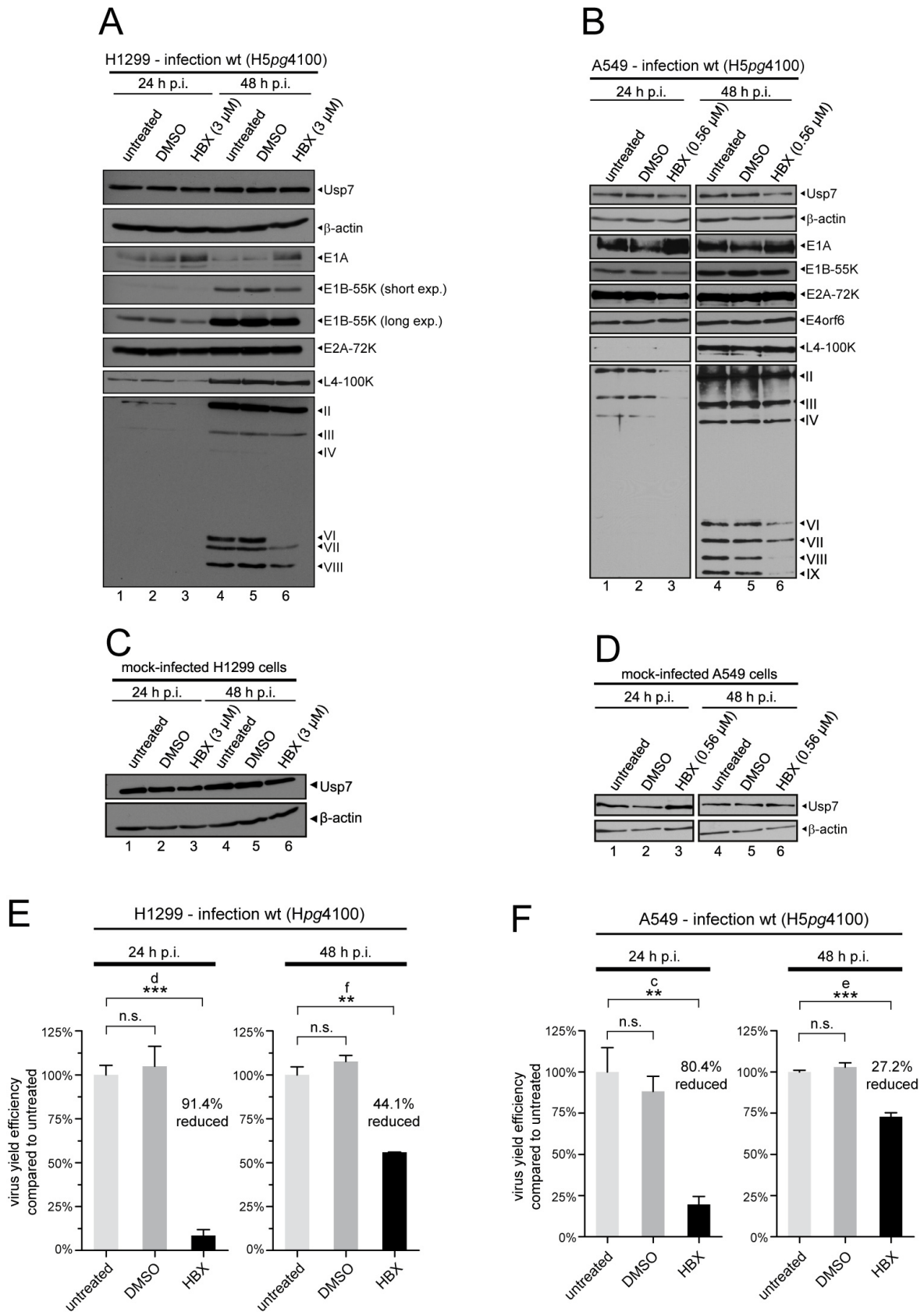


FIG 28 HBX treatment leads to negative effects on adenoviral proteins and virus growth. (A+B) H1299 and A549 cells were infected with H5pg4100 (wt) (MOI=20 FFU/cell). 15 h before harvest cells were treated with DMSO or HBX with the indicated concentrations and harvested at the indicated time points post infection. Total cell extracts were prepared, separated by SDS-PAGE, and immunoblotted for the indicated proteins. (C+D) Same as (A+B). Exception: Cells were left uninfected. (E+F) Same as (A+B). Exception: Virus was extracted at the indicated time points and virus yield determined as described in 27B. Three independent experiments were performed. S.e.m. \*\*  $P < 0.01$ , \*\*\*  $P < 0.001$ . n.s.=not significant.

Importantly, upon compound treatment (A549  $GI_{50} = 0.56 \mu\text{M}$ ; H1299  $GI_{50} = 3 \mu\text{M}$ ), virus growth was severely impaired in both cell lines and even at a later time point of inhibitor application (start 33 h p.i. with harvest 48 h p.i., Fig. 28E and F), clearly supporting the notion that Usp7 may exert its effects not only during early, but also at late times of infection reflected by the reduction of structural capsid proteins (Fig. 28A and B, each lane 6). Moreover, the degree of virus yield inhibition was comparable to that of Usp7 knockdown (compare with Fig. 27B), indicating a good efficacy and comparability in both approaches and importantly, stressing the specificity of the Usp7 inhibition. Notably, negative cell growth characteristics at later time points were taken into consideration for calculating the virus yield, as virus yield was determined by virus per cell and then normalized to untreated-infected cells.

### **6.12 Impact of Usp7 inhibition on adenoviral oncogene-mediated cellular transformation**

Numerous experiments have investigated the role of plasmid-based adenoviral oncogene-mediated transformation for primary mammalian rodent cells, especially with the adenoviral oncogenes E1A and E1B-55K. Partial or incomplete transformation can be achieved with E1A alone, whereas a complete transformation phenotype can only be gained with concurrent E1B-55K activity upon p53 (Berk, 2005). Previous studies performed in the Dobner group revealed that Usp7 is a positive factor supporting adenoviral-mediated cell transformation (Koyuncu, 2009). These experiments involved shRNA-mediated Usp7 knockdown.

Expecting similar results, the Usp7 inhibitor HBX was applied in similar transformation assays to substantiate the role of Usp7 in adenoviral oncogene-mediated cell transformation processes.

As illustrated in Fig. 29A plasmid-based transformation of primary rodent cells with E1A and E1B encoding plasmids could be achieved and was visualized by crystal violet staining of cell foci (representative plates). Quantification of several experiments revealed a marked reduction in cell foci number upon HBX treatment according to the shRNA experiments (Koyuncu, 2009). Interestingly, applying the inhibitor resulted in foci number reduction comparable to E1A-induced transformation alone, suggesting that the effect of HBX treatment was specifically exerted upon E1B-55K. DMSO control-treated cells showed no significant change in foci formation in comparison to untreated cells (Fig. 29B). Since interaction of Usp7 and E1B-55K was only shown in transformed human cells, it was necessary to demonstrate that this binding also occurs in transformed rat cells. Indeed, it was

possible to coprecipitate E1B-55K from E1B-plasmid transfected Brk1 cells (a spontaneously transformed rat cell line derived from primary Brk cells used for the transformation assay), indirectly implying that this interaction also plays an important role in this setting (Fig. 29C lane 2).

In order to assess the relevance of the adenoviral oncogene-mediated cell transformation concerning Usp7 in a human system, a newly introduced cell and lentiviral vector system (Speiseder ongoing work) was used to induce cell transformation of primary human cells. Here, lentiviral vectors containing E1A or E1B-55K as well as empty vector controls were used to transduce primary human mesenchymal stroma cells (hMSC). As shown in Fig. 29D, it was possible to efficiently induce foci formation in hMSCs (representative crystal violet-stained plates). DMSO control treatment did not lead to a significant decrease of foci numbers, whereas HBX treatment led to a dose-dependent severe reduction of foci numbers, as also shown above in the rat cell system (Fig. 29E,  $GI_{50}$  0.18  $\mu$ M). Immunoblot analyses of transduced and HBX-treated hMSCs revealed that equivalent to A549 and H1299 cells, E1B-55K levels were modestly reduced upon HBX treatment, whereas E1A levels were not obviously affected, leading to the conclusion that simple E1B-55K steady-state reduction might lead to the reduction in foci numbers after HBX treatment (Fig. 29F, lane 7). To display the transformed phenotype of hMSC cells, non-transformed and E1A-E1B-55K transformed hMSC images are presented in direct comparison (Fig. 29G).

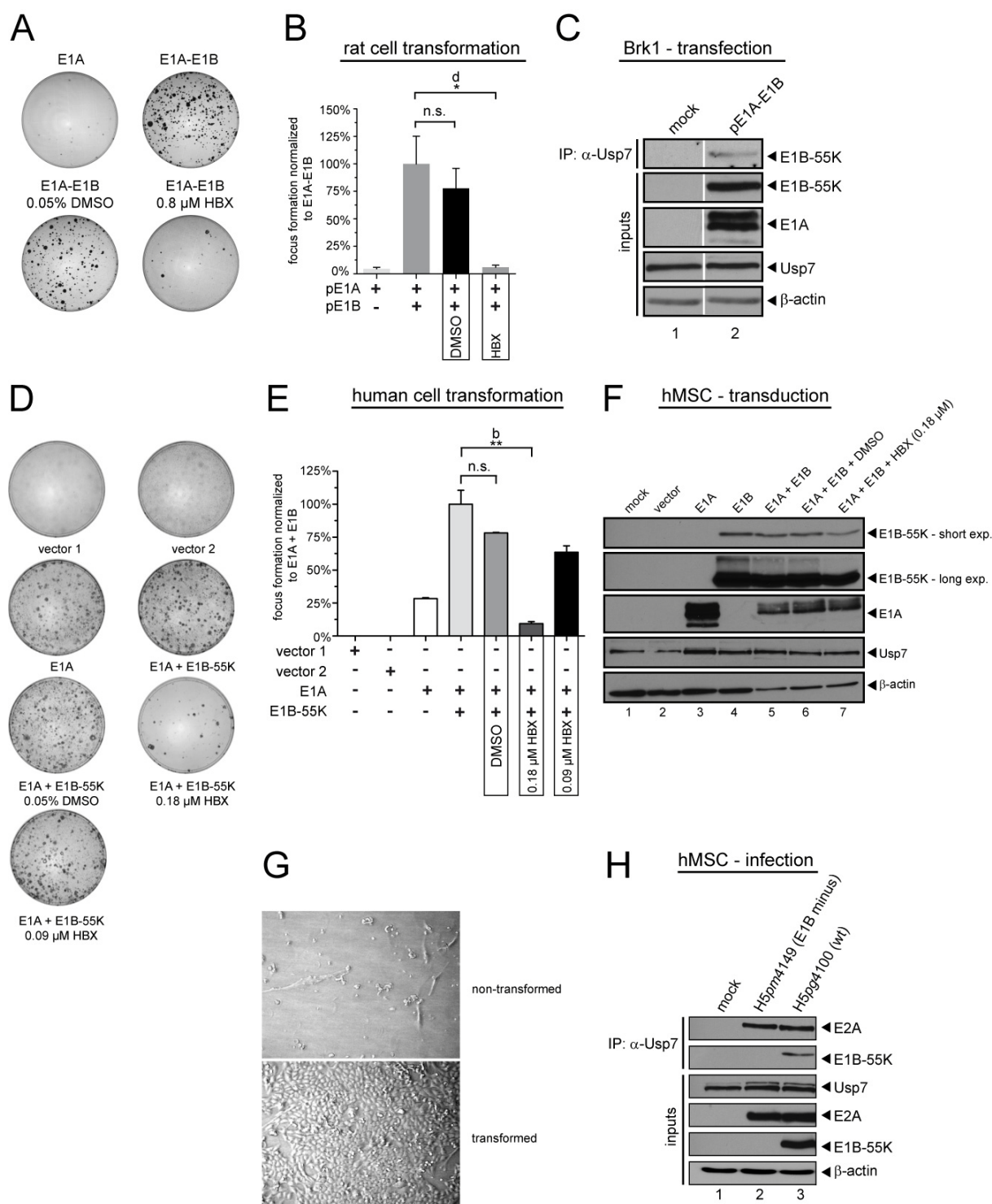


FIG 29 The effect of HBX on cell transformation. (A)  $1 \times 10^6$  primary baby rat kidney cells were transfected with 1-1.5  $\mu$ g E1A (pE1A) or E1A-E1B (pXC15) and were treated with DMSO (solvent), HBX or left untreated for several weeks until foci were visible. Crystal violet staining followed. Representative plates of three independent experiments are shown. (B) Statistical analyses of (A). S.e.m. of foci number normalized to E1A-E1B induced focus formation. Analysis with GraphPad Prism 5: t-test, unpaired, two-tailed. n.s.=not significant. \*  $P < 0.05$ . (C) Brk1 cells were transfected with pXC15. Coimmunoprecipitation followed with Usp7 antibody 3D8 as described in Fig. 22G. (D) Human mesenchymal stroma cells (hMSC) were infected with 0.3 lentiviral particles per cell containing empty vectors (LeGo-iVNL2 or LeGo-iBLB2), E1A (LeGo-iVNL2 E1A) or E1A+E1B-55K (LeGo-iBLB2 E1B-55K), and were treated with DMSO, HBX or left untreated. Plates were fixed and stained with crystal violet when foci became visible. Representative plates of three independent experiments are shown. (E) Statistical analyses of three independent experiments with hMSC. S.e.m. of foci number from three independent experiments normalized to E1A-E1B-55K induced foci. Analysis with GraphPad Prism 5: t-test, unpaired, two-tailed. n.s.=not significant. \*\*  $P < 0.01$ . (F) hMSCs were infected as in (D) and 8-10 days post infection cells were subjected to immunoblotting for the indicated proteins. (G) Representative images of non-transformed and transformed hMSCs before staining. (H) 70-80% confluent hMSCs were infected with  $1 \times 10^8$  virus particles (indicated) and subjected to coimmunoprecipitation analyses as described in Fig. 22G.

In accordance to the coimmunoprecipitation experiments conducted in A549, H1299 and Brk1 cells, E1B-55K could be coprecipitated along with Usp7 and E2A in infected hMSC cells (viruses are indicated), strongly supporting the global nature of Usp7-E1B-55K interaction since this has been proven in different cell systems.

These results clearly demonstrate the important role of Usp7 in adenoviral oncogene-mediated transformation processes and show that small-molecule inhibitor treatment can efficiently reduce the number of transformed cells in the experimental set-ups. Additionally, successful transformation could efficiently be shown in the new human cell system along with emphasizing the extraordinary relevance of Usp7 in this process.

## **7 Discussion**

### **7.1 The Usp7-E1B relationship**

Since Usp7's first discovery as a herpesviral interacting protein by Michayla Meredith and colleagues (Meredith et al., 1994), intense studies have contributed to the knowledge of the enzyme and defined the outstanding role of this deubiquitinating enzyme (DUB) in herpesviral diseases but more in cancer-related processes. However, Usp7 is the only cellular DUB so far known to be directly involved in virus infections. To date, only herpesviruses are known to use mechanisms to exploit Usp7 function. So far, four viruses have been described to be associated with Usp7: Herpes simplex virus type 1 (HSV-1), Epstein-Barr virus (EBV), Kaposi's sarcoma-associated herpesvirus (KSHV) and Human cytomegalovirus (HCMV).

HSV-1 ICP0 binds strongly to Usp7 and this interaction contributes to ICP0's ability to stimulate gene expression and viral lytic growth (Everett et al., 1997, 1999). This is probably achieved by promoting ICP0's stability under lytic infection conditions through Usp7-mediated deubiquitination (Canning et al., 2004; Boutell et al., 2005). Moreover, ICP0 has been shown to usurp Usp7's functions in order to terminate TLR-mediated NF $\kappa$ B and JNK activation (Daubeuf et al., 2009).

In contrast to ICP0, EBV EBNA1 does not require enzymatic activity of Usp7 for its own stability. In the EBV system, sole interaction of EBNA1 with Usp7 is sufficient to induce PML degradation by polyubiquitination. Work from Lee and colleagues could impressively demonstrate that peptide fragments derived from another viral protein, KSHV vIRF4, bind and inhibit Usp7. However, these studies are missing any infection relevance (Lee et al.,

2011). The next viral proteins, HCMV UL35 and UL35a, have also been shown to be associated with Usp7 and UL35 has been found to alter Usp7's subcellular localization.

In fact, extensive infection studies have only been performed in HSV-1 and EBV infection model systems. Based on these findings, it can be assumed that Usp7 displays rather positive than negative regulatory properties toward viral replication. In an analogous manner to the HSV-1 and EBV proteins described above, adenoviral E1B-55K has been shown to be associated with specific PML isoforms and degradation of p53, and to be a key player in ensuring proper viral lytic cycle progression. Along these lines, Usp7 could be identified as a positive regulator related to the family of *Adenoviridae*.

## **7.2 Usp7 is redistributed in a complex manner during adenoviral infection**

Indeed, it was possible to demonstrate that the adenoviral E1B-55K interacts with Usp7 by using classical coimmunoprecipitation assays from transfected and infected cells. Another method, the recently developed technique of the flow cytometry-based FRET analyses, (Banning et al., 2010) could successfully be applied in the experiments to verify Usp7-E1B-55K interaction in an intact cellular environment (*in vivo*) with quantitative relevance. These different set-ups unambiguously demonstrate a clearly defined interaction between both proteins which is independent of other adenoviral proteins or p53.

Since it has been reported that HSV-1 ICP0, EBV EBNA1 and HCMV UL35 induce a fine but distinct change in Usp7 localization, it can be assumed that binding of Usp7 to E1B-55K might also lead to a change in Usp7 location. Strikingly, immunofluorescence analyses revealed an infection time-dependent, strong nuclear relocalization of Usp7 and the kinetics of this relocalization do not allow an exclusive involvement of the respective binding partner E1B-55K (at least at the beginning of infection). This is because pronounced changes in Usp7 localization in early-infection-phase cells (see Fig. 19C, panels E to L category 3 and 4) are lacking any spatial correlation to E1B-55K, which is only seen at later stages of infection (16 h p.i. onwards, Fig. 19C, panels M to T). Here, Usp7 redistribution into round centers at the early stage of infection and colocalization with E1B-55K at later stages discloses striking similarities to the kinetics of viral ssDNA accumulations, namely adenoviral replication centers. These kinetics, clearly presented by Pombo et al. (Pombo et al., 1994), are defined by early and late stages of infection with regard to the formation of adenoviral replication centers. In this respect and in simple terms, E2A foci and small ring-like structures are formed at the beginning and bigger ring-like formations are found at the late phase of infection which

eventually become smaller at an even later stage of infection. In this work, this could clearly be observed and also quantified to a certain degree for Usp7 redistribution (Fig. 19A to 19E).

Hence, *in situ* costaining investigations of Usp7 and E2A, which is commonly used as a marker for viral DNA replication centers, were conducted. The immunofluorescence studies performed in this work clearly correlate Usp7 redistribution to sites of E2A protein presence. If so, the IF observations suggest an association of Usp7 with early viral DNA replication as Usp7 is directly found at sites of E2A staining early in infection (Fig. 21C, panels E to H). It has to be kept in mind, that although Usp7 colocalizes reliably with E2A, which is supported by the Imaris colocalization analyses (Fig. 22A to E), there is never a 100% perfect overlap in both stainings. Especially at late times of infection, it rather seems as if a certain part of the Usp7 population is simply surrounded by E2A. Due to the IF observations, it is probable that in the late stage of infection E1B-55K comes into play. Especially, the colocalization of Usp7 and E1B-55K is not showing any peripheral E1B localization like it was observed for E2A (Fig. 21F). The kinetics of the different redistribution patterns imply that Usp7 is used independently by two different viral proteins at different stages of infection. More specifically, E2A might induce Usp7 redistribution at the beginning of infection (which is supported by previous observations in single E2A transfection experiments; [Koyuncu, 2009]) to promote early functions of E2A or the transition to the late phase like DNA replication. In the course of replication center formation or more probably at the end of formation, E1B-55K “takes over” in order to support late functions (e.g. viral RNA transport). These functions can for example be inhibition of Usp7’s stabilizing properties toward p53 in order to facilitate p53 degradation. On the one hand, coimmunoprecipitation experiments demonstrated binding of Usp7 to E2A even in the absence of E1B-55K shown by E1B minus virus (H5 $pm$ 4149; Fig. 22G) infection, clearly supporting the *in situ* observations and the hypothetical assumptions made before. On the other hand, interaction experiments illustrated that E1B-55K binds to Usp7 independently of E2A shown by the transfection assays (Fig. 18A). Interestingly and supporting the theory that Usp7 might foster DNA replication (at the beginning of infection), Usp7 has been demonstrated to facilitate DNA binding activities of EBNA1 to latent viral genome *oriP* elements and the sequence-specific DNA binding activity of p53 (Sarkari et al., 2009). Therefore, it is not digressive to assume that Usp7 exerts similar functions on E2A. Nevertheless, it has to be considered that for efficient DNA replication *in vitro*, three viral and three cellular elements have been found to be sufficient: Adenovirus DNA-polymerase, precursor- or preterminal protein (pTP), E2A (also termed DNA binding protein [DBP]), cellular NFI, NFII and topoisomerase I (Liu et al., 2003). In this respect, Usp7 would rather

have supportive than essential functions. While a detailed investigation of the Usp7-E2A interaction was beyond the scope of this work, only some general considerations for adenoviral replication are presented here and in the following sections.

However, it is tempting to conduct experiments concerning the binding pattern of Usp7 to E1B-55K and E2A during the whole course of infection in order to distinguish between functions exerted on E2A and E1B-55K. In the following sections functional consequences will be discussed resulting from Usp7 functional inactivation.

In sum, Usp7 displays an intricate redistribution pattern which probably reflects the multiple pathways this protein has to take during adenoviral infection.

### **7.2.1 Usp7 knockdown or inhibition leads to similar negative effects on adenoviral replication**

Many efforts have been invested to find new drugs against DUBs or other proteins related to the ubiquitin-proteasome system (UPS). Aberrantly regulated DUBs are described to be involved in specific human diseases like cancer and neurodegenerative disorders (Hussain et al., 2009).

Since Usp7 is the only DUB directly connected to cancer and infectious diseases at the same time, it is very enticing to find suitable inhibitors that can be used efficiently and specifically against Usp7 enzymatic activity. Several companies set out to develop such chemical substances and were eventually successful in finding them and developing more specific derivatives. In this respect, Progenra identified novel small-molecule inhibitors against Usp7 that stabilize p53 and inhibit cancer cell progression (Nicholson and Suresh Kumar, 2011). Additionally, Hybrigenics described in a patent from 2006 several cyano-indenopyrazine substances which have been demonstrated to exert functional inhibition upon Usp7.

One of these Hybrigenics substances was resynthesized (HBX) and used in this study to perform inhibitor assays on adenovirus-infected cells in order to underline and investigate the functional consequences of Usp7-E1B-55K (or Usp7-E2A) interaction and to prove that Usp7 inhibition can efficiently reduce virus replication. In fact, it was possible to show that Usp7 inhibition and knockdown follow the same route of negatively affecting adenovirus-associated processes leading either to reduced virus growth or negative effects upon adeno-oncogene-primed cellular transformation.

At the start of characterizing the effects of an inhibitor compound on a given system, no-observable adverse-effect levels (NOAEL) are determined. Initially in this work, no cytotoxic

effects, which are normally taken as the first output factor characterizing newly found compounds, could be observed (Chen et al., 2010; Wang et al., 2011a, 2011b; Xie et al., 2011; Figure 23). On that note, inhibitor treatment did not alter subcellular localization of investigated proteins and did not change cell morphology. Additionally, the experimental setups chosen in this study in which all infection experiments were performed, only displayed (modest) growth inhibitory effects at later time points of examination. This was observed, even though every experimental condition for the infection studies included the same inhibitor incubation duration of 15 hours. Such an effect might be explained by cell cycle differences between cells harvested 24 h p.m.i. or 48 h p.m.i. (not only for mock but also normal infection). Assuming that more cells enter/are in S-phase the longer they are cultivated (48 h p.m.i.), the gap or growth inhibition between HBX-treated and DMSO-treated cells becomes more discernable than for cells which have been investigated earlier (24 h p.m.i.). Taking these effects into consideration, meaningful results can be attained.

The initial motivation of this study was to profile new interaction partners of E1B-55K. Due to E1B-55K's involvement in the p53 stress response and DNA damage response pathway many investigations have concentrated on E1B-55K's function in circumventing and inhibiting these antiviral pathways. As a result, nearly all significantly investigated cellular interaction partners of E1B-55K (which have been proven to bind to E1B-55K) turned out to be negatively regulated through proteasomal degradation, mislocalized in order to inhibit antiviral functions or do not show any effect at all on virus growth. Interestingly, Usp7 cannot be classified into this type of proteins with adverse effects for viral replication even though it is a major component of the p53 stress-response pathway and should be seen as a positive regulator of p53 functions.

This study provides significant evidence that Usp7 is a major positive determinant for HAdV5 viral replication. To prove that the effects of the HBX compound can be specifically traced back to Usp7, a cell line was created with stable Usp7 shRNA-mediated knockdown. In effect, the obtained cell clone with a suitable Usp7 knockdown efficiency (HU5) showed no growth inhibition at all and therefore served as a good instrument to study the effects of Usp7 knockdown in parallel with Usp7 inhibition.

Several different experiments in this work demonstrated a marked reduction in E1B-55K levels (knockdown + transfection, knockdown + infection, transfection + inhibitor and infection + inhibitor with immunofluorescence or Western blot analyses as output) indicative for Usp7 having stabilizing effects upon E1B-55K. However, this E1B-55K reduction could

not be detected or was mitigated 48 h p.i. in both investigated cell lines and in the knockdown setting (Fig. 25). It can be hypothesized that other factors come into play for E1B-55K stabilization later in infection and/or Usp7 exerts its function on E1B-55K until 24 h p.i. and can be neglected later on, which is supported by the observation that accumulation of Usp7-E1B-55K overlap in the *in situ* analyses occurs at this time point (Fig. 19). Concerning the stabilizing effect, such a circumstance has been described for the HSV-1 protein ICP0 which is stabilized by Usp7's deubiquitination activity (Boutell et al., 2005). Interestingly, in a similar functional environment as ICP0, E1B-55K forms a multi-protein complex E3 ubiquitin ligase with several cellular factors. In keeping with this information and assuming that E1B-55K is destabilized through polyubiquitination, it can be hypothesized that Usp7 stabilizes E1B-55K through deubiquitination. However, there is no report showing ubiquitinated E1B-55K. Moreover, attempts to start mode-of-action *in vitro* ubiquitination analyses have been impeded by one major drawback: the extremely low yield of full length recombinant E1B-55K, probably owing to the toxic effect of overexpressed E1B-55K in *E. coli*. In this respect, other measures for full length E1B-55K expression have to be taken into consideration to tackle this question.

During the course of this study, it became clear that Usp7 not only specifically targets E1B-55K, but also exerts (mainly) positive effects on E1A, to a certain degree E2A and some late adenovirus structural proteins, since reduction in steady-state levels could also be observed for most of these proteins after Usp7 knockdown or inhibition. However, certain differences between knockdown and inhibition existed. For instance, E1A protein levels are clearly diminished by comparing knockdown *versus* control cell line, but showed no difference or even increased protein levels after inhibitor treatment (Fig. 28). It is clear that specific (subtle) disparities exist between knockdown and inhibition settings. One general explanation to this observation: while knockdown affects the protein level *in toto*, inhibitor treatment might affect only one function of a protein while other functions are not affected at all. In case of Usp7, it has been well established that due to its multi-domain structure, Usp7 exerts functions which are not solely traced back to the enzymatic deubiquitination activity but to other parts of the protein (Faesen et al., 2011; Sarkari et al., 2011). However, the specificity of both approaches upon other viral proteins like E1B-55K or structural proteins clearly suggests that Usp7 functions are necessary during the whole course of infection which is indirectly underlined by the *in situ* observations. It can only be speculated that Usp7 operates on the other adenoviral proteins in the same manner as described for ICP0 deubiquitination. Remarkably, negatively affecting Usp7 can reduce virus yield up to 91%, even after an

established and ongoing infection pointing to the importance of Usp7 for the late phase of adenoviral infection. Addressing this issue more in detail involves first steps in identifying the Usp7-adenovirus interactome using standard binding assays.

In conclusion, blocking the activity of Usp7 could be used in the treatment of adenovirus infections. Particularly, pediatric patients undergoing allogeneic stem cell transplantation are vulnerable to disseminated adenovirus infections with a high rate of mortality (Walls et al., 2003). Hence, there is a need for potent antiviral therapeutics against adenoviruses that allow suppression of the virus at different steps in the replication cycle (Lenaerts et al., 2008). In this context, Usp7, having enzymatic activity, represents a potent target for small-molecule inhibitors. These results here clearly propose that an efficient reduction of adenoviral progeny virions can even be achieved after an established infection with an inhibitor against Usp7 which could also be confirmed with RNAi experiments.

### **7.3 Usp7 in adenoviral transformation processes**

In simple terms, adenoviral oncogene-mediated transformation involves only two viral proteins. The adenoviral E1A protein facilitates uncontrolled S-phase progression and E1B-55K counteracts subsequent p53 activation and detrimental effects like apoptosis. To bring more complexity into this matter, several studies could demonstrate that there are mechanisms involved in E1A-E1B-55K-mediated transformation independent of the p53 status and more relying on different cellular interaction partners (Barral et al., 2005; Sieber and Dobner, 2007; Härtl et al., 2008).

In previous RNAi experiments, Usp7 was shown to be involved in adenoviral oncogene-mediated transformation processes (Koyuncu, 2009). Along with the inhibitor experiments performed here, it was possible to show that this does not only apply for the rat cell system but also, and even more interestingly, for a human cell system. Strikingly, in comparison to the rat cell transformation assay, in the human cell system fewer foci numbers could be detected after inhibitor treatment than during sole E1A-mediated transformation. This may suggest that other mechanisms are involved relying on Usp7's ability to promote the transformed phenotype in human cells which are inhibited by HBX. With respect to already known involvements of Usp7 in tumor pathways, the observed phenotypes may be explained by two to three possible scenarios: First, p53 is activated, accumulates and promotes antiproliferative activities due to instability of its negative regulator Mdm2. It has been shown that Mdm2 is the primary target of Usp7-mediated stabilization. Thus, inhibition of Usp7 in this setting might lead to reduced Mdm2 levels. Second, tumor suppressors PTEN and

FOXO4 stimulate expression of proapoptotic/cell cycle arrest genes due to increased monoubiquitination and nuclear activity. In both cases, several reports demonstrated that Usp7 can deubiquitinate both transcription factors leading to their nuclear exclusion. Third, increased Daxx proapoptotic activity supports cell death. Like in the case of p53, Daxx levels increase due to a lack of negative Mdm2 regulation after Usp7 inhibition. Additionally, in transformation settings, Daxx functions are antagonized by E1B-55K and as shown in Part II E1B-55K levels definitely depend on functional Usp7. Indeed, it was possible to demonstrate interaction of E1B-55K in rat and human cells (Fig. 29), indirectly supporting the direct relation of Usp7 and E1A-E1B-55K-mediated cellular transformation. More importantly, transduction with E1B-55K-containing lentiviruses with subsequent Usp7 inhibitor treatment resulted in lower E1B-55K protein levels. Therefore, similar Usp7-dependent mechanisms may play an important role during adenoviral lytic infection and adenoviral-oncogene-mediated transformation processes specifying the extraordinary relationship between Usp7 and E1B-55K.

In summary, for the first time, efficient virus yield reduction can be linked with efficient reduction of virus-mediated cellular transformation, making Usp7 a striking drug target.

# Part III

## **8 Connecting CK2-mediated phosphorylation of E1B-55K and Usp7**

The last part of this work tries to present a link between CK2-mediated E1B-55K phosphorylation and the E1B-55K-Usp7 interaction. Intriguingly, CK2 phosphorylation is a prerequisite for E1B-55K to bind Usp7. In this section, Part I and Part II become interlinked forming Part III.

Several studies from Lori Frappier's lab showed that the two host cellular factors CK2 and Usp7 are hijacked by EBV EBNA1 for efficient degradation of PML nuclear bodies (PML-NBs) (Frappier, 2011) in order to promote EBV latent infection or EBV-induced carcinogenic processes. Outstanding work from Everett et al. introduced an extraordinary relationship between PML nuclear bodies (PML-NBs), HSV-1 ICP0 and Usp7 (Everett et al., 1997, 1999). Here, efficient degradation of PML-NBs is induced by ICP0 which requires Usp7 to counteract its own ubiquitination and proteasomal degradation. Also, adenoviruses affect PML-NBs by disrupting the foci structure of different PML proteins which are constituents of the PML-NBs. Here, the adenoviral protein E4orf3 has been demonstrated to cause track-like transformation of PML proteins (Yondola and Hearing, 2007). However, E1B-55K, extensively elaborated in this work, also participates in PML binding and probably modulation. More specifically, different isoforms of PML proteins are bound in an infection time-dependent manner by E1B-55K depending on the SUMOylation status of the viral regulatory protein (Wimmer et al., 2010). On top of that, PML-NBs have been shown to negatively regulate Usp7's function in a Daxx-dependent manner (Song et al., 2008).

### **8.1 The extent of binding deficiency toward Usp7 affects E1B-55K protein stability which is a matter of E1B-55K's phosphorylation status**

Further studies into the role of E1B-55K phosphorylation revealed that the phosphorylation determines the SUMO-specific modification of E1B-55K (coauthored in Wimmer et al., 2012; in revision) and presumably its binding to specific PML isoforms which might have important implications for E1B-55K-assisted oncogenic transformation. Since this topic has been studied extensively elsewhere, the next steps involved analyses of the functional consequences of E1B-55K phosphorylation for Usp7.

In keeping with the observations that Usp7 regulates E1B-55K stability and that the phospho-mutant (E1B-P minus) exerts similar stability defects in H1299 cells, like wt E1B-55K in Usp7 knockdown cells (compare Fig. 16 with Fig. 27), it is tempting to ask whether the phosphonegative E1B-55K mutant (E1B-P minus) exerts defects in Usp7 binding. Therefore, coimmunoprecipitation binding assays were employed. For this, A549 and H1299 cells were infected in parallel (same infection master) with wt (H5pg4100) and E1B-P minus (H5pm4174) virus at an MOI of 20 FFU/cell. Subsequent precipitation of endogenous Usp7 from mock-infected and infected cells and immunoblotting for E1B-55K and E2A revealed interaction. Strikingly, in A549 cells and E1B-P minus virus (H5pm4174) infection, binding of Usp7 toward E1B-P minus was severely impaired almost in the same extent as interaction with E2A was “enhanced” in comparison to wt (H5pg4100) infection, indicating a significant role of E1B-55K phosphorylation for the interplay of E1B-55K and E2A with Usp7. Notably, identical steady-state levels of wt and mutant E1B-55K could be detected in A549 cell lysates (Fig. 30, lanes 2 and 3). In comparison to A549 cells, in H1299 cells the binding defect of the phosphonegative E1B-55K toward Usp7 was more pronounced and no E1B-55K could be precipitated in this set-up. Moreover, as shown before, E1B-55K from E1B-P minus also exerted lower steady-state levels, suggesting that “totally” abolished Usp7 binding may be responsible for lower E1B-55K levels. Interestingly neither wt nor mutant E1B-55K displayed Usp7-E2A interaction in H1299 cells probably due to the low amounts of E2A used in the assay reaction (compare input A549 and H1299 Fig. 30).

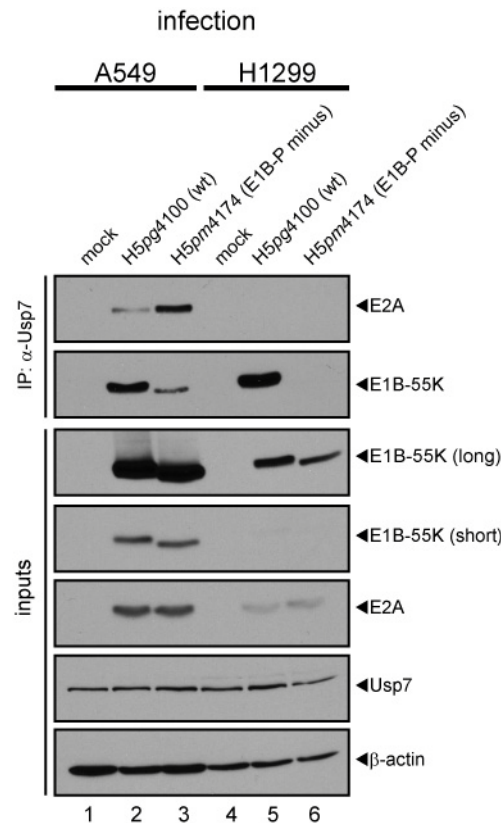


FIG 30 Phosphonegative E1B-55K (E1B-P minus) interaction towards Usp7 is severely reduced. A549 and H1299 cells either mock-infected or infected (MOI=20 FFU/cell) with H5pg4100 (wt) and H5pm4174 (E1B-P minus) virus were analyzed by immunoprecipitation assays using protein A-Sepharose-coupled anti-Usp7 antibody (3D8). Proteins separated by SDS-PAGE were detected by immunoblotting with anti-E1B (2A6) and anti-E2A (B6-8) antibodies. Immunoblot analyses of protein input levels are shown below for Usp7 (3D8), E1B-55K (2A6), E2A (B6-8), and  $\beta$ -actin (AC-15).

## 8.2 Usp7 is relocalized during E1B-P minus virus (H5pm4174) infection in the same manner as during wt virus infection

To analyze whether differences in the relocalization pattern of Usp7 during E1B-P minus and wt virus occur, double-label immunofluorescence analyses were performed. A549 cells were infected with indicated viruses at an MOI of 20 FFU/cell and methanol-fixed 24 h p.i. (Fig. 31). However, no difference in the relocalization pattern between wt and E1B-P minus virus infection could be observed. According to these analyses and as seen in Part I, phosphonegative E1B-55K (from H5pm4174 infection) mainly displayed cytosolic and diffuse localization and no visible association to viral replication centers. The absence of binding (Fig. 30) and no discernable colocalization, support the hypothesis that Usp7 redistribution is independent of E1B-55K.

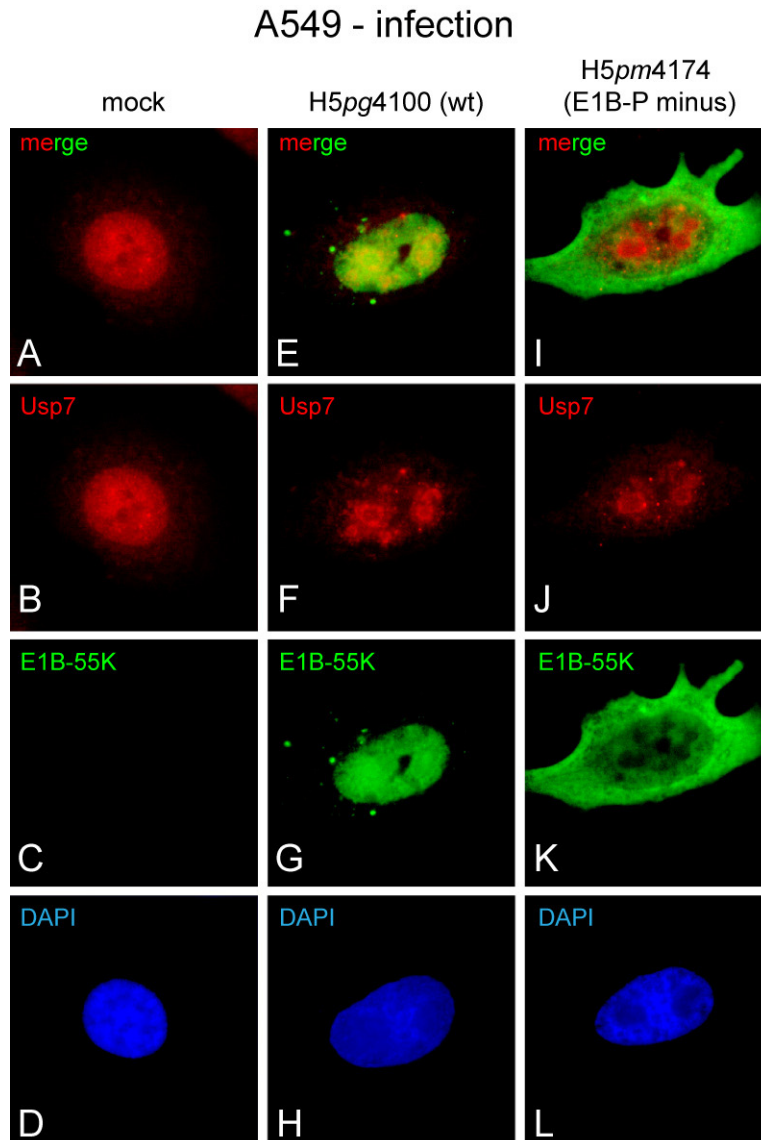


FIG 31 No obvious difference in the Usp7 redistribution pattern between wt (H5pg4100) and E1B-P minus (H5pm4174) virus infection. A549 cells mock-infected or infected with H5pg4100 (wt) and (H5pm4174) (MOI=20 FFU/cell) were analyzed by *in situ* immunofluorescence staining for E1B-55K (2A6), Usp7 (3D8), and DNA content (DAPI) 24 hours post infection.

### 8.3 TBB-mediated inhibition of CK2 results in reduced Usp7 binding of E1B-55K

As a possibility, lower E1B-55K levels in H1299 cells could be the reason why coprecipitation of E1B-55K after Usp7 precipitation in E1B-P minus virus-infected cells failed. Therefore, H1299 cells were infected with H5pm4174 (E1B-P minus) at an MOI of 50 FFU/cell and H5pg4100 (wt) at an MOI of 20 FFU/cell to compensate for the lower E1B-55K levels in E1B-P minus infection (as described in section 4.2). Furthermore, wt virus-infected cells were also treated with the CK2 inhibitor TBB as described in section 4.7. As shown in Figure 32, almost identical amounts of E1B-P minus (even a bit more) and wt E1B-55K could

be used for the coimmunoprecipitation experiments (compare lanes 3 and 4). However, mutant E1B-55K (E1B-P minus) still failed to be coprecipitated with Usp7 from H5pm4174 virus-infected cells (Fig. 32). Similarly, CK2 inhibitor treatment reduced the binding affinity of E1B-55K toward Usp7. A control immunoprecipitation using another fraction of the same lysates, showing the reduction of phospho-E1B-55K after CK2 inhibitor treatment, was also performed. Different amounts of detected phospho-E1B-55K probably reflect divergent inhibition efficacies in the samples due to different inhibitor concentrations used. Of note, the E1B-55K steady-state levels were also slightly reduced in H1299 cells upon CK2 inhibitor treatment (Fig. 32, lane 5), supporting the notion that CK2-mediated Usp7 binding stabilizes E1B-55K. Nevertheless, the modest reduction of E1B-55K protein steady-state levels is unlikely to account for the reduced binding of E1B-55K toward Usp7.

In summary, it was possible to demonstrate for the first time a direct link between CK2 phosphorylation of E1B-55K and its ability to bind and probably be stabilized by Usp7.

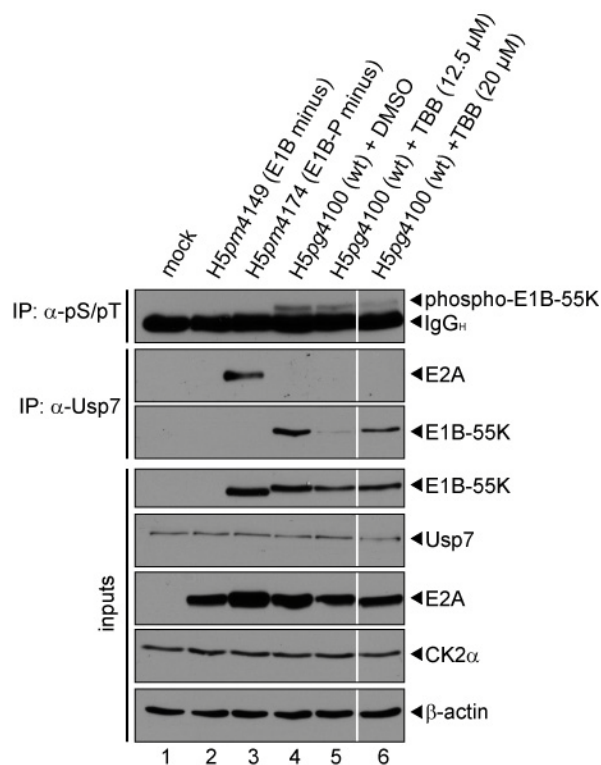


FIG 32 CK2 inhibition reduces binding capacity of E1B-55K towards Usp7. H1299 cells were mock infected or infected with H5pm4149 (E1B minus), H5pg4100 (wt), and H5pm4174 (E1B-P minus; MOI of 50=FFU/cell) virus at an MOI of 20 FFU/cell. As indicated, cells were also treated with DMSO and TBB 4 h p.i. until harvesting the cells at 24 h p.i. Immunoprecipitation assays were performed with anti-phosphoserine/phosphothreonine (pS/pT, 22a) and anti-Usp7 (3D8). Proteins separated by SDS-PAGE were immunoblotted with anti-E1B (2A6) and anti-E2A (B6-8) antibodies. Protein steady-state levels were detected by immunoblotting with antibodies specific for E1B-55K (2A6), Usp7 (3D8), E2A (B6-8), CK2α (ab13410), and β-actin (AC-15).

#### **8.4 Usp7 inhibition through HBX further reduces virus yield of the E1B-P minus virus**

Having established the connection between CK2, Usp7 and E1B-55K, it was necessary to demonstrate that Usp7 inhibition during wt (H5pg4100) infection and the defect in virus yield after E1B-P minus virus (H5pm4174) infection are quantitatively comparable. Moreover, it was of interest to investigate whether HBX inhibitor treatment further reduces virus yield after E1B-P minus virus infection. In case the specific defect during E1B-P minus infection solely depends on the disruption of Usp7 binding, no further negative effect of an Usp7 inhibitor upon virus yield would be expected. However, as results from Part II point to a “global” involvement of Usp7, this was not expected.

Next, A549 cells were infected with wt and E1B-P minus virus at an MOI of 20 FFU/cell and 52 h p.i. virus particles were extracted. Moreover, DMSO control solution and Usp7 inhibitor HBX were applied 20 hours before harvest.

As anticipated, HBX treatment resulted in ca. 40% reduction of virus growth and (almost identically) E1B-P minus (H5pm4174) was also found to have ca. 40% less virus progenies compared to wt (H5pg4100) infection. Interestingly, HBX treatment after E1B-P minus infection reduced virus yield by additional 30% (Fig. 33A).

In parallel performed binding assays and protein steady-state immunoblots revealed that HBX treatment had a modest negative effect on E1B-55K from E1B-P minus (Fig. 33B), and in contrast to the previous observations, also reduced wt E1B-55K protein levels at a later infection time point of application. This is probably owing to the longer incubation period of the Usp7 inhibitor (20 hours compared to 15 hours). As a consequence, less E1B-55K could be coprecipitated from Usp7 in HBX-treated cells and the binding defect was even more pronounced in E1B-P minus virus infection (Fig. 33B, compare lanes 3 and 5).

In summary, these results further suggest that Usp7 is involved in multiple steps of the adenoviral life cycle.

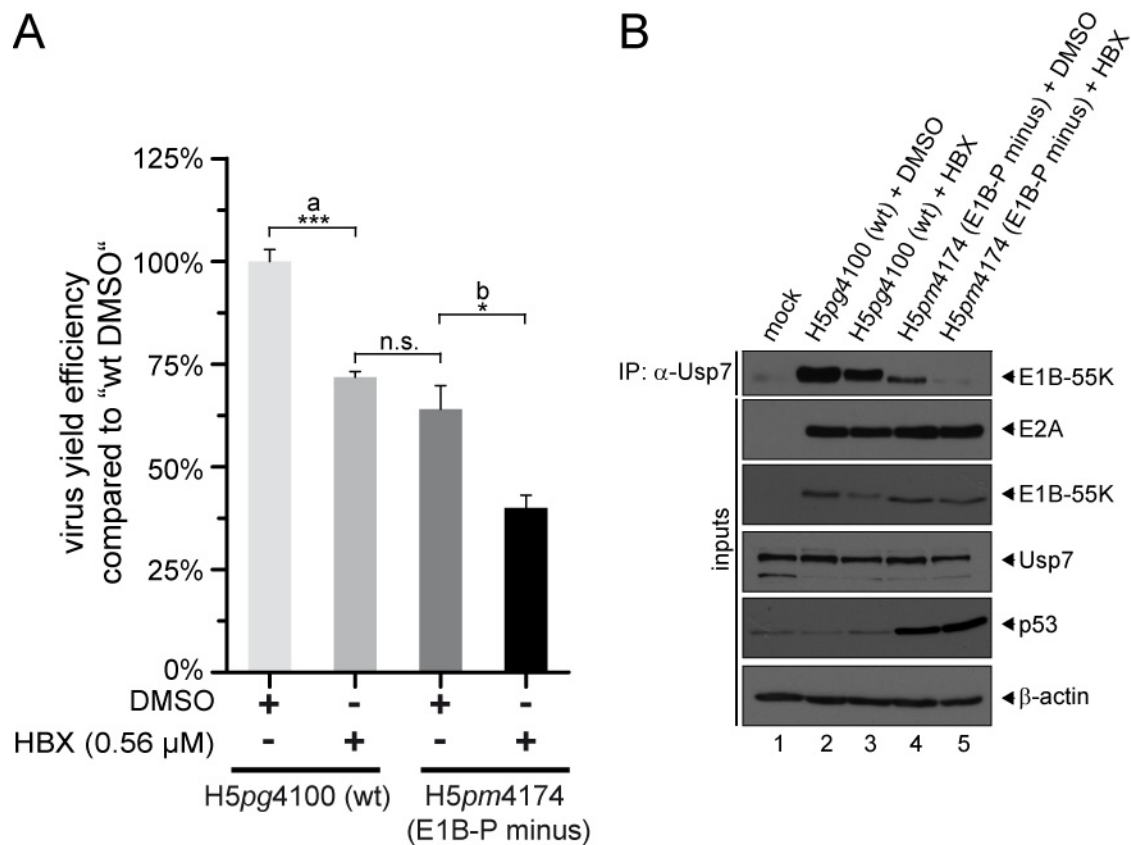


FIG 33 The Usp7 inhibitor HBX decreases virus yield of the E1B-P minus virus (H5pm4174). (A) A549 cells were infected with wt and E1B-P minus virus at an MOI of 20 FFU/cell and harvested at 52 h p.i. In addition, the cells were also treated with DMSO or HBX 20 before harvest. Virus yield was determined by quantitative E2A-72K immunofluorescence staining (B6-8) on HEK293 cells. The results represent the average of at least three independent experiments. P values of unpaired, two-tailed t tests (GraphPad Prism 5) were determined. n.s.=not significant. \*  $P < 0.05$ , \*\*\*  $P < 0.001$ . (B) A549 cells were treated as described in (A). Additionally, immunoprecipitation assays were performed with anti-Usp7 antibody 3D8. Proteins separated by SDS-PAGE were immunoblotted with anti-E1B (2A6) and anti-E2A (B6-8) antibodies. Protein steady-state levels were detected by immunoblotting with antibodies specific for E1B-55K (2A6), Usp7 (3D8), E2A (B6-8), p53 (D0-1), and  $\beta$ -actin (AC-15).

## 8.5 Concluding subsections – Giving an outlook of possible investigation pathways

In the last two subsections, data will be presented that point to an involvement of PML proteins in the regulatory CK2-E1B-55K-Usp7 triad. The purpose is to provide a fertile ground for further investigations into the fascinating topic of virus-host interaction in adenovirus infections.

### 8.5.1 The amount of PML tracks during wt and E1B-P minus virus infection differs significantly

Owing to the nature of PML functions, among them antitumorigenic and antiviral properties, it is not surprising that track-like reorganization of PML proteins during adenoviral infection is discussed as a mechanism counteracting PML antiviral activity.

As shown in Part I, CK2 is an important regulator of E1B-55K phosphorylation. Interestingly, CK2 and E1B-55K are both associated to PML-NBs, whereas direct functional regulation has only been shown for CK2. In this context, E1B-55K was shown to bind specific isoforms via its SUMOylation and probably also phosphorylation status and CK2 has been demonstrated to directly induce phosphorylation of PML with subsequent PML degradation (Scaglioni et al., 2006). Therefore, it is possible that CK2 phosphorylation is used by E1B-55K in order to modulate not only its own but also PML functions.

In an initial step to investigate the formation of track-like structures during phosphonegative E1B-55K (H5pm4174) infection, immunofluorescence studies were employed as described above. A549 cells were infected with wt (H5pg4100) and E1B-P minus (H5pm4174) virus at an MOI of 20 FFU/cell and methanol-fixed 24 h p.i. As shown in Figure 34A, PML foci could be detected in the nucleus of uninfected cells (Fig. 34A, panels A to D). As expected, infection-induced tracks were formed after wt and E1B-P minus infection (Fig. 34A, panels E to L). Interestingly, not only track-like structures were formed but also a minor fraction of ring-like structures similarly to those formed during Usp7 redistribution (Fig. 34B, panel F) and - more pronounced in E1B-P minus infection - other not definable relocalization patterns (Fig. 34B, panel B and D), probably mirroring intermediate stages of PML reorganization. Along the same lines previously described PML subpopulations have been reported to surround viral replication centers (Carvalho et al., 1995; Doucas et al., 1996; Yondola and Hearing, 2007). Importantly, quantification of the observed phenotypes of PML rearrangement revealed that 24 h p.i. ca. 56% of the E1B-positive cells showed PML in tracks after wt infection, whereas the amount of track-like structures after E1B-P minus (H5pm4174) infection was only 18% (Fig. 34C). In general, the formation of tracks during E1B-P minus infection seemed to be incomplete with less and shorter tracks (Fig. 34A, panel J). Surprisingly, in this context, the amount of E1B-positive cells displaying a general change of PML staining was comparable to wt-infected cells, indirectly indicating that phosphorylated E1B-55K might be involved in the formation of PML tracks. However, it is more likely that a certain cellular factor involved in E1B-55K phosphorylation might be involved in PML track formation.

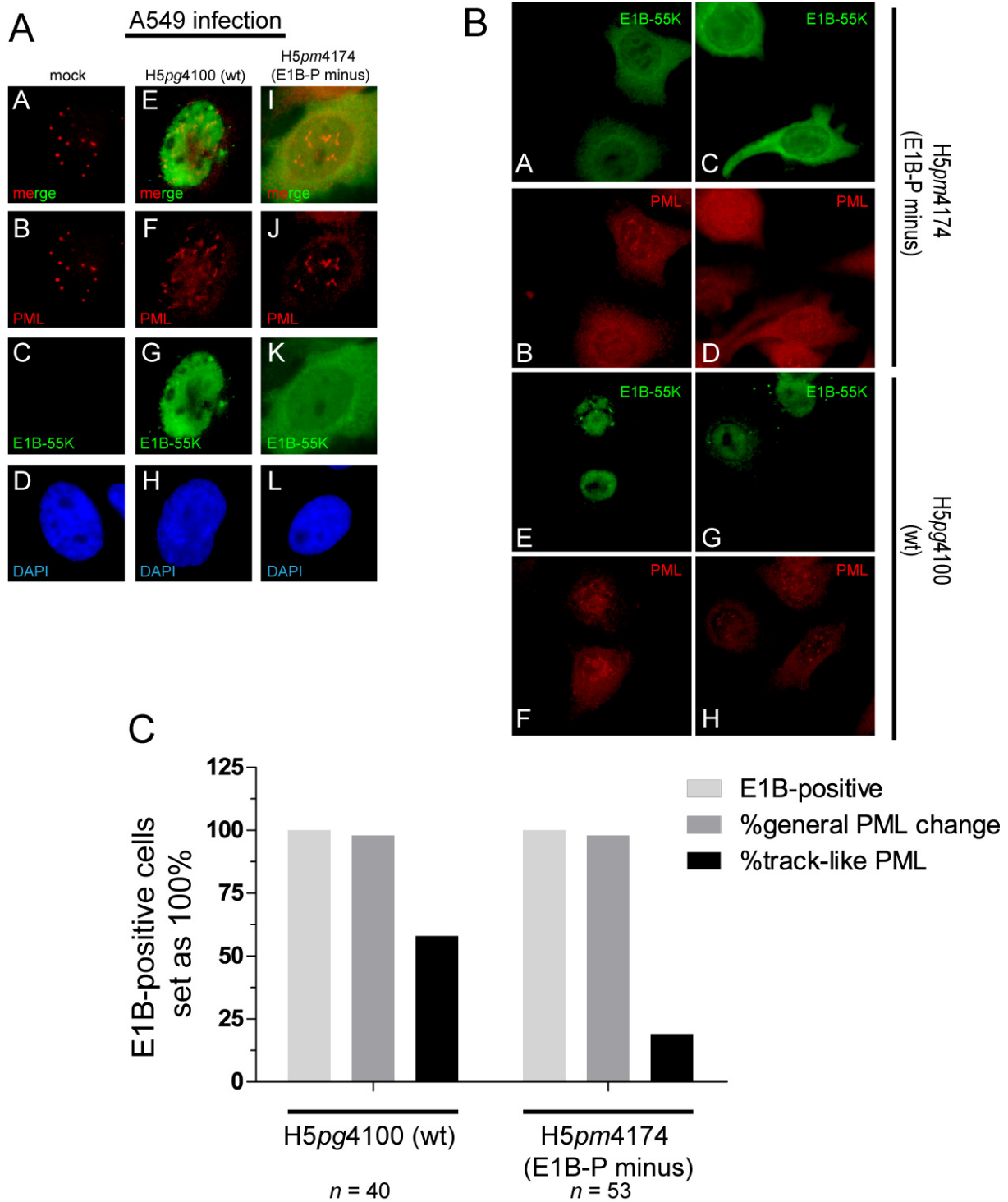


FIG 34 The amount of PML tracks during wt and E1B-P minus virus infection differs significantly. (A+B) A549 cells mock-infected or infected with H5pg4100 (wt) and (H5pm4174) (MOI=20 FFU/cell) were analyzed by *in situ* immunofluorescence staining for E1B-55K (7C11), PML (5E10), and DNA content (DAPI) 24 hours post infection. (C) Cell phenotypes were counted and plotted in GraphPad prism for graphical visualization.

### **8.5.2 Adenoviral infection induces the spatial proximity of Usp7 and PML into ring-like structures**

As previously described, Usp7 transiently associates with PML-NBs to negatively regulate PML protein levels which is enhanced upon EBV EBNA1 presence (Sarkari et al., 2011). To analyze whether a similar enhanced association could be observed during adenoviral infection, *in situ* analyses of Usp7 and PML were conducted. Quantification of cells showing aberrant PML location in this setting revealed that ca. one third of the cells, after wt (H5pg4100) and E1B-P minus (H5pm4174) virus infection, displayed significant partial colocalization of Usp7 with PML in the aforementioned ring-like structures (Fig. 35B). Mock-infected cells served as a negative control to specify gating in Imaris colocalization analyses. However, the  $R^2$  values displayed no significant differences between wt and E1B-P minus-induced staining overlap (Fig. 35C). As shown in Fig 35, Usp7 is relocalized in the same manner during wt and E1B-P minus infection suggesting that the phosphorylation status of E1B-55K has no effect on Usp7 redistribution as seen before (Fig. 31). Nevertheless, comparing the amount of PML tracks, revealed that E1B-P minus infection induces less tracks with a general different morphology than wt induced PML tracks (Fig. 35D and E). As described before, also under uninfected conditions some Usp7 foci associate in the vicinity of PML foci (Fig. 35F).

These results suggest that a specific fraction of Usp7 is relocalized to regions overlapping with PML staining. However, phosphorylation does not determine the outcome or “quality” of Usp7 relocalization, but obviously the amount of PML tracks formed, indirectly indicating passive mechanisms.

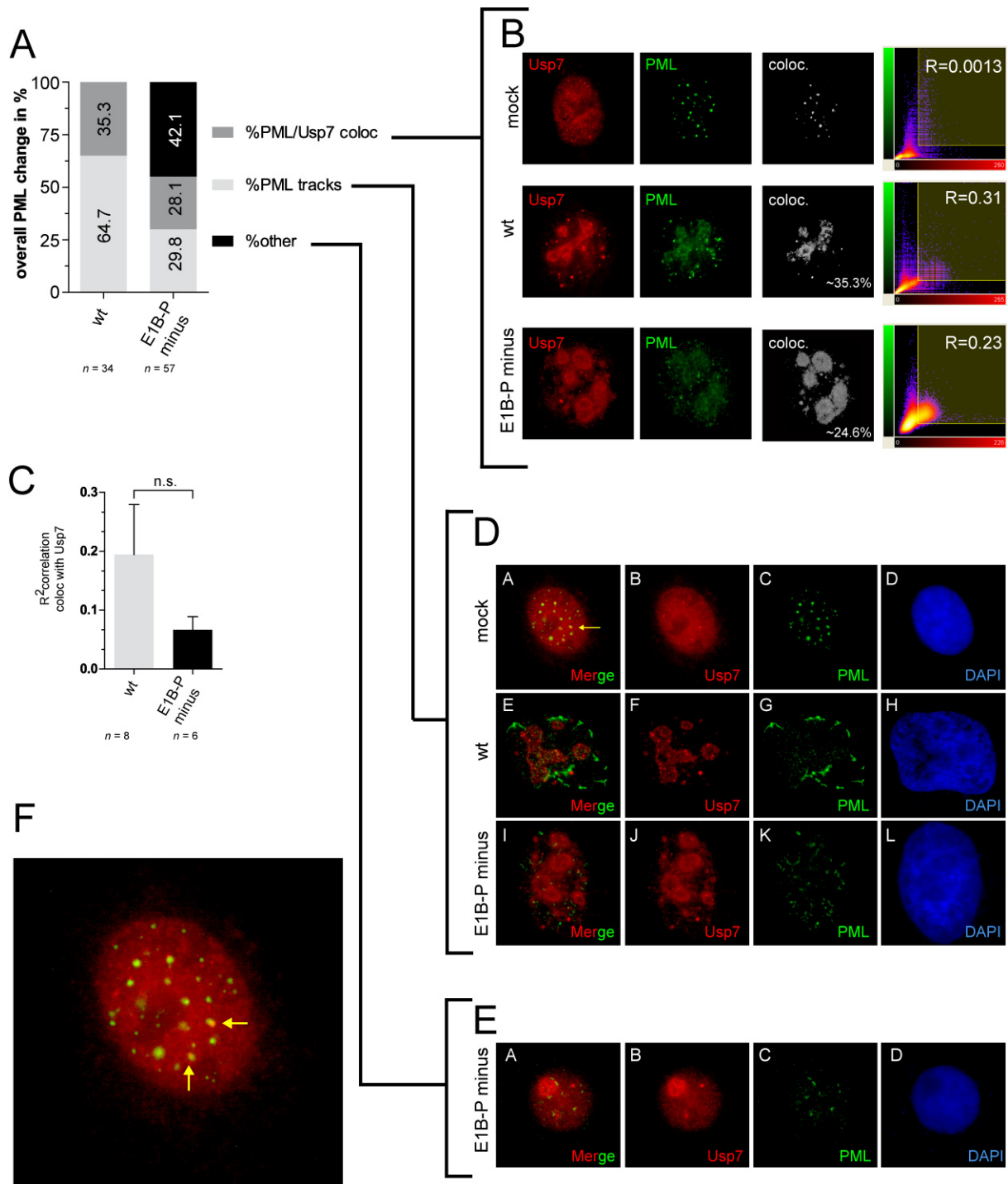


FIG 35 Usp7 and PML localization during adenoviral infection. (A) Quantification of the different Usp7 and PML phenotypes observed after wt (H5pg4100) and E1B-P minus (H5pm4174) virus infection in A549 cells (24 h p.i., MOI 20=FFU/cell). (B+C) Immunofluorescence data from cells displaying Usp7-PML colocalization were analyzed using Imaris 7.2.3. (Bitplane) to obtain the Pearson's correlation coefficient and the  $R^2$  values were plotted in the presented graph. Student *t* test was performed to assess statistical significance (GraphPad Prism 5). (D+E) Displayed are representative images showing different phenotypes as assigned by (A). (F) Image magnification showing colocalized Usp7 and PML (yellow arrows). All cells were analyzed by *in situ* immunofluorescence staining for Usp7 (3D8), PML (5E10), and DNA content (DAPI) 24 hours post infection. n.s.=not significant.

## 9 Discussion

### 9.1 E1B-55K and the dependence upon two cellular factors

Several circumstances prompted the investigations of a possible link between CK2 and Usp7 in adenovirus infection:

First, in Part I and Part II, E1B-55K faced stability problems either through ablation of the phosphosites as shown by the phosphonegative E1B-55K mutant protein E1B-P minus in H1299 cells or in the functional absence of Usp7 for wt E1B-55K. The question arose: Is this phenomenon connected to CK2 and Usp7 action on E1B-55K at the same time?

Secondly, like E1B-55K, EBV EBNA-1 interacts with CK2, Usp7 and PML-NBs. While EBNA-1 does so to disrupt PML-NBs, there is a dearth of evidence explaining a functional consequence for E1B-55K-PML-NB interaction. The question arose: Is there any functional analogy?

As hypothesized, the phosphonegative E1B-55K displayed severely reduced binding efficiency toward Usp7. Intriguingly, residual Usp7 binding remained in A549 cells, and in H1299 cells almost complete ablation of this interaction occurred (which will be discussed later). In combination with the stabilizing role of Usp7 for E1B-55K, it is appealing to think that exactly this (residual) interaction is necessary to stabilize E1B-55K. So far, the experiments in this work have provided a phenotypical description of a functional relationship between Usp7 and E1B-55K. Now, it seems quite obvious that CK2-mediated phosphorylation precedes and contributes to this functional interaction which is supported by the CK2 inhibitor experiments.

However, one question emerges: What makes the phosphonegative E1B-55K (E1B-P minus) stable in A549 cells and unstable in H1299 cells? There is a possible and quite obvious explanation for this phenomenon: As previously described, Usp7 is one of the two most important p53 binding partners and regulators. Although, E1B-P minus shows a severe defect in p53 binding some residual binding remains which is further facilitated by the accumulation of high p53 protein levels during E1B-P minus virus (H5pm4174) infection (Part I; Schwartz et al., 2008). In effect, this might be sufficient for p53-bound Usp7 to act on E1B-P minus *trans*; enough to ensure stability and at the same time suggesting an enzymatic activity behind the stabilizing effect. In the absence of p53, for example in H1299 cells, this *trans* effect is not exerted, thus E1B-P minus cannot be stabilized in this setting. This is further supported by results of other infection experiments in MRC5, hMSC and U2OS cells (all p53-positive, data

not shown) where E1B-P minus displayed no reduced protein steady-state levels. As another two examples to strengthen this idea, first, it has been shown that the Mdm2-p53-Usp7 interplay exactly allows *trans* deubiquitination of p53 (Brooks and Gu, 2004; Brooks et al., 2007), and secondly, CK2 phosphorylation-dependent protein stability has been demonstrated for ataxin-3 (Mueller et al., 2009). To analyze this hypothesis, p53 could be transfected into H1299 or depleted in A549 cells with subsequent infection of the cells with E1B-P minus and wt virus. However, it cannot be ruled out that also another protein plays a mediating role.

Another finding underlining the causal relationship between Usp7 and CK2, is the almost identical quantitative virus yield reduction in the background of HBX treatment or E1B-P minus virus (H5pm4174) infection. Intriguingly, further E1B-P minus virus growth inhibition could be achieved after Usp7 inhibitor application, again raising the possibility of Usp7 regulation of different adenoviral proteins.

So far, a mechanistic explanation was provided to understand the intricate relationship between two cellular and one viral protein.

## **9.2 PML-NBs and phospho-E1B-55K – more complexity to the CK2-Usp7 matter**

However, further analyses revealed that the amount of long track-like PML structures, which normally occur after adenovirus infection, are significantly reduced in their appearance in E1B-P minus virus infection (from 64.7 (wt) to 29.8% (E1B-P minus), and that the overall track-like formation was impaired. It has been well established that the adenoviral protein E4orf3 is responsible for transforming the PML-NBs from dot-like to track-like structures (Doucas et al., 1996; Evans and Hearing, 2003). Nevertheless, it has also been well established that E1B-55K associates to specific isoforms of PML (IV and V) (Wimmer et al., 2010). Interestingly, the PML IV isoform is discussed to be the entry site for ICP0 or EBNA-1 to gain access to other PML proteins in the PML-NBs and induce marked changes of/in the structure of the protein complex (Sivachandran et al., 2008; Sarkari et al., 2009, 2011; Frappier, 2011). Thus it is not digressive to assume that the same applies for E1B-55K. Additionally, and as elaborated above, CK2 and Usp7 are both negative regulators of PML proteins working independently of each other. In keeping with the observed phenotype of the phosphonegative E1B-55K mutant not being able to bind Usp7 and CK2 $\alpha$  and the reduction in the amount of PML tracks during E1B-P minus infection, it is tempting to speculate that E1B-55K usurps the function of both proteins in order to manipulate, assist or maintain the track formation of PML-NBs.

Another striking observation of this work and in this context, describes the relocalization of a subset or an intermediate stage of PML-NBs into ring-shaped structures as it has been reported elsewhere (Carvalho et al., 1995; Doucas et al., 1996; Weitzman et al., 1996; Rosa-Calatrava et al., 2003). Very important, these structures colocalized also significantly with Usp7 in these rings. This work demonstrates unambiguously Usp7's redistribution into viral replication centers and this may suggest that PML proteins are found there, too. In 2002 Souquerre-Besse et al. (Souquere-Besse et al., 2002) and in 2003 Rosa-Calatrava et al. (Rosa-Calatrava et al., 2003), reported PML redistribution into clear amorphous inclusions in a pIX dependent manner. Interestingly, CK2 $\alpha$  was found to be relocalized into these structures as well, along with pIX indicating CK2 $\alpha$  also playing a role in this context.

By considering all these information presented in this work, a possible model that accounts for the observations made in this study can be developed:

## 10 Thesis model

### 10.1 Phosphorylation of E1B-55K impacts its localization

E1B-55K needs to be phosphorylated in order to localize, bind and promote its functions properly. Presumably, this may happen in the cytoplasm as well as in the nucleus since colocalization or spatial proximity with CK2 $\alpha$  could be verified in both compartments. The specific relocalization of the CK2 subunits during adenoviral infection is therefore needed to:

First, dissociate the CK2 $\alpha$  subunit from the  $\beta$  subunit indirectly derivable from reduced *in vitro* E1B phosphorylation by the CK2 holoenzyme and electron microscopy imaging from Souquerre-Besse et al. (Fig. 36 model; Fig. 13) (Souquere-Besse et al., 2002).

Secondly, this will enhance E1B-55K phosphorylation since E1B-55K will be produced in larger amounts with increasing infection time.

However, CK2 phosphorylation of E1B-55K assures the balance between cytoplasmic and nuclear E1B-55K. Without CK2 phosphorylation, the equilibrium between cytoplasmic and nuclear E1B-55K will be in favor of the cytoplasmic localized E1B-55K. Since the majority of phosphonegative E1B-55K (E1B-P minus) is continuously transported out of the nucleus in a CRM1-dependent manner. This circumstance could be demonstrated in E1B-P minus infected cells where LMB treatment led to nuclear retention of the mutant protein (Fig. 36C). Hence, phosphorylation has profound effects on E1B-55K localization. A specific E1B-55K subpopulation is probably responsible for CK2 $\beta$  interaction in order to hinder CK2 $\alpha$  and

CK2 $\beta$  reassociation and keep CK2 $\alpha$  “active” (indirectly shown by *in situ* analyses and coimmunoprecipitation analyses; Fig. 12). Surprisingly, CK2 $\alpha$  is also relocalized independently of E1B-55K since this occurs in E1B minus virus infection (Fig. 11) pointing to the involvement of another viral protein in CK2 exploitation.

### **10.2 Phosphorylation of E1B-55K – An interaction issue**

The interaction of CK2 $\alpha$  and E1B-55K is probably of transient nature since E1B-55K inherits many other interaction partners. The majority of E1B-55K associates in a virus-induced E3 ubiquitin ligase complex with E4orf6 (Ad E3 Ub ligase). However, phospho-E1B-55K has a higher affinity for E4orf6 than phosphonegative E1B-55K (E1B-P minus exhibits ~52% binding reduction; Fig. 15) and thus formation of the complete and functional Ad E3 Ub ligase is also dependent on CK2-mediated phosphorylation. Additionally, other interaction partners like p53, Mre11, CK2 $\beta$  and probably DNA ligase IV are also bound with higher affinity by phospho-E1B-55K indicating that this binding is necessary for time-dependent and efficient degradation of p53, DNA ligase IV and Mre11 (shown by Western blots; Fig. 15, 16 and 36).

### **10.3 Usp7 - A very special interaction partner**

In the nucleus E1B-55K transiently translocates to regions in the proximity of the adenoviral replication centers (shown by costainings with Usp7; Fig. 19, 36). This might be the region where E1B-55K interacts with many different cellular proteins, one of them Usp7. Usp7 is also translocated with increasing infection time to those sites (shown by costaining with E2A; Fig. 21, 36 model). However, very probable, CK2 $\alpha$  is also redirected to the same regions during adenoviral infection (compare Fig. 36D). This might have several functional outcomes and reasons:

- I. since phosphorylation is a reversible process and more E1B-55K is produced, a certain E1B-55K subpopulation needs to be phosphorylated there (again),
- II. E1B-55K can remain in the nucleus especially in the vicinity of the replication centers,
- III. and this is the prerequisite for interaction with Usp7,
- IV. this interaction is necessary for E1B-55K's stability (as shown by lower E1B-P minus levels in H1299 cells; Fig. 16+30). Nonetheless, functions can still be exerted on E1B-55K in *trans*, if a mediating protein is available (discussed in section 9.1).

- V. In fact, the nuclear redistribution of CK2 $\alpha$  and Usp7 is not solely for the good of E1B-55K *per se*. Also, E2A interacts with Usp7 (shown by coimmunoprecipitation experiments; Fig. 22) and possibly promotes E2A functions (Fig. 36 model).
- VI. Especially interaction with E2A demonstrates the role of Usp7 as a “global” player for adenoviral infection which is underlined by the defect of other adenoviral proteins in the functional absence of Usp7 (Fig 27.). However, this is only under one condition: E1B-55K must localize to the same regions as Usp7 to modulate its functions. This is indirectly shown by the virus yield reduction in E1B-P minus (H5pm4174) and E1B-P minus’ inability to bind Usp7 (Figs. 31 and 32).

#### **10.4 Possible role of CK2 $\alpha$ and Usp7 in the modulation of downstream targets**

Eventually, the nuclear redirection of Usp7 and CK2 $\alpha$  may imply that both proteins are needed to act in a certain microenvironment in order to function on each other and/or other proteins which are relocated there, too. For the former possibility, studies from others have shown that Usp7 interacts with CK2 and is phosphorylated at a CK2 consensus site (Fernández-Montalván et al., 2007). For the latter possibility, it has been demonstrated that Usp7 and CK2 associate with and can negatively regulate PML proteins. In the context of virus infection (Scaglioni et al., 2006; Sarkari et al., 2011), this may mean that E1B-55K uses both proteins, in the late phase of infection, in this microenvironment for several other reasons:

(I) PML-NBs represent a CK2-phosphorylation-dependent SUMOylation platform and due to CK2 $\alpha$  phosphorylation of E1B-55K, SUMO moieties can be attached to E1B-55K at PML platforms. E1B-55K’s substrate specificity and functional activities might be modulated in that way. This is supported by the fact that E1B-55K associates with specific PML isoforms (Wimmer et al., 2010).

(II) Assuming PML proteins exert antiviral functions upon adenovirus replication, CK2 $\alpha$  and Usp7 might be “forced” to be associated with certain isoforms of PML proteins and modulate their function due to the nature of both cellular factors as being negative regulators of PML proteins. Probably, this modulation will affect PML IV or V since E1B-55K has been shown to bind these isoforms (Wimmer et al., 2010). Moreover, immunofluorescence analyses showing increased overlap support this hypothesis (Fig. 35). Furthermore, a similar

mechanism has been described by Rosa-Calatrava et al. and would certainly conform the model stated in that publication (Rosa-Calatrava et al., 2003).

(III) Another aspect of the importance of CK2-mediated phosphorylation: phospho-E1B-55K is needed to counteract certain antiviral mechanisms. Daxx for example is not bound and degraded by phosphonegative E1B-55K (data not shown, and Wimmer et al., 2012). Under physiologic conditions Daxx is stabilized by Usp7 and degraded by Mdm2 (Tang et al., 2010). In case of adenoviral infection, Usp7 as well as Daxx are bound by E1B-55K this might lead to inhibition of Daxx stabilization and consequently increased Daxx destabilization in a proteasomal manner. Using this model, an explanation for Daxx degradation in a sole E1B-55K-dependent manner could be explained (Schreiner et al., 2010) and another reason why Usp7 binding of E1B-55K is so important.

It is clear that the model presented here lacks completeness. However, for a visual summary and better understanding of the key points discussed here, a graphical abstract is provided (Fig. 36).

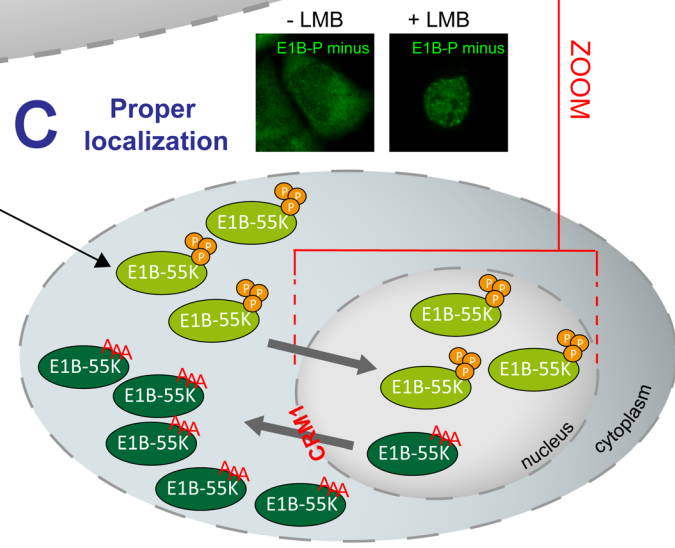
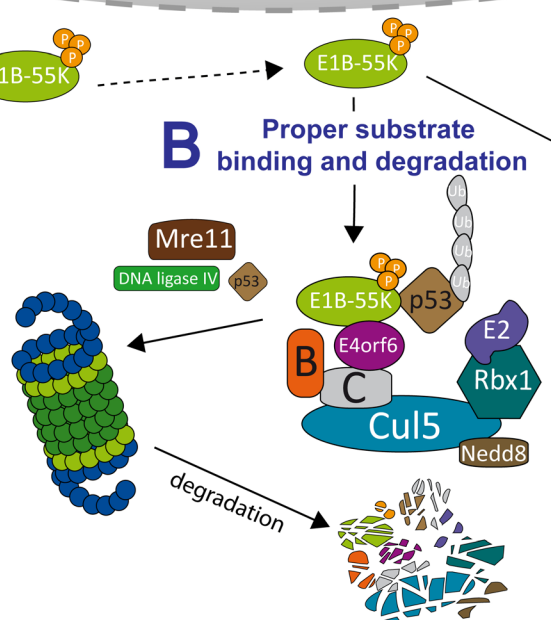
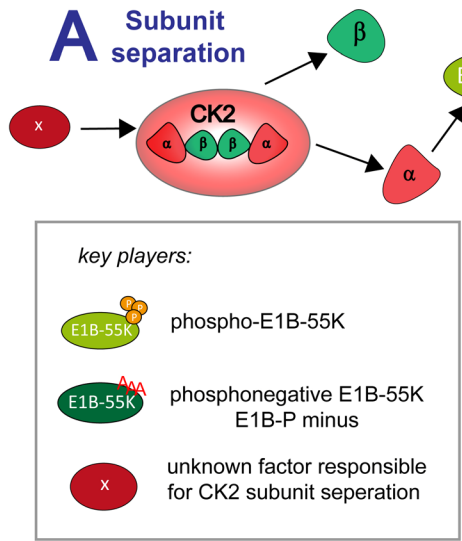
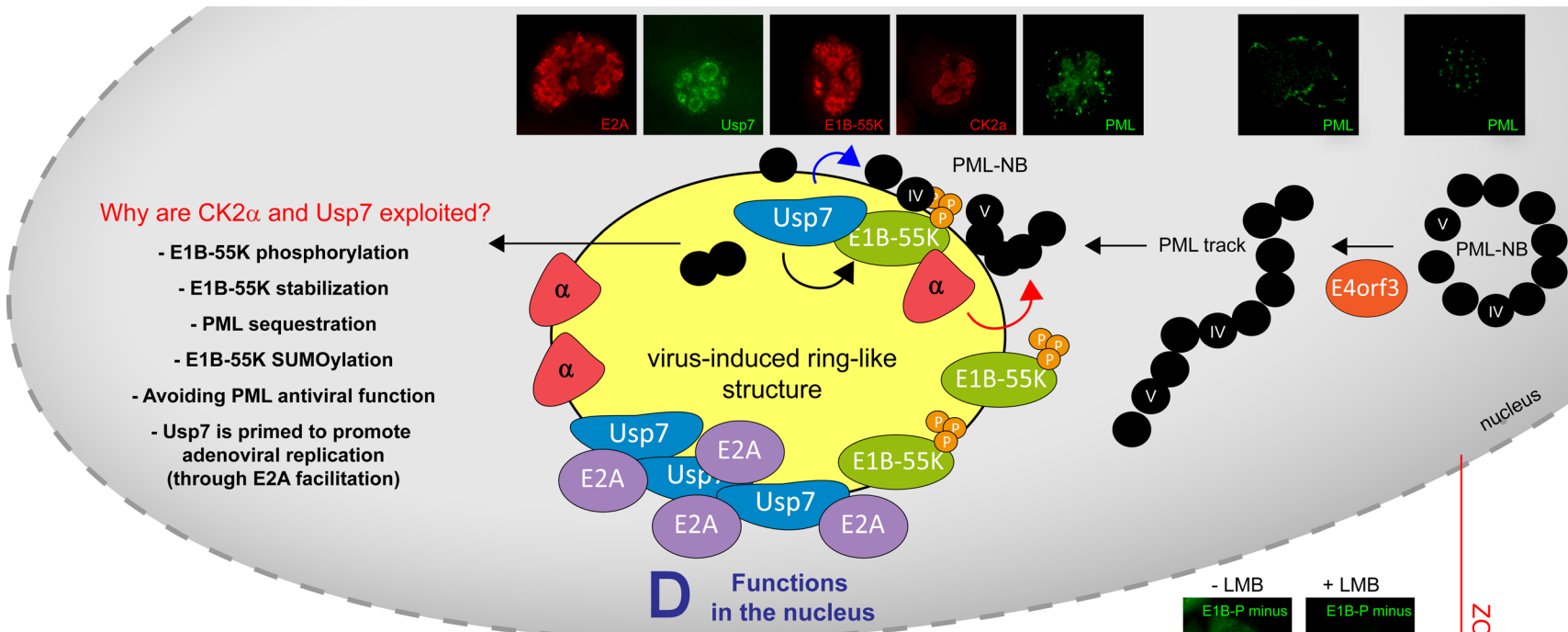


FIG 36 A visualization of certain key points discussed in the thesis model. (A) After separation from CK2 $\beta$ , CK2 $\alpha$  phosphorylates E1B-55K. (B) Phosphorylated E1B-55K assembles with E4orf6 an E3 ubiquitin ligase complex for substrate targeting. (C) Correct localization is only guaranteed after phosphorylation. Phosphonegative E1B-55K (E1B-P minus) is constantly exported out of the nucleus; LMB treatment stops this process. (D) In the nucleus phospho-E1B-55K exerts diverse functions in concert with CK2 $\alpha$  and Usp7 at virus-induced ring-like structures. For example, specific PML isoforms-targeting to promote or inhibit PML functions. Also, other proteins are bound at those sites or interact with Usp7 (E2A).

## 11 Conclusion and Outlook

In the first part of this work, the decisive relationship between cellular CK2 $\alpha$  and adenoviral E1B-55K was elucidated. For the first time, it was possible to demonstrate that a cellular factor is directly involved in posttranslational modifications of the adenoviral protein E1B-55K. Analysis of the phenotype exerted by a virus mutant with mutated phosphosites in E1B-55K (H5pm4174, E1B-P minus) revealed that this virus mutant exerts severely reduced virus growth. Especially in H1299 cells this defect is well articulated and can be explained by the following: reduced protein stability of E1B-55K and late structural proteins and a reduced/lowered viral DNA replication ability. On the contrary, these results are challenged by the fact that such negative phenotypes could not be observed during infection in A549 cells although virus yield was severely impaired making it difficult to explain the obvious negative effect during E1B-P minus infection. However, at the end of the first part, it was possible to demonstrate a functional relevance of the E1B-55K-CK2 $\alpha$  interaction.

In the second part of this work, the decisive relationship between cellular Usp7 and E1B-55K was investigated. Initial interaction analyses substantiated binding between E1B-55K and Usp7. Inhibition or knockdown of Usp7 induced a decrease in steady-state levels of E1B-55K, but surprisingly affected other adenoviral proteins in a negative way as well. More importantly, for the first time in adenovirology, it was possible to show that the application of a small-molecule inhibitor (HBX) against a cellular factor leads to severely reduced virus progeny numbers as well as impaired foci formation efficiency. However, more detailed mode-of-action analyses are favorable and planned to dissect the mechanisms lying behind Usp7 effects on the adenoviral life cycle.

In the third part of this work, an exciting link between CK2 phosphorylation of E1B-55K and the binding capability of E1B-55K towards Usp7 was presented. The phosphonegative E1B-55K exhibited severely impaired binding towards Usp7 which could be substantiated with the CK2 inhibitor experiments. Moreover, the extent of binding deficiency towards Usp7 has specific negative effects on the stability of E1B-55K (from E1B-P minus) since almost complete abolished binding led to severely reduce E1B-55K steady-state levels whereas a certain degree of residual binding could stabilize phosphonegative E1B-55K. Nevertheless, using the Usp7 model, it was possible to give a partial explanation for the observed differences between A549 and H1299 cells in Part I.

This work provides insights into the molecular mechanisms of the HAdV5 E1B-55K protein and its intricate interaction with two host cell proteins. CK2 is the kinase phosphorylating E1B-55K and Usp7 provides stability of the viral protein. Either ablation of the CK2-mediated phosphorylation on E1B-55K or inhibition of Usp7 functions, results in a profound negative outcome for the viral life cycle. With this knowledge it is therefore possible to think of strategies, which lead to targeted reduction of adenoviral particles after a disseminated adenovirus spread. As an example, this is especially important for immunocompromised patients awaiting hematopoietic stem cell transplantation. These patients face serious adenoviral infection in an increasing number of cases. In this respect, it is not digressive to assume that Usp7 inhibition alone or in combination with CK2 inhibition might result in the desired effect of diminishing the viral load. Nevertheless, similar studies involving other adenovirus types or other viruses (e.g. HSV-1, EBV) will certainly prove valuable and will help understanding the probable global nature of Usp7 and CK2 exploitation by other viral pathogens.

Undoubtedly, on the molecular level, still many questions remain and await an answer.

## 12 References

- Arrigoni, G., Marin, O., Pagano, M.A., Settimo, L., Paolin, B., Meggio, F., and Pinna, L.A. (2004). Phosphorylation of calmodulin fragments by protein kinase CK2. Mechanistic aspects and structural consequences. *Biochemistry* 43, 12788–12798.
- Babiss, L.E., and Ginsberg, H.S. (1984). Adenovirus type 5 early region 1b gene product is required for efficient shutoff of host protein synthesis. *J. Virol.* 50, 202–212.
- Babiss, L.E., Ginsberg, H.S., and Darnell, J.E., Jr (1985). Adenovirus E1B proteins are required for accumulation of late viral mRNA and for effects on cellular mRNA translation and transport. *Mol. Cell. Biol.* 5, 2552–2558.
- Baker, A., Rohleder, K.J., Hanakahi, L.A., and Ketner, G. (2007). Adenovirus E4 34k and E1b 55k oncoproteins target host DNA ligase IV for proteasomal degradation. *J. Virol.* 81, 7034–7040.
- Banning, C., Votteler, J., Hoffmann, D., Koppensteiner, H., Warmer, M., Reimer, R., Kirchhoff, F., Schubert, U., Hauber, J., and Schindler, M. (2010). A flow cytometry-based FRET assay to identify and analyse protein-protein interactions in living cells. *PLoS ONE* 5, e9344.
- Barral, P.M., Rusch, A., Turnell, A.S., Gallimore, P.H., Byrd, P.J., Dobner, T., and Grand, R.J.A. (2005). The interaction of the hnRNP family member E1B-AP5 with p53. *FEBS Lett.* 579, 2752–2758.
- Benkő, M., and Harrach, B. (1998). A proposal for a new (third) genus within the family Adenoviridae. *Arch. Virol.* 143, 829–837.
- Bergelson, J.M., Cunningham, J.A., Droguett, G., Kurt-Jones, E.A., Krithivas, A., Hong, J.S., Horwitz, M.S., Crowell, R.L., and Finberg, R.W. (1997). Isolation of a common receptor for Coxsackie B viruses and adenoviruses 2 and 5. *Science* 275, 1320–1323.
- Berget, S.M., and Sharp, P.A. (1977). A spliced sequence at the 5'-terminus of adenovirus late mRNA. *Brookhaven Symp. Biol.* 332–344.
- Berk, A.J. (2005). Recent lessons in gene expression, cell cycle control, and cell biology from adenovirus. *Oncogene* 24, 7673–7685.
- Berk, A.J. (2007). Adenoviridae: The viruses and their replication. pp. 2355–2394.
- Blackford, A.N., and Grand, R.J.A. (2009). Adenovirus E1B 55-kilodalton protein: multiple roles in viral infection and cell transformation. *J. Virol.* 83, 4000–4012.
- Blanchette, P., Cheng, C.Y., Yan, Q., Ketner, G., Ornelles, D.A., Dobner, T., Conaway, R.C., Conaway, J.W., and Branton, P.E. (2004). Both BC-box motifs of adenovirus protein E4orf6 are required to efficiently assemble an E3 ligase complex that degrades p53. *Mol. Cell. Biol.* 24, 9619–9629.
- Blanchette, P., Kindsmüller, K., Groitl, P., Dallaire, F., Speiseder, T., Branton, P.E., and Dobner, T. (2008). Control of mRNA export by adenovirus E4orf6 and E1B55K proteins during productive infection requires E4orf6 ubiquitin ligase activity. *J. Virol.* 82, 2642–2651.

- Boutell, C., Canning, M., Orr, A., and Everett, R.D. (2005). Reciprocal activities between herpes simplex virus type 1 regulatory protein ICP0, a ubiquitin E3 ligase, and ubiquitin-specific protease USP7. *J. Virol.* *79*, 12342–12354.
- Bradford, M. M. (1976). A rapid and sensitive method for the quantitation of microgram quantities of protein utilizing the principle of protein-dye binding. *Anal Biochem*, *72*, 248-54.
- Brennan, C.M., Gallouzi, I.E., and Steitz, J.A. (2000). Protein ligands to HuR modulate its interaction with target mRNAs in vivo. *J. Cell Biol.* *151*, 1–14.
- Brooks, C.L., and Gu, W. (2004). Dynamics in the p53-Mdm2 ubiquitination pathway. *Cell Cycle* *3*, 895–899.
- Brooks, C.L., Li, M., Hu, M., Shi, Y., and Gu, W. (2007). The p53--Mdm2--HAUSP complex is involved in p53 stabilization by HAUSP. *Oncogene* *26*, 7262–7266.
- Buchou, T., Vernet, M., Blond, O., Jensen, H.H., Pointu, H., Olsen, B.B., Cochet, C., Issinger, O.-G., and Boldyreff, B. (2003). Disruption of the regulatory beta subunit of protein kinase CK2 in mice leads to a cell-autonomous defect and early embryonic lethality. *Mol. Cell. Biol.* *23*, 908–915.
- Bullock, W.O., Fernandez, J.M., and Short, J.M. (1987). XL1-Blue: A high efficiency plasmid transforming recA *Escherichia coli* strain with b-galactosidase selection. In *In Biotechniques* *5*, p.
- Burgert, H.G., and Blusch, J.H. (2000). Immunomodulatory functions encoded by the E3 transcription unit of adenoviruses. *Virus Genes* *21*, 13–25.
- Canning, M., Boutell, C., Parkinson, J., and Everett, R.D. (2004). A RING finger ubiquitin ligase is protected from autocatalyzed ubiquitination and degradation by binding to ubiquitin-specific protease USP7. *J. Biol. Chem.* *279*, 38160–38168.
- Carvalho, T., Seeler, J.S., Ohman, K., Jordan, P., Pettersson, U., Akusjärvi, G., Carmo-Fonseca, M., and Dejean, A. (1995). Targeting of adenovirus E1A and E4-ORF3 proteins to nuclear matrix-associated PML bodies. *J. Cell Biol.* *131*, 45–56.
- Catalucci, D., Sporeno, E., Cirillo, A., Ciliberto, G., Nicosia, A., and Colloca, S. (2005). An adenovirus type 5 (Ad5) amplicon-based packaging cell line for production of high-capacity helper-independent deltaE1-E2-E3-E4 Ad5 vectors. *J. Virol.* *79*, 6400–6409.
- Cathomen, T., and Weitzman, M.D. (2000). A functional complex of adenovirus proteins E1B-55kDa and E4orf6 is necessary to modulate the expression level of p53 but not its transcriptional activity. *J. Virol.* *74*, 11407–11412.
- Chahal, J.S., and Flint, S.J. (2012). Timely Synthesis of the Adenovirus Type 5 E1B 55-Kilodalton Protein Is Required for Efficient Genome Replication in Normal Human Cells. *J. Virol.* *86*, 3064–3072.
- Chakraborty, A.A., and Tansey, W.P. (2009). Adenoviral E1A function through Myc. *Cancer Res.* *69*, 6–9.
- Chemnitz, J., Pieper, D., Grüttner, C., and Hauber, J. (2009). Phosphorylation of the HuR ligand APRIL by casein kinase 2 regulates CD83 expression. *Eur. J. Immunol.* *39*, 267–279.

- Chen, Y.-L., Yin, Z., Lakshminarayana, S.B., Qing, M., Schul, W., Duraiswamy, J., Kondreddi, R.R., Goh, A., Xu, H.Y., Yip, A., et al. (2010). Inhibition of dengue virus by an ester prodrug of an adenosine analog. *Antimicrob. Agents Chemother.* *54*, 3255–3261.
- Chow, L.C., Gelinas, R.E., Broker, T.R., and Roberts, R.J. (2000). An amazing sequence arrangement at the 5' ends of adenovirus 2 messenger RNA. 1977. *Rev. Med. Virol.* *10*, 362–371; discussion 355–356.
- Chow, L.T., Lewis, J.B., and Broker, T.R. (1980). RNA transcription and splicing at early and intermediate times after adenovirus-2 infection. *Cold Spring Harb. Symp. Quant. Biol.* *44 Pt 1*, 401–414.
- Cuconati, A., Mukherjee, C., Perez, D., and White, E. (2003). DNA Damage Response and MCL-1 Destruction Initiate Apoptosis in Adenovirus-Infected Cells. *Genes Dev.* *17*, 2922–2932.
- Cummins, J.M., and Vogelstein, B. (2004). HAUSP is required for p53 destabilization. *Cell Cycle* *3*, 689–692.
- Dallaire, F., Blanchette, P., Groitl, P., Dobner, T., and Branton, P.E. (2009). Identification of integrin alpha3 as a new substrate of the adenovirus E4orf6/E1B 55-kilodalton E3 ubiquitin ligase complex. *J. Virol.* *83*, 5329–5338.
- Daubeuf, S., Singh, D., Tan, Y., Liu, H., Federoff, H.J., Bowers, W.J., and Tolba, K. (2009). HSV ICP0 recruits USP7 to modulate TLR-mediated innate response. *Blood* *113*, 3264–3275.
- Davison, A.J., Benko, M., and Harrach, B. (2003). Genetic content and evolution of adenoviruses. *J. Gen. Virol.* *84*, 2895–2908.
- Defer, C., Belin, M.T., Caillet-Boudin, M.L., and Boulanger, P. (1990). Human adenovirus-host cell interactions: comparative study with members of subgroups B and C. *J. Virol.* *64*, 3661–3673.
- Desagher, S., Osen-Sand, A., Montessuit, S., Magnenat, E., Vilbois, F., Hochmann, A., Journot, L., Antonsson, B., and Martinou, J.C. (2001). Phosphorylation of bid by casein kinases I and II regulates its cleavage by caspase 8. *Mol. Cell* *8*, 601–611.
- Doble, B.W., and Woodgett, J.R. (2003). GSK-3: tricks of the trade for a multi-tasking kinase. *J. Cell. Sci.* *116*, 1175–1186.
- Dobner, T., and Kzhyshkowska, J. (2001). Nuclear export of adenovirus RNA. *Curr. Top. Microbiol. Immunol.* *259*, 25–54.
- Doerr, H.W., and Gerlich, W.H. (2009). *Medizinische Virologie: Grundlagen, Diagnostik, Prävention und Therapie viraler Erkrankungen* (Thieme, Stuttgart).
- Doucas, V., Ishov, A.M., Romo, A., Juguilon, H., Weitzman, M.D., Evans, R.M., and Maul, G.G. (1996). Adenovirus replication is coupled with the dynamic properties of the PML nuclear structure. *Genes Dev.* *10*, 196–207.
- DuBridge, R.B., Tang, P., Hsia, H.C., Leong, P.M., Miller, J.H., and Calos, M.P. (1987). Analysis of mutation in human cells by using an Epstein-Barr virus shuttle system. *Mol. Cell. Biol.* *7*, 379–387.

- El-Guindy, A.S., and Miller, G. (2004). Phosphorylation of Epstein-Barr virus ZEBRA protein at its casein kinase 2 sites mediates its ability to repress activation of a viral lytic cycle late gene by Rta. *J. Virol.* *78*, 7634–7644.
- Endter, C., and Dobner, T. (2004). Cell transformation by human adenoviruses. *Curr. Top. Microbiol. Immunol.* *273*, 163–214.
- Endter, C., Härtl, B., Spruss, T., Hauber, J., and Dobner, T. (2005). Blockage of CRM1-dependent nuclear export of the adenovirus type 5 early region 1B 55-kDa protein augments oncogenic transformation of primary rat cells. *Oncogene* *24*, 55–64.
- Endter, C., Kzhyshkowska, J., Stauber, R., and Dobner, T. (2001). SUMO-1 modification required for transformation by adenovirus type 5 early region 1B 55-kDa oncoprotein. *Proc. Natl. Acad. Sci. U.S.A.* *98*, 11312–11317.
- Evans, J.D., and Hearing, P. (2003). Distinct roles of the Adenovirus E4 ORF3 protein in viral DNA replication and inhibition of genome concatenation. *J. Virol.* *77*, 5295–5304.
- Everett, R.D., Meredith, M., and Orr, A. (1999). The ability of herpes simplex virus type 1 immediate-early protein Vmw110 to bind to a ubiquitin-specific protease contributes to its roles in the activation of gene expression and stimulation of virus replication. *J. Virol.* *73*, 417–426.
- Everett, R.D., Meredith, M., Orr, A., Cross, A., Kathoria, M., and Parkinson, J. (1997). A novel ubiquitin-specific protease is dynamically associated with the PML nuclear domain and binds to a herpesvirus regulatory protein. *Embo J.* *16*, 1519–1530.
- Everts, M., and Curiel, D.T. (2004). Transductional targeting of adenoviral cancer gene therapy. *Curr Gene Ther* *4*, 337–346.
- Faesen, A.C., Dirac, A.M.G., Shanmugham, A., Ovaa, H., Perrakis, A., and Sixma, T.K. (2011). Mechanism of USP7/HAUSP activation by its C-terminal ubiquitin-like domain and allosteric regulation by GMP-synthetase. *Mol. Cell* *44*, 147–159.
- Fernández-Montalván, A., Bouwmeester, T., Joberty, G., Mader, R., Mahnke, M., Pierrat, B., Schlaeppli, J.-M., Worpenberg, S., and Gerhartz, B. (2007). Biochemical characterization of USP7 reveals post-translational modification sites and structural requirements for substrate processing and subcellular localization. *Febs J.* *274*, 4256–4270.
- Filhol, O., Cochet, C., Wedegaertner, P., Gill, G.N., and Chambaz, E.M. (1991). Coexpression of both alpha and beta subunits is required for assembly of regulated casein kinase II. *Biochemistry* *30*, 11133–11140.
- Filhol, O., Nueda, A., Martel, V., Gerber-Scokaert, D., Benitez, M.J., Souchier, C., Saoudi, Y., and Cochet, C. (2003). Live-cell fluorescence imaging reveals the dynamics of protein kinase CK2 individual subunits. *Mol. Cell. Biol.* *23*, 975–987.
- Flint, S.J., and Gonzalez, R.A. (2003). Regulation of mRNA production by the adenoviral E1B 55-kDa and E4 Orf6 proteins. *Curr. Top. Microbiol. Immunol.* *272*, 287–330.
- Franck, N., Le Seyec, J., Guguen-Guillouzo, C., and Erdtmann, L. (2005). Hepatitis C virus NS2 protein is phosphorylated by the protein kinase CK2 and targeted for degradation to the proteasome. *J. Virol.* *79*, 2700–2708.

- Frappier, L. (2011). Viral disruption of promyelocytic leukemia (PML) nuclear bodies by hijacking host PML regulators. *Virulence* 2, 58–62.
- Giard, D.J., Aaronson, S.A., Todaro, G.J., Arnstein, P., Kersey, J.H., Dosik, H., and Parks, W.P. (1973). In vitro cultivation of human tumors: establishment of cell lines derived from a series of solid tumors. *J. Natl. Cancer Inst.* 51, 1417–1423.
- Gonzalez, R., Huang, W., Finnen, R., Bragg, C., and Flint, S.J. (2006). Adenovirus E1B 55-kilodalton protein is required for both regulation of mRNA export and efficient entry into the late phase of infection in normal human fibroblasts. *J. Virol.* 80, 964–974.
- Gonzalez, R.A., and Flint, S.J. (2002). Effects of mutations in the adenoviral E1B 55-kilodalton protein coding sequence on viral late mRNA metabolism. *J. Virol.* 76, 4507–4519.
- Gooding, L.R., and Wold, W.S. (1990). Molecular mechanisms by which adenoviruses counteract antiviral immune defenses. *Crit. Rev. Immunol.* 10, 53–71.
- Goodrum, F.D., and Ornelles, D.A. (1998). p53 status does not determine outcome of E1B 55-kilodalton mutant adenovirus lytic infection. *J. Virol.* 72, 9479–9490.
- Graham, F.L., Rowe, D.T., McKinnon, R., Bacchetti, S., Ruben, M., and Branton, P.E. (1984). Transformation by human adenoviruses. *J Cell Physiol Suppl* 3, 151–163.
- Graham, F.L., Smiley, J., Russell, W.C., and Nairn, R. (1977). Characteristics of a human cell line transformed by DNA from human adenovirus type 5. *J. Gen. Virol.* 36, 59–74.
- Graham, K.C., and Litchfield, D.W. (2000). The regulatory beta subunit of protein kinase CK2 mediates formation of tetrameric CK2 complexes. *J. Biol. Chem.* 275, 5003–5010.
- Grässer, F.A., Göttel, S., Haiss, P., Boldyreff, B., Issinger, O.G., and Mueller-Lantzsch, N. (1992). Phosphorylation of the Epstein-Barr virus nuclear antigen 2. *Biochem. Biophys. Res. Commun.* 186, 1694–1701.
- Guedat, P., Boissy, G., Borg-Capra, C., Colland, F., Daviet, L., Formstecher, E., Jacq, X., Rain, J.-C., Delansorn, R., Vallese, S., et al. (2007). Novel cysteine protease inhibitors and their therapeutic applications.
- Guerra, B., Götz, C., Wagner, P., Montenarh, M., and Issinger, O.G. (1997). The carboxy terminus of p53 mimics the polylysine effect of protein kinase CK2-catalyzed MDM2 phosphorylation. *Oncogene* 14, 2683–2688.
- Gustafsson, B., Huang, W., Bogdanovic, G., Gauffin, F., Nordgren, A., Talekar, G., Ornelles, D.A., and Gooding, L.R. (2007). Adenovirus DNA is detected at increased frequency in Guthrie cards from children who develop acute lymphoblastic leukaemia. *Br. J. Cancer* 97, 992–994.
- Hahn, W.C., Counter, C.M., Lundberg, A.S., Beijersbergen, R.L., Brooks, M.W., and Weinberg, R.A. (1999). Creation of human tumour cells with defined genetic elements. *Nature* 400, 464–468.
- Harlow, E., Franza, B.R., Jr, and Schley, C. (1985). Monoclonal antibodies specific for adenovirus early region 1A proteins: extensive heterogeneity in early region 1A products. *J. Virol.* 55, 533–546.

- Härtl, B., Zeller, T., Blanchette, P., Kremmer, E., and Dobner, T. (2008). Adenovirus type 5 early region 1B 55-kDa oncoprotein can promote cell transformation by a mechanism independent from blocking p53-activated transcription. *Oncogene* 27, 3673–3684.
- Horwitz, M.S. (2001a). Adenovirus immunoregulatory genes and their cellular targets. *Virology* 279, 1–8.
- Horwitz, M.S. (2001b). Adenovirus immunoregulatory genes and their cellular targets. *Virology* 279, 1–8.
- Hu, M., Li, P., Li, M., Li, W., Yao, T., Wu, J. W., Gu, W., Cohen, R. E., and Shi, Y. (2002). Crystal structure of a UBP-family deubiquitinating enzyme in isolation and in complex with ubiquitin aldehyde. *Cell*, 111, 1041-1054.
- Hu, M., Gu, L., Li, M., Jeffrey, P. D., Gu, W., Shi, Y (2006). Structural basis of competitive recognition of p53 and MDM2 by HAUSP/USP7: implications for the regulation of the p53-MDM2 pathway. *PLoS Biol*, 4,e27
- Hussain, S., Zhang, Y., and Galardy, P.J. (2009). DUBs and cancer: the role of deubiquitinating enzymes as oncogenes, non-oncogenes and tumor suppressors. *Cell Cycle* 8, 1688–1697.
- Kindsmüller, K., Groitl, P., Härtl, B., Blanchette, P., Hauber, J., and Dobner, T. (2007). Intranuclear targeting and nuclear export of the adenovirus E1B-55K protein are regulated by SUMO1 conjugation. *Proc. Natl. Acad. Sci. U.S.A.* 104, 6684–6689.
- Kindsmüller, K., Schreiner, S., Leinenkugel, F., Groitl, P., Kremmer, E., and Dobner, T. (2009). A 49-kilodalton isoform of the adenovirus type 5 early region 1B 55-kilodalton protein is sufficient to support virus replication. *J. Virol.* 83, 9045–9056.
- Koffa, M.D., Kean, J., Zachos, G., Rice, S.A., and Clements, J.B. (2003). CK2 protein kinase is stimulated and redistributed by functional herpes simplex virus ICP27 protein. *J. Virol.* 77, 4315–4325.
- Koppensteiner, H., Banning, C., Schneider, C., Hohenberg, H., and Schindler, M. (2012). Macrophage Internal HIV-1 Is Protected from Neutralizing Antibodies. *J. Virol.* 86, 2826–2836.
- Kosulin, K., Haberler, C., Hainfellner, J.A., Amann, G., Lang, S., and Lion, T. (2007). Investigation of adenovirus occurrence in pediatric tumor entities. *J. Virol.* 81, 7629–7635.
- Koyuncu, E. (2009). Ubiquitin-specific Protease 7 Plays a Critical Role in Control of Lytic Infection and Cell Transformation by Human Adenovirus Type 5. Dissertation.
- Kuwano, K., Kawasaki, M., Kunitake, R., Hagimoto, N., Nomoto, Y., Matsuba, T., Nakanishi, Y., and Hara, N. (1997). Detection of group C adenovirus DNA in small-cell lung cancer with the nested polymerase chain reaction. *J. Cancer Res. Clin. Oncol.* 123, 377–382.
- Kzhyshkowska, J., Kremmer, E., Hofmann, M., Wolf, H., and Dobner, T. (2004). Protein arginine methylation during lytic adenovirus infection. *Biochem. J.* 383, 259–265.

- Landesman-Bollag, E., Song, D.H., Romieu-Mourez, R., Sussman, D.J., Cardiff, R.D., Sonenshein, G.E., and Seldin, D.C. (2001). Protein kinase CK2: signaling and tumorigenesis in the mammary gland. *Mol. Cell. Biochem.* *227*, 153–165.
- Lange, C., Schroeder, J., Stute, N., Lioznov, M.V., and Zander, A.R. (2005). High-potential human mesenchymal stem cells. *Stem Cells Dev.* *14*, 70–80.
- Lee H. J., Kim M. S., Kim Y. K., Oh Y. K., and Baek K. H. (2005). HAUSP, a deubiquitinating enzyme for p53, is polyubiquitinated, polyubiquitinated, and dimerized. *FEBS Lett.* *579*, 4867–4872.
- Lee, H.-R., Choi, W.-C., Lee, S., Hwang, J., Hwang, E., Guchhait, K., Haas, J., Toth, Z., Jeon, Y.H., Oh, T.-K., et al. (2011). Bilateral inhibition of HAUSP deubiquitinase by a viral interferon regulatory factor protein. *Nat. Struct. Mol. Biol.* *18*, 1336–1344.
- Lenaerts, L., De Clercq, E., and Naesens, L. (2008). Clinical features and treatment of adenovirus infections. *Rev. Med. Virol.* *18*, 357–374.
- Lilley, C.E., Schwartz, R.A., and Weitzman, M.D. (2007). Using or abusing: viruses and the cellular DNA damage response. *Trends Microbiol.* *15*, 119–126.
- Liu, H., Naismith, J.H., and Hay, R.T. (2003). Adenovirus DNA replication. *Curr. Top. Microbiol. Immunol.* *272*, 131–164.
- Llorens, F., Roher, N., Miró, F.A., Sarno, S., Ruiz, F.X., Meggio, F., Plana, M., Pinna, L.A., and Itarte, E. (2003). Eukaryotic translation-initiation factor eIF2beta binds to protein kinase CK2: effects on CK2alpha activity. *Biochem. J.* *375*, 623–631.
- Lowe, S.W., and Ruley, H.E. (1993). Stabilization of the p53 tumor suppressor is induced by adenovirus 5 E1A and accompanies apoptosis. *Genes Dev.* *7*, 535–545.
- Malette, P., Yee, S.P., and Branton, P.E. (1983). Studies on the phosphorylation of the 58000 dalton early region 1B protein of human adenovirus type 5. *J. Gen. Virol.* *64*, 1069–1078.
- Malik, P., and Clements, J.B. (2004). Protein kinase CK2 phosphorylation regulates the interaction of Kaposi's sarcoma-associated herpesvirus regulatory protein ORF57 with its multifunctional partner hnRNP K. *Nucleic Acids Res.* *32*, 5553–5569.
- Marton, M.J., Baim, S.B., Ornelles, D.A., and Shenk, T. (1990). The adenovirus E4 17-kilodalton protein complexes with the cellular transcription factor E2F, altering its DNA-binding properties and stimulating E1A-independent accumulation of E2 mRNA. *J. Virol.* *64*, 2345–2359.
- Mathews, M.B., and Shenk, T. (1991). Adenovirus virus-associated RNA and translation control. *J. Virol.* *65*, 5657–5662.
- Mathias, P., Wickham, T., Moore, M., and Nemerow, G. (1994). Multiple adenovirus serotypes use alpha v integrins for infection. *J. Virol.* *68*, 6811–6814.
- McBride, W.D., and Wiener, A. (1964). In Vitro Transformation of Hamster Kidney Cells By Human Adenovirus Type 12. *Proc. Soc. Exp. Biol. Med.* *115*, 870–874.

- Medina-Palazon, C., Gruffat, H., Mure, F., Filhol, O., Vingtdoux-Didier, V., Drobecq, H., Cochet, C., Sergeant, N., Sergeant, A., and Manet, E. (2007). Protein kinase CK2 phosphorylation of EB2 regulates its function in the production of Epstein-Barr virus infectious viral particles. *J. Virol.* *81*, 11850–11860.
- Meggio, F., and Pinna, L.A. (2003). One-thousand-and-one substrates of protein kinase CK2? *Faseb J.* *17*, 349–368.
- Meredith, M., Orr, A., and Everett, R. (1994). Herpes simplex virus type 1 immediate-early protein Vmw110 binds strongly and specifically to a 135-kDa cellular protein. *Virology* *200*, 457–469.
- Mitsudomi, T., Steinberg, S.M., Nau, M.M., Carbone, D., D'Amico, D., Bodner, S., Oie, H.K., Linnoila, R.I., Mulshine, J.L., and Minna, J.D. (1992). p53 gene mutations in non-small-cell lung cancer cell lines and their correlation with the presence of ras mutations and clinical features. *Oncogene* *7*, 171–180.
- Montenarh, M. (2010). Cellular regulators of protein kinase CK2. *Cell Tissue Res.* *342*, 139–146.
- Moore, M., Horikoshi, N., and Shenk, T. (1996). Oncogenic potential of the adenovirus E4orf6 protein. *Proc Natl Acad Sci U S A* *93*, 11295–11301.
- Mueller, T., Breuer, P., Schmitt, I., Walter, J., Evert, B.O., and Wüllner, U. (2009). CK2-dependent phosphorylation determines cellular localization and stability of ataxin-3. *Hum. Mol. Genet.* *18*, 3334–3343.
- Münstermann, U., Fritz, G., Seitz, G., Lu, Y.P., Schneider, H.R., and Issinger, O.G. (1990). Casein kinase II is elevated in solid human tumours and rapidly proliferating non-neoplastic tissue. *Eur. J. Biochem.* *189*, 251–257.
- Nevels, M., Rubenwolf, S., Spruss, T., Wolf, H., and Dobner, T. (1997). The Adenovirus E4orf6 Protein Can Promote E1A/E1B-Induced Focus Formation by Interfering with P53 Tumor Suppressor Function. *Pnas* *94*, 1206–1211.
- Nevels, M., Spruss, T., Wolf, H., and Dobner, T. (1999a). The adenovirus E4orf6 protein contributes to malignant transformation by antagonizing E1A-induced accumulation of the tumor suppressor protein p53. *Oncogene* *18*, 9–17.
- Nevels, M., Täuber, B., Kremmer, E., Spruss, T., Wolf, H., and Dobner, T. (1999b). Transforming Potential of the Adenovirus Type 5 E4orf3 Protein. *J Virol* *73*, 1591–1600.
- Nevins, J.R., and Vogt, P.K. (1996). Cell transformation by viruses. In *Virology*, (Lippincott-Raven, New York), pp. 301–343.
- Nicholson, B., and Suresh Kumar, K.G. (2011). The multifaceted roles of USP7: new therapeutic opportunities. *Cell Biochem. Biophys.* *60*, 61–68.
- Niefind, K., Pütter, M., Guerra, B., Issinger, O.G., and Schomburg, D. (1999). GTP plus water mimic ATP in the active site of protein kinase CK2. *Nat. Struct. Biol.* *6*, 1100–1103.
- Ohman, K., Nordqvist, K., Linder, S., and Akusjarvi, G. (1995). Effect of adenovirus-2 early region-4 products on e1-transformation. *Int. J. Oncol.* *6*, 663–668.

- Orazio, N.I., Naeger, C.M., Karlseder, J., and Weitzmann, M.D. (2011). The adenovirus E1b55K/E4orf6 complex induces degradation of the Bloom helicase during infection. *J. Virol.* *85*, 1887-1892.
- Pagano, M.A., Bain, J., Kazimierczuk, Z., Sarno, S., Ruzzene, M., Di Maira, G., Elliott, M., Orzeszko, A., Cozza, G., Meggio, F., et al. (2008). The selectivity of inhibitors of protein kinase CK2: an update. *Biochem. J.* *415*, 353–365.
- Pagano, M.A., Meggio, F., Ruzzene, M., Andrzejewska, M., Kazimierczuk, Z., and Pinna, L.A. (2004). 2-Dimethylamino-4,5,6,7-tetrabromo-1H-benzimidazole: a novel powerful and selective inhibitor of protein kinase CK2. *Biochem. Biophys. Res. Commun.* *321*, 1040–1044.
- Park, J.W., and Bae, Y.S. (1999). Phosphorylation of ribosomal protein L5 by protein kinase CKII decreases its 5S rRNA binding activity. *Biochem. Biophys. Res. Commun.* *263*, 475–481.
- Pegg, A.E., and McCann, P.P. (1982). Polyamine metabolism and function. *Am. J. Physiol.* *243*, C212–221.
- Piazza, F., Manni, S., Ruzzene, M., Pinna, L.A., Gurrieri, C., and Semenzato, G. (2012). Protein kinase CK2 in hematologic malignancies: reliance on a pivotal cell survival regulator by oncogenic signaling pathways. *Leukemia: Official Journal of the Leukemia Society of America, Leukemia Research Fund, U.K.*
- Pilder, S., Moore, M., Logan, J., and Shenk, T. (1986). The adenovirus E1B-55K transforming polypeptide modulates transport or cytoplasmic stabilization of viral and host cell mRNAs. *Mol. Cell. Biol.* *6*, 470–476.
- Pinna, L.A. (1990). Casein kinase 2: an “eminence grise” in cellular regulation? *Biochim. Biophys. Acta* *1054*, 267–284.
- Pinna, L.A. (1997). Protein kinase CK2. *Int. J. Biochem. Cell Biol.* *29*, 551–554.
- Pinna, L.A. (2002). Protein kinase CK2: a challenge to canons. *J. Cell. Sci.* *115*, 3873–3878.
- Pistorius, K., Seitz, G., Remberger, K., and Issinger, O.G. (1991). Differential CKII Activities in Human Colorectal Mucosa, Adenomas and Carcinomas. *Onkologie* *14*, 256–260.
- Pombo, A., Ferreira, J., Bridge, E., and Carmo-Fonseca, M. (1994). Adenovirus replication and transcription sites are spatially separated in the nucleus of infected cells. *Embo J.* *13*, 5075–5085.
- Puvion-Dutilleul, F., Chelbi-Alix, M.K., Koken, M., Quignon, F., Puvion, E., and de Thé, H. (1995). Adenovirus infection induces rearrangements in the intranuclear distribution of the nuclear body-associated PML protein. *Exp. Cell Res.* *218*, 9–16.
- Querido, E., Morrison, M.R., Chu-Pham-Dang, H., Thirlwell, S.W., Boivin, D., Branton, P.E., and Morrison, M.R. (2001). Identification of three functions of the adenovirus e4orf6 protein that mediate p53 degradation by the E4orf6-E1B55K complex. *J. Virol.* *75*, 699–709.
- Reich, N.C., Sarnow, P., Duprey, E., and Levine, A.J. (1983). Monoclonal antibodies which recognize native and denatured forms of the adenovirus DNA-binding protein. *Virology* *128*, 480–484.

- Rojas, S., Corbin-Lickfett, K.A., Escudero-Paunetto, L., and Sandri-Goldin, R.M. (2010). ICP27 phosphorylation site mutants are defective in herpes simplex virus 1 replication and gene expression. *J. Virol.* *84*, 2200–2211.
- Rosa-Calatrava, M., Puvion-Dutilleul, F., Lutz, P., Dreyer, D., de Thé, H., Chatton, B., and Kedinger, C. (2003). Adenovirus protein IX sequesters host-cell promyelocytic leukaemia protein and contributes to efficient viral proliferation. *EMBO Rep.* *4*, 969–975.
- Salvi, M., Sarno, S., Cesaro, L., Nakamura, H., and Pinna, L.A. (2009). Extraordinary pleiotropy of protein kinase CK2 revealed by weblogo phosphoproteome analysis. *Biochim. Biophys. Acta* *1793*, 847–859.
- Sarkari, F., Sanchez-Alcaraz, T., Wang, S., Holowaty, M.N., Sheng, Y., and Frappier, L. (2009). EBNA1-mediated recruitment of a histone H2B deubiquitylating complex to the Epstein-Barr virus latent origin of DNA replication. *PLoS Pathog.* *5*, e1000624.
- Sarkari, F., Wang, X., Nguyen, T., and Frappier, L. (2011). The herpesvirus associated ubiquitin specific protease, USP7, is a negative regulator of PML proteins and PML nuclear bodies. *PLoS ONE* *6*, e16598.
- Sarnow, P., Sullivan, C.A., and Levine, A.J. (1982). A monoclonal antibody detecting the adenovirus type 5-E1b-58Kd tumor antigen: characterization of the E1b-58Kd tumor antigen in adenovirus-infected and -transformed cells. *Virology* *120*, 510–517.
- Scaglioni, P.P., Yung, T.M., Cai, L.F., Erdjument-Bromage, H., Kaufman, A.J., Singh, B., Teruya-Feldstein, J., Tempst, P., and Pandolfi, P.P. (2006). A CK2-dependent mechanism for degradation of the PML tumor suppressor. *Cell* *126*, 269–283.
- Schneider, E., Kartarius, S., Schuster, N., and Montenarh, M. (2002). The cyclin H/cdk7/Mat1 kinase activity is regulated by CK2 phosphorylation of cyclin H. *Oncogene* *21*, 5031–5037.
- Schreiner, S., Wimmer, P., Sirma, H., Everett, R.D., Blanchette, P., Groitl, P., and Dobner, T. (2010). Proteasome-dependent degradation of Daxx by the viral E1B-55K protein in human adenovirus-infected cells. *J. Virol.* *84*, 7029–7038.
- Schuster, N., Götz, C., Faust, M., Schneider, E., Prowald, A., Jungbluth, A., and Montenarh, M. (2001). Wild-type p53 inhibits protein kinase CK2 activity. *J. Cell. Biochem.* *81*, 172–183.
- Schwartz, R.A., Lakdawala, S.S., Eshleman, H.D., Russell, M.R., Carson, C.T., and Weitzman, M.D. (2008). Distinct requirements of adenovirus E1b55K protein for degradation of cellular substrates. *J. Virol.* *82*, 9043–9055.
- Seeber, S., Issinger, O.G., Holm, T., Kristensen, L.P., and Guerra, B. (2005). Validation of protein kinase CK2 as oncological target. *Apoptosis* *10*, 875–885.
- Seldin, D.C., Lou, D.Y., Toselli, P., Landesman-Bollag, E., and Dominguez, I. (2008). Gene targeting of CK2 catalytic subunits. *Mol. Cell. Biochem.* *316*, 141–147.
- Shen, Y., Kitzes, G., Nye, J.A., Fattaey, A., and Hermiston, T. (2001). Analyses of Single-Amino-Acid Substitution Mutants of Adenovirus Type 5 E1B-55K Protein. *J. Virol.* *75*, 4297–4307.

- Shenk, T. (2001). Adenoviridae: the viruses and their replication. In *Virology*, (New York, Lippincott-Raven), pp. 2265–2300.
- Sieber, T., and Dobner, T. (2007). Adenovirus type 5 early region 1B 156R protein promotes cell transformation independently of repression of p53-stimulated transcription. *J. Virol.* *81*, 95–105.
- Sivachandran, N., Sarkari, F., and Frappier, L. (2008). Epstein-Barr nuclear antigen 1 contributes to nasopharyngeal carcinoma through disruption of PML nuclear bodies. *PLoS Pathog.* *4*, e1000170.
- Slaton, J.W., Unger, G.M., Sloper, D.T., Davis, A.T., and Ahmed, K. (2004). Induction of apoptosis by antisense CK2 in human prostate cancer xenograft model. *Mol. Cancer Res.* *2*, 712–721.
- Song, M.S., Salmena, L., Carracedo, A., Egia, A., Lo-Coco, F., Teruya-Feldstein, J., and Pandolfi, P.P. (2008). The deubiquitinylation and localization of PTEN are regulated by a HAUSP-PML network. *Nature* *455*, 813–817.
- Soria, C., Estermann, F.E., Espantman, K.C., and O’Shea, C.C. (2010). Heterochromatin silencing of p53 target genes by a small viral protein. *Nature* *466*, 1076–1081.
- Souquere-Besse, S., Pichard, E., Filhol, O., Legrand, V., Rosa-Calatrava, M., Hovanessian, A.G., Cochet, C., and Puvion-Dutilleul, F. (2002). Adenovirus infection targets the cellular protein kinase CK2 and RNA-activated protein kinase (PKR) into viral inclusions of the cell nucleus. *Microsc. Res. Tech.* *56*, 465–478.
- Soussi, T., Caron de Fromental, C., and May, P. (1990). Structural aspects of the p53 protein in relation to gene evolution. *Oncogene* *5*, 945–952.
- St-Denis, N.A., and Litchfield, D.W. (2009). Protein kinase CK2 in health and disease: From birth to death: the role of protein kinase CK2 in the regulation of cell proliferation and survival. *Cell. Mol. Life Sci.* *66*, 1817–1829.
- Stehmeier, P., and Muller, S. (2009). Phospho-regulated SUMO interaction modules connect the SUMO system to CK2 signaling. *Mol. Cell* *33*, 400–409.
- Stracker, T.H., Carson, C.T., and Weitzman, M.D. (2002). Adenovirus oncoproteins inactivate the Mre11-Rad50-NBS1 DNA repair complex. *Nature* *418*, 348–352.
- Stuurman, N., de Graaf, A., Floore, A., Josso, A., Humbel, B., de Jong, L., and van Driel, R. (1992). A monoclonal antibody recognizing nuclear matrix-associated nuclear bodies. *J. Cell. Sci.* *101 (Pt 4)*, 773–784.
- Tang, J., Qu, L., Pang, M., and Yang, X. (2010). Daxx is reciprocally regulated by Mdm2 and Hausp. *Biochem. Biophys. Res. Commun.* *393*, 542–545.
- Tatsis, N., and Ertl, H.C.J. (2004). Adenoviruses as vaccine vectors. *Mol. Ther.* *10*, 616–629.
- Täuber, B., and Dobner, T. (2001). Molecular regulation and biological function of adenovirus early genes: the E4 ORFs. *Gene* *278*, 1–23.

- Teodoro, J.G., and Branton, P.E. (1997). Regulation of p53-dependent apoptosis, transcriptional repression, and cell transformation by phosphorylation of the 55-kilodalton E1B protein of human adenovirus type 5. *J. Virol.* *71*, 3620–3627.
- Teodoro, J.G., Halliday, T., Whalen, S.G., Takayesu, D., Graham, F.L., and Branton, P.E. (1994). Phosphorylation at the carboxy terminus of the 55-kilodalton adenovirus type 5 E1B protein regulates transforming activity. *J. Virol.* *68*, 776–786.
- Trembley, J.H., Wang, G., Unger, G., Slaton, J., and Ahmed, K. (2009). Protein kinase CK2 in health and disease: CK2: a key player in cancer biology. *Cell. Mol. Life Sci.* *66*, 1858–1867.
- Trentin, J.J., Yabe, Y., and Taylor, G. (1962). The quest for human cancer viruses. *Science* *137*, 835–841.
- Ubersax, J.A., and Ferrell, J.E., Jr (2007). Mechanisms of specificity in protein phosphorylation. *Nat. Rev. Mol. Cell Biol.* *8*, 530–541.
- Walls, T., Shankar, A.G., and Shingadia, D. (2003). Adenovirus: an increasingly important pathogen in paediatric bone marrow transplant patients. *Lancet Infect Dis* *3*, 79–86.
- Wang, G., Unger, G., Ahmad, K.A., Slaton, J.W., and Ahmed, K. (2005). Downregulation of CK2 induces apoptosis in cancer cells--a potential approach to cancer therapy. *Mol. Cell. Biochem.* *274*, 77–84.
- Wang, H., Davis, A., Yu, S., and Ahmed, K. (2001). Response of cancer cells to molecular interruption of the CK2 signal. *Mol. Cell. Biochem.* *227*, 167–174.
- Wang, Q.-Y., Bushell, S., Qing, M., Xu, H.Y., Bonavia, A., Nunes, S., Zhou, J., Poh, M.K., Florez de Sessions, P., Niyomrattanakit, P., et al. (2011a). Inhibition of dengue virus through suppression of host pyrimidine biosynthesis. *J. Virol.* *85*, 6548–6556.
- Wang, Q.-Y., Kondreddi, R.R., Xie, X., Rao, R., Nilar, S., Xu, H.Y., Qing, M., Chang, D., Dong, H., Yokokawa, F., et al. (2011b). A translation inhibitor that suppresses dengue virus in vitro and in vivo. *Antimicrob. Agents Chemother.* *55*, 4072–4080.
- Weber, K., Bartsch, U., Stocking, C., and Fehse, B. (2008). A multicolor panel of novel lentiviral “gene ontology” (LeGO) vectors for functional gene analysis. *Mol. Ther.* *16*, 698–706.
- Weitzman, M.D., Fisher, K.J., and Wilson, J.M. (1996). Recruitment of wild-type and recombinant adeno-associated virus into adenovirus replication centers. *J. Virol.* *70*, 1845–1854.
- Weitzman, M.D., and Ornelles, D.A. (2005). Inactivating intracellular antiviral responses during adenovirus infection. *Oncogene* *24*, 7686–7696.
- Wickham, T.J., Filardo, E.J., Cheresch, D.A., and Nemerow, G.R. (1994). Integrin alpha v beta 5 selectively promotes adenovirus mediated cell membrane permeabilization. *J. Cell Biol.* *127*, 257–264.

- Wickham, T.J., Mathias, P., Cheresch, D.A., and Nemerow, G.R. (1993). Integrins alpha v beta 3 and alpha v beta 5 promote adenovirus internalization but not virus attachment. *Cell* 73, 309–319.
- Wimmer, P., Blanchette, P., Schreiner, S., Ching, W., Groitl, P., Berscheminski, J., Branton, P.E., Will, H., and Dobner, T. (2012). Cross-talk Between Phosphorylation and SUMOylation Regulates Transforming Activities of an Adenoviral Oncoprotein. *Oncogene*.
- Wimmer, P., Schreiner, S., Everett, R.D., Sirma, H., Groitl, P., and Dobner, T. (2010). SUMO modification of E1B-55K oncoprotein regulates isoform-specific binding to the tumour suppressor protein PML. *Oncogene* 29, 5511–5522.
- Xie, X., Wang, Q.-Y., Xu, H.Y., Qing, M., Kramer, L., Yuan, Z., and Shi, P.-Y. (2011). Inhibition of dengue virus by targeting viral NS4B protein. *J. Virol.* 85, 11183–11195.
- Xu, R.-H., Yuan, Z.-Y., Guan, Z.-Z., and Li, S. (2005). [Reverse effect of genetically modified adenovirus H101 on drug-resistance of A549/DDP cells to cisplatin]. *Ai Zheng* 24, 975–979.
- Yaron, Y., McAdara, J.K., Lynch, M., Hughes, E., and Gasson, J.C. (2001). Identification of novel functional regions important for the activity of HOXB7 in mammalian cells. *J. Immunol.* 166, 5058–5067.
- Yondola, M.A., and Hearing, P. (2007). The adenovirus E4 ORF3 protein binds and reorganizes the TRIM family member transcriptional intermediary factor 1 alpha. *J. Virol.* 81, 4264–4271.
- Zapata, J. M., Pawlowski, K., Haas, E., Ware, C. F., Godzik, A., and Reed J. C. (2001). A diverse family of proteins containing tumor necrosis factor receptor-associated factor domains. *J Biol Chem*, 276, 24242-24252.

## 13 List of figures

FIG 1 Simplified taxonomic illustration of the family of <i>Adenoviridae</i> .....	2
FIG 2 Electron micrograph and schematic representation of an adenoviral virion .....	4
FIG 3 Schematic representation of a linear double-stranded DNA genome of HAdV5. ....	5
FIG 4 Schematic representation of the HAdV5 E1B-55K protein .....	9
FIG 5 Schematic representation of CK2 $\alpha$ and CK2 $\beta$ .....	12
FIG 6 CK2 inhibitor TBB and DMAT.....	13
FIG 7 Usp7 at the center of p53 and Mdm2 regulation.....	15
FIG 8 Functionally important domains of Usp7 .....	16
FIG 9 CK2 phosphorylation consensus motif of E1B-55K and E1B-55K phosphorylation.....	44
FIG 10 Coimmunoprecipitation to analyze E1B-55K and its interaction with CK2 $\alpha$ in infected cells.....	46
FIG 11 Indirect immunofluorescence to analyze E1B-55K and CK2 $\alpha$ in infected cells.....	48
FIG 12 Coimmunoprecipitation and indirect immunofluorescence to analyze E1B-55K and its interaction with CK2 $\beta$ in infected cells.....	50
FIG 13 CK2 $\alpha$ , but not the CK2 holoenzyme, phosphorylates E1B-55K's C terminus <i>in vitro</i> .....	52
FIG 14 The 156R splice product of E1B-55K is also phosphorylated by CK2 $\alpha$ but not by the holoenzyme .....	53
FIG 15 Phosphorylation of E1B-55K determines interaction with several proteins .....	55
FIG 16 Phenotypic characterization of H5pg4100 (wt) and H5pm4174 (E1B-P minus) viruses.....	58
FIG 17 Inhibitors TBB and DMAT reduce Mre11 and DNA ligase IV degradation efficiency but have no effect on inducing viral genome concatemerization although virus yield is significantly decreased.....	60
FIG 18 Usp7-E1B-55K interaction in different set-ups .....	68
FIG 19 Indirect immunofluorescence to analyze Usp7 localization during adenoviral infection in comparison to E1B-55K .....	71
FIG 20 Image processing of immunofluorescence data from Usp7-E1B-55K costainings.....	73
FIG 21 Indirect immunofluorescence to analyze the Usp7 localization during adenoviral infection in comparison to E2A.....	75
FIG 22 Image processing of immunofluorescence data from Usp7-E2A costaining to underline Usp7-E2A interaction .....	77
FIG 23 Assessing Dose-response curves of different cell lines upon Usp7 inhibitor HBX treatment.....	79
FIG 24 Analyses of the growth behavior of A549 and H1299 cells upon HBX treatment.....	81
FIG 25 HBX treatment causes no change in the localization patterns of Usp7 and E1B-55K in infected cells but reduces the amount of E1B-positive cells .....	83
FIG 26 Usp7 knockdown and its effect on E1B-55K .....	85

---

FIG 27 Usp7 knockdown in H1299 cells has a negative effect on adenoviral proteins and virus growth .....	87
FIG 28 HBX treatment leads to negative effects on adenoviral proteins and virus growth. ....	88
FIG 29 The effect of HBX on cell transformation. ....	91
FIG 30 Phosphonegative E1B-55K (E1B-P minus) interaction towards Usp7 is severely reduced.....	102
FIG 31 No obvious difference in the Usp7 redistribution pattern between wt (H5pg4100) and E1B-P minus (H5pm4174) virus infection .....	103
FIG 32 CK2 inhibition reduces binding capacity of E1B-55K towards Usp7 .....	104
FIG 33 The Usp7 inhibitor HBX decreases virus yield of the E1B-P minus virus (H5pm4174).....	106
FIG 34 The amount of PML tracks during wt and E1B-P minus virus infection differs significantly.....	108
FIG 35 Usp7 and PML localization during adenoviral infection .....	110
FIG 36 A visualization of certain key points discussed in the thesis model .....	118

## 14 Acknowledgements

**I want to say thank you to** Prof. Dr. Thomas Dobner, Dr. Habil. Nicole Fischer, Prof. Dr. Hans Will, Prof. Dr. Udo Wienand, Prof. Dr. Alexander Haas, Prof. Georg Mayr, Dr. Jan Chemnitz, Dr. Nicole Walz, Dr. Cornelia Heinze, Dr. Christina Arbelo, Rüdiger Meyer and Prof. Chris Meier

Thanks to the Leibniz Graduate School

I want to point out that Dr. Timo Sieber deserves special respect since he is one hell of a scientist, entertainer and was one of the nicest lab mate ;)

Thanks to Julie Sellau and Franziska Muscate for being so helpful and nice Bachis;) – How Am I supposed to eat all that sweet stuff

Big, Big thanks to my best friend Finn, big help, great effort, a guy you can trust...;) At this point, I will read your dissertation. Great input!

Also big thanks to Sonia! man I was lucky working with such a nice and talented Master's student together hehe!! whatsapp!! Also great input

much credit belongs to my family: Ivan, Carmen, Yipeng, Max, Josy, mom and dad. What can I say? Without family nothing's working

Last but not least:

Cindy mein Schatz ohne Dich hätte ich das nicht geschafft. Vielen vielen Dank. Auch für Dein Verständnis wenn ich "mal" spät nach Hause gekommen bin. Ich verspreche Dir 2.5 Jahre ohne Urlaub und ohne Wochenende mache ich nicht mehr!

Ich liebe dich für immer und das wir zusammen sind ist eigentlich alles was zählt!!! ILU Dein Willi